Applications of Remote Hyperspectral Sensing in the Characterization of Alberta's Oil Sands Tailings

by

Iman Entezari Najafabadi

A thesis submitted in partial fulfillment of the requirements for the degree of

Doctor of Philosophy

Department of Earth and Atmospheric Sciences
University of Alberta

Abstract

The bitumen production from oil sands surface-mining operations produces large volumes of mineral wastes called tailings. Characterization of the oil sands tailings is of importance to monitor their state for trafficability and reclamation issues, to assess the tailings operation performance, and to develop more effective measures for tailings operations and management.

This thesis investigates the use of hyperspectral remote sensing data to develop spectral models capable of predicting key characteristic of oil sands tailings surfaces including: 1) water content and normalized evaporation; 2) swelling potential or activity as indicated by the methylene blue index (MBI), and 3) clay mineral species and their abundance as well as the abundance of quartz.

In Chapter two, hyperspectral time-series laboratory observations are collected from different tailings samples displaying variations in swelling potential and bitumen concentration. From these data effective spectral models were developed for the estimation of moisture content and normalized evaporation with best results achieved using the Normalized Soil Moisture Index (NSMI). Application of the predictive models to field setting would require a validation of initial results.

In Chapter three shortwave and longwave infrared hyperspectral data are used to estimate the swelling potential or activity of oil sands soft tailings indicated by the Methylene Blue Index (MBI). Spectral features, in particular those attributed to the presence of clay and quartz minerals, are characterized and their correlation with MBI is investigated. In the SWIR, a band ratio of reflectance at 1.773 μm to 1.307 μm provided an estimation of MBI of tailings that could be applied to field settings. A water sensitivity analysis showed that the model based on these

bands is robust against variations in the tailings moisture content for values less than 20 wt%. At moisture levels above 20 wt%, the MBI value was overestimated. The best MBI predictions were obtained in the LWIR using reflectance peaks at 9.67 μm and 11 μm attributed to total clays and kaolinite, respectively.

The aim of Chapter four is to gain an understanding of the changes in reflectance response with change in mineralogy of oil sands and to investigate the effectiveness of hyperspectral sensing for the prediction of the mineral composition of oil sands ore and tailings, particularly clays. The results demonstrate that longwave infrared observations are of significant value for the prediction of clay and quartz content in oil sands ore and tailings. Also, spectral tools can be developed to monitor the ratio of swelling to non-swelling clays in ore and tailings.

Overall, the results of this thesis offer a key enabling technology to remotely assess tailings characteristics related to establishing the geotechnical stability of a tailings deposit. Such observations and derived information would complement standard geotechnical testing and sampling campaigns (using manual techniques), which are expensive, time consuming, potentially hazardous to personnel, and necessarily limited to a small number of locations. In future efforts, the methods developed in this thesis can contribute in generating real-time maps of tailings properties for operational decision-making in predicting engineered tailings process performance.

Acknowledgements

First and foremost, I would like to express my deepest gratitude to my supervisor Dr. Benoit Rivard for all his guidance, insightful comments, and support. His passion for doing distinguished research, his expertise in hyperspectral remote sensing, his openness to research ideas, and his professional attitude made my PhD studies truly joyful.

Besides, I would like to thank my committee advisors Dr. Michael Lipsett and Dr. Ward Wilson for their valuable comments and encouragement. Their expertise in the field of oil sands incented me to broaden my research from various perspectives and their interest in my work was a great source of inspiration.

I am grateful to Dr. Jilu Feng (University of Alberta) for training me to use several spectral instruments and for his guidance. I am also thankful to my fellow graduate student Michelle Speta for all her collaboration and constructive discussions we had throughout our PhD journey. Dr. Heather Kaminsky (Suncor Energy) is acknowledged for her valuable comments and input. Dr. Reza Nik (Shell Canada) and Mr. Mirjavad Geramian (University of Alberta) are thanked for providing samples for this research.

I would also like to thank my fellow graduate students and office/lab mates Dr. Kati Laakso, Philip Lypaczewski, Yaqian Long, Dominica Harrison, and Leila Taheriazad at the Centre for Earth Observation Sciences (CEOS), University of Alberta, who provided a friendly and collaborative environment suited for research. Mei Mei Chong (CEOS) is also appreciated for her support.

This thesis would not have been completed without financial support from the University of Alberta, the Institute for Oil Sands Innovation (IOSI), and Canada's Oil Sands Innovation

Alliance (COSIA). Shell Canada Energy is also acknowledged for providing the samples used in this study.

Last but not least, I must thank my lovely wife Sara for all her love and encouragement throughout my years of study. I am also grateful to my parents for all their support and for everything they have done for my success.

Table of Contents

List of Tables

List of Figures

Chapter 1 Introduction

1.1 Background

A vast reservoir of oil sands is located in northern Alberta, Canada. Oil sands are a natural mixture of sand, clay and other minerals, water, and a type of very thick and heavy oil called bitumen. To produce crude oil and other petroleum products, bitumen must be removed from the solids and water and then refined. Depending on the burial depth of the oil sand deposits, two methods of bitumen extractions are used: i) surface mining and ii) in-situ extraction. The former method is used for deposits at burial depths of less than 75 meters (National Energy Board 2004) while the later extracts deep underground deposits. In surface mining, the extraction process uses massive volumes of water to float the bitumen from the ore material. This results in large volumes of high water content tailings composed predominantly of sand, silt, clay, and residual bitumen. The long term goal in tailings management is to remove the water from solids so that a trafficable load-bearing surface, which is no longer mobile, can be produced for the purpose of reclamation (BGC Engineering Inc. 2010). Thus, characterization of the oil sands tailings is of importance for tailings processing and evaluating the tailings operation performance, monitoring the tailings state for trafficability, and tailings deposition and capping.

The capability of tailings to discharge water is of importance because after a few years of placement, the oil sands tailings can still contain 60-70 wt% water and such tailings are known as mature fine tailings (MFT). The separation of water from solids is thus an operational and environmental challenge of tailings management. In the past decades, several engineering techniques have been proposed and tested to accelerate water removal and increase the performance of the consolidation process. Kasperski (1992) and Chalaturnyk et al. (2002) have

summarized most of the tailings treatment options. As of 2012, there were five process methods being used by oil sands operators to accelerate the dewatering of fine tailings (COSIA/OSTC 2012): i) Centrifugation of flocculated tailings, ii) thin-lift deposition of in-line flocculated tailings, iii) deep-lift deposition of in-line flocculated tailings, iv) thin- or deep-lift deposition of flocculated and thickened fine tailings, and v) deep-deposit of blended sand slurry and flocculated or coagulated fine tailings. To assess the efficiency of the operational techniques, periodic estimation of tailings characteristics is required.

The surface properties of the minerals within the tailings control the water holding capacity and thus the rate of consolidation of the tailings (Kotlyar et al. 1992). Among the minerals present, clay minerals, which can be inert (like kaolinite) or active (like smectite and vermiculite), constitute a significant fraction of the tailings solids. Many studies have shown that kaolinite and illite are major clays present in the Alberta oil sands ores and tailings (Kessick 1979; Kotlyar et al. 1995; Mercier et al. 2008). However, other clay species have been observed such as smectite, chlorite, vermiculite and mixed-layer clays including kaolinite-smectite and illite-smectite (Yong and Sethi 1978; Scott et al. 1985; Omotoso and Mikula 2004; Omotoso et al. 2006, Kaminsky 2008). It is generally believed that challenges in the extraction of bitumen (oil sands processability) and the dewatering of tailings are largely related to the abundance of illite and mixed-layer clays in oil sands (BGC Engineering Inc. 2010). Therefore, the identification of clays and their abundance in tailings can help in improving the tailings processing and dewatering technologies but also help to evaluate the geotechnical properties of the tailings. Assessment of such properties, including the swelling potential and shear strength, is important as tailings management aims to produce load-bearing surfaces that can be reclaimed and revegetated. It has been reported that the typical shear strength of MFT is much less than

1kPa which is indicative of their fluid-like behaviour (FTFC 1995). During the process of dewatering and consolidation, the tailings strength increases depending on the type of minerals and the particle size distribution of the solids. Determining the particles size distribution of a tailing in a given state is also contributing to the evaluation of the strength of the tailings. The swelling potential generally refers to the ability of clays to undergo a large change in volume in the presence of water. The activity of clays significantly affects the settling and consolidation of tailings (Omotoso and Mikula 2004) and the geotechnical stability of a final tailings deposit for reclamation purposes. Also, the effectiveness of many polymer-based technologies, developed to reduce tailings inventories, depends on the type and abundance of clay minerals (Omotoso and Mikula 2004; Omotoso et al. 2006; Kaminsky et al. 2009; Kaminsky 2014). The Methylene Blue Index (MBI) is the most commonly used index to estimate the activity of clays in the ore, froth, and tailings of oil sands. MBI quantifies the cation exchange capacity (CEC) of a sample by measuring the amount of methylene blue cations required to cover the total available surface of the anionic clay particles present in the sample that has had the bitumen and connate water removed so that only solid material remains.

Considerable work has been done characterizing oil sands ore and tailings (e.g. Bayliss and Levinson 1976; Bichard 1987; Hepler and His 1989; Omotoso and Mikula 2004; Omotoso et al. 2006; Wallace et al. 2004; Mercier et al. 2008; Kaminsky 2008; Hooshiar Fard 2011; Osacky et al. 2013). However, most of the laboratory methods used to measure tailings properties are time consuming, costly, and limited to a small number of samples or locations. Therefore, introducing reliable and accurate methods, which are quick and cost effective, capable of monitoring and measuring the characteristics of tailings at a large scale is potentially of benefit for tailings management. The current research aims to develop and test hyperspectral remote sensing

methods to meet some of these needs and assess the accuracy of these methods for the characterization of oil sands tailings.

Hyperspectral sensing (so-called reflectance spectroscopy) is an emerging technology used for the characterization of materials, such as the identification and quantification of minerals. Hyperspectral sensors collect the natural radiation reflected from or emitted by materials for an extended portion of the electromagnetic spectrum. These sensors divide the electromagnetic spectrum in hundreds of narrow continuous wavelength intervals, so-called spectral bands, and measure the radiation in these bands. Depending on the instrument used, the radiation is acquired in optical (0.4-2.5 μm) and longwave portions (7.5-11.5 μm) of the electromagnetic spectrum, where unique features about the measured object are revealed. The spectral response from each material is wavelength dependent and is largely controlled by the chemical composition and crystal structure of the minerals and other materials within. Owing to advances in high spatial resolution hyperspectral imaging systems (so-called imaging spectrometers), it is now feasible to collect spectra for every pixel of the acquired image, associated with a small footprint on the object (a few millimetres or less per pixel), resulting in detailed compositional spatial context following analysis and interpretation.

Thus far, remotely sensed data have been widely used to study the properties of natural soils (e.g. Barnes et al., 2003; Bindlish et al., 2003; Ben-Dor et al., 2009). Significant work has been done to estimate the moisture of such soils using multi and hyperspectral data (e.g. Weidong et al., 2002, 2003; Whiting et al., 2004; Haubrock et al., 2008). There is ample literature on the characterization of clay minerals using reflectance spectroscopy (e.g. Farmer and Russell 1964; Oinuma and Hayashi 1965; Clark et al. 1990; Salisbury et al. 1991; Chabrillat et al. 2002; Ellis and Scott 2004; Gates 2005; Bishop et al. 2008, 2011; Yitagesu et al. 2011). The effectiveness of

reflectance spectroscopy for mapping active clays and for the determination of engineering parameters (such as Atterberg limits, coefficient of linear extensibility (COLE), and CEC) of natural expansive soils has been investigated in several studies (Van der Meer 1999; Goetz et al. 2001; Kariuki et al. 2003, 2004; Shouxun and Jin 2004; Yitagesu et al. 2009, 2012). The effects of particle size and compaction of natural soils on their spectra have also been studied to some extent (Clark and Roush 1984; Salisbury and Wald 1992; Hapke 1993; Cooper and Mustard 1999). In the context of oil sands studies have investigated the applications of hyperspectral sensing to estimate several characteristics of oil sands ore, particularly the estimation of bitumen content (Rivard et al. 2010; Speta et al. 2015). However there is no comprehensive research on the use of hyperspectral remote sensing to characterize oil sands tailings, to the author's knowledge. This study thus represents the first investigation of the spectroscopy of oil sands tailings and it assesses the potential applications of hyperspectral remote sensing to reveal information of relevance to tailings management.

1.2 Thesis Objectives and Hypotheses

The current study aims to develop quantitative estimates of characteristics of tailings surfaces using shortwave infrared (SWIR, 1.0-2.5 μm) and longwave infrared (LWIR, 7.5-11.5 μm) hyperspectral observations. Among the different tailings characteristics, focus is given to the estimation of some crucial and trackable properties including water content and the normalized evaporation, and the swelling potential and mineral content particularly clay mineral species and their abundances. The outcome of this study could be beneficial to the industry by providing new monitoring tools for the management of tailings operations. Specific objectives and the hypotheses to achieve each objective are:

1) To develop spectral models for the accurate estimation of water content and normalized evaporation from oil sands tailings surfaces using hyperspectral observations. It is hypothesised that the moisture content from the tailings surface can be estimated and quantified using spectral measurements and spectral features relating to the overtones and combination absorption bands of the water molecules around 1400 nm and 1900 nm. The overall reflectance in the SWIR may also be of value for water content quantification as it dramatically changes with water content.
2) To explore the capability of SWIR and LWIR hyperspectral sensing for the estimation of the swelling potential or activity of oil sands tailings. In doing so it should be possible to estimate the methylene blue index (MBI) of tailings, which is measured in the laboratory and is an indicator of the swelling potential of the oil sands tailings. The hypothesis is that variations in clay content and clay types in the tailings, which results in variation in the swelling potential and thus MBI values, cause variations in the tailings spectra in the SWIR and LWIR. Reflectance spectra collected from tailings samples spanning a range of known MBI values can thus be used to explore spectral metrics, including features attributed to clay and quartz minerals in the SWIR and LWIR, to develop predictive models for the estimation of MBI.
3) To assess the potential of hyperspectral data for the detection and identification of clay mineral species and their abundance in oil sands and to develop tools to characterize the clay minerals in oil sands ore and tailings. The hypothesis is that clay minerals can be identified using characteristic absorption features and reflectance peaks, in the SWIR and LWIR, caused by vibrations of the hydroxyl (OH) group and structural water molecules as well as vibrations involving silicon, oxygen, and octahedral, tetrahedral, and interlayer cations. The

variation in the overall shape of the spectra (i.e. continuum) can also be diagnostic of the mineralogy.

1.3 Thesis Outline

This thesis is in paper-based format based on the completion of three stand-alone manuscripts submitted or ready for submission to peer-reviewed journals. Following the Introduction Chapter, Chapters two, three, and four address the three specific objectives of this thesis. Chapter 5 presents the conclusions and suggests avenues for future research.

Chapter two presents the challenge of estimating the water content and evaporative fluxes from oil sands soft tailings surfaces using hyperspectral sensing. The resulting manuscript is being edited based on first reviews and appears as Entezari, I., Rivard, B., Lipsett, M., and Wilson, G.W., "Prediction of water content and normalized evaporation from oil sand soft tailings surfaces using hyperspectral observations," *Canadian Geotechnical Journal*. Dr. Rivard, Dr. Lipsett, and Dr. Wilson helped in designing the experimental protocol, provided critiques, and edited the manuscript. Dr. Wilson also provided input for the introduction. Dr. Rivard was the supervisory author and was involved with paper composition. All the experiments, data collection and data analysis was done by the author of this thesis.

Chapter three discusses the use of SWIR and LWIR hyperspectral sensing for the estimation of the swelling potential or activity of oil sands tailings. The relationships between sample reflectance spectral features and the Methylene Blue Index (MBI), which is an indicative of the activity of the tailings, were investigated in this chapter. The resulting manuscript has been accepted for publication after minor revisions and appears as: Entezari, I., Rivard, B., and Lipsett, M., "Estimation of Methylene Blue Index in oil sands tailings using hyperspectral data."

in the Canadian Journal of Chemical Engineering. Dr. Lipsett provided feedback on the results and edited the manuscript. Dr. Rivard provided critiques on the results and was the supervisory author of the manuscript.

Chapter four investigates the effectiveness of hyperspectral sensing for the prediction of the mineral make up of oil sands ore and tailings, particularly clays species and their abundance. This chapter is ready for submission as a publication. The authors are Iman Entezari, Benoit Rivard, Mirjavad Geramian, and Michael Lipsett. Mr. Geramian provided the samples with mineralogical data and helped in sample preparation for spectral measurements. Dr. Lipsett helped in editing the manuscript. As in Chapters two and three, Dr. Rivard was the supervisory author and was involved with the manuscript composition.

If not mentioned above, this thesis is an original work by Iman Entezari Najafabadi.

References

Barnes, E.M., Sudduth, K.A., Hummel, J.W., Lesch, S.M., Corwin, D.L., Yang, C.H., Daughtry, C.S.T., and Bausch, W.C., 2003. Remote- and ground-based sensor techniques to map soil properties. Photogrammetric Engineering and Remote Sensing 69(6): 619–630.

Bayliss, P., and Levinson, A.A., 1976. Mineralogical review of the Alberta oil sand deposits (Lower Cretaceous, Mannville Group). Bulletin of Canadian Petroleum Geology, 24(2): 211–224.

Ben-Dor, E., Chabrillat, S., Dematte, J.A.M, Taylor, G.R., Hill, J., Whiting, M.L., and Sommer, S., 2009. Using imaging spectroscopy to study soil properties. Remote Sensing of Environment 113(1): 38–55.

BGC Engineering Inc., 2010. Oil sands tailings technology review. Oil Sands Research and Information Network, University of Alberta, School of Energy and the Environment, Edmonton, Alberta. OSRIN Report No. TR-1. 136 pp.

Bichard, J.A., 1987. Oil sands composition and behaviour research. Edmonton: Alberta Oil Sands Technology and Research Authority.

Bindlish, R., Jackson, T.J., Wood, E., Gao, H., Starks, P., Bosch, D., and Lakshmi, V., 2003. Soil moisture estimates from TRMM Microwave Imager observations over the southern United States. Remote Sensing of Environment 85(4): 507–515.

Bishop, J.L., Lane, M.D., Dyar, M.D., and Brown, A.J., 2008. Reflectance and emission spectroscopy study of four groups of phyllosilicates: Smectites, kaolinite-serpentines, chlorites and micas. Clay Minerals 43: 35-54.

Bishop, J.L., Gates, W.P., Makarewicz, H.D., McKeown, N.K., and Hiroi, T. 2011. Reflectance spectroscopy of beidellites and their importance for Mars. Clays and Clay Minerals. 59(4): 378–399.

Chabrillat, S., Goetz, A.F.H., Krosley, L., and Olsen, H.W., 2002. Use of hyperspectral images in the identification and mapping of expansive clay soils and the role of spatial resolution. Remote Sensing of Environment 82: 431-445.

Chalaturnyk, R.J., Scott, J.D, and Ozum, B., 2002. Management of oil sands tailings. Petroleum Science and Technology 20: 1025–1046.

Clark, R.N., King, T.V., Klejwa, M., Swayze, G.A., and Vergo, N., 1990. High spectral resolution reflectance spectroscopy of minerals. Journal of Geophysical Research 95(B8): 12653-12680.

Clark, R.N. and Roush, T.L., 1984. Reflectance spectroscopy: Quantitative analysis techniques for remote sensing applications. Journal of Geophysical Research 89: 6329−6340.

Cooper, C., and Mustard, J., 1999. Effects of very fine particle size on reflectance spectra of smectite and palagonitic soil. Icarus 142: 557-570.

COSIA/OSTC, 2012. Technical guide for fluid fine tailings management.

Ellis, R.J., and Scott, P.W., 2004. Evaluation of hyperspectral remote sensing as a means of environmental monitoring in the St. Austell China clay (kaolin) region, Cornwall, UK. Remote Sensing of Environment 93: 118-130.

Farmer, V. C., Russell, J.D. 1964. The infrared spectra of layer silicates. Spectrochimica Acta 20: 1149–1173.

FTFC (Fine Tailings Fundamentals Consortium), 1995. Advances in oil sands tailings research. Alberta Department of Energy, Oil Sands and Research Division, Edmonton, Canada.

Gates W.P., 2005. Infrared spectroscopy and the chemistry of dioctahedral smectites. Pp. 125-168 in: The Application of Vibrational Spectroscopy to Clay Minerals and Layered Double Hydroxides (J.T. Kloprogge, editors). The Clay Minerals Society, Aurora, Colorado, USA.

Goetz, A.F.H., Chabrillat, S., and Lu, Z., 2001. Field reflectance spectrometry for detection of swelling clays at construction sites. Field Analytical Chemistry and Technology 5(3): 143-155.

Hapke, B., 1993. Theory of reflectance and emittance spectroscopy. Cambridge Univ. Press, Cambridge.

Haubrock, S.N., Chabrillat, S., Lemmintz, C., and Kaufmann, H., 2008. Surface soil moisture quantification models from reflectance data under field condition. International Journal of Remote Sensing 29(1): 3-39.

Hepler, L. (ed.) and Hsi, C. (ed.), 1989. AOSTRA technical handbook on oil sands, bitumens and heavy oils. Edmonton: Alberta Oil Sands Technology and Research Authority.

Hooshiar Fard, M.A., 2011. Characterization of clay minerals in the Athabasca oil sands in water extraction and nonaqueous solvent extraction processes. Ph.D. Thesis, Department of Chemical and Materials Engineering, University of Alberta, Canada.

Kaminsky, H., 2008. Characterization of an athabasca oil sands ore and process streams. PhD Thesis, Department of Chemical and Materials Engineering, University of Alberta.

Kaminsky, H., 2014. Demystifying the Methylene Blue Index. Proc. Fourth International Oil Sands Tailings Conference, 7-10 December 2014, Lake Louise, AB, Canada, 221-229.

Kaminsky, H.A.W., Etsell, T.H., Ivey, D.G., and Omotoso, O., 2009. Distribution of clay minerals in the process streams produced by the extraction of bitumen from Athabasca oil sands. Canadian Journal of Chemical Engineering 87(1): 85-93.

Kariuki, P.C., Van der Meer, F., and Verhoef, P.N.W., 2003. Cation exchange capacity (CEC) determination from spectroscopy. International Journal of Remote Sensing 24(1): 161-167.

Kariuki, P.C., Woldai, T., Van der Meer, F.D., 2004. Effectiveness of spectroscopy in identification of swelling indicator clay minerals. International Journal of Remote Sensing 25(2): 455–469.

Kasperski, K.L., 1992. A review of properties and treatment of oil sands tailings. AOSTRA Journal of Research 8(1): 11–53.

Kessick, M., 1979. Structure and properties of oil sands and clay tailings. Journal of Canadian Petroleum Technology 18(1): 49–52.

Kotlyar, L.S., Capes, C.E., and Sparks, B.D., 1992. Gel-forming attributes of colloidal solids from fine tails formed during extraction of bitumen from Athabasca oil sands by the hot water process. AOSTRA Journal of Research 8: 55-61.

Kotlyar, L.S., Sparks, B.D., Woods, J., Capes, C.E., and Schutte, R., 1995. Biwetted ultrafine solids and structure formation in oil sands fine tailings. Fuel 74: 1146–1149.

Mercier, P.H.J., Le page, Y., Tu, Y., and Kotlyar, L.S., 2008. Powder X-ray diffraction determination of phyllosilicate mass and area versus particle thickness distributions for clays from the Athabasca oil sands. Petroleum Science and Technology 26(3): 307–321.

National Energy Board, 2004. Canada's Oil Sands: opportunities and challenges to 2015 [Pamphlet], Calgary, AB.

Oinuma, K. and Hayashi, H., 1965. Infrared study of mixed-layer clay minerals. American Mineralogist 50: 1213-1227.

Omotoso, O., and Mikula, R., 2004. High surface areas caused by smectitic interstratification of kaolinite and illite in Athabasca oil sands. Applied Clay Science 25: 37-47.

Omotoso, O., Mikula, R., Urquhart, S., Sulimma, H., and Stephens, P., 2006. Characterization of clays from poorly processing oil sands using synchrotron techniques. Clay Science 12(2): 88–93.

Osacky, M., Geramian, M., Dyar, M.D., Sklute, E.C., Valter, M., Ivey, D.G., Liu, Q., Etsell, T.H., 2013. Characterisation of petrologic end members of oil sands from the Athabasca region, Alberta, Canada. The Canadian Journal of Chemical Engineering 9999: 1–14.

Rivard, B., Lyder, D., Feng, J., Gallie, A., Cloutis, E., Dougan, P., Gonzalez, S., Cox, D., and Lipsett, M.G., 2010, Bitumen content estimation of Athabasca oil sand from broad band infrared reflectance spectra. The Canadian Journal of Chemical Engineering 88: 830–838

Salisbury, J. W., and Wald, A., 1992. The role of volume scattering in reducing spectral contrast in spectra of powdered minerals. Icarus 96: 121–128.

Salisbury J.W., Walter L.S., Vergo, N. and D'Aria D.M., 1991. Infrared (2.1-25 mm) spectra of minerals. Johns Hopkins University Press, Baltimore, USA.

Scott, J.D., Dusseault, M.B., and Carrier III, W.D., 1985. Behaviour of the clay/bitumen/water sludge system from oil sands extraction plants. Applied Clay Science 1: 207–218.

Shouxun, Y., and Jin, P., 2004. A study on the correlation relationships between smectite contents and spectral absorption indices of swelling soils. Proc. International Geoscience and Remote Sensing Symposium (IGARSS '04), 20-24 Sept. 2004, Anchorage, AK, USA.

Speta, M., Rivard, B., Feng, J., Lipsett, M., and Gingras, M.K., 2015, Hyperspectral imaging for the determination of bitumen content in Athabasca oil sands core samples: AAPG Bulletin 99(7): 1245–1259.

Van der Meer, F.D., 1999. Can we map swelling clay with remote sensing? International Journal of Applied Earth Observation & Geoinformation (JAG) 1: 27–35.

Wallace, D., Tipman, R., Komishke, B., Wallwork, V., and Perkins, E., 2004. Fines/water interactions and consequences of the presence of degraded illite on oil sands extractability. The Canadian Journal of Chemical Engineering 82: 667–677.

Weidong, L., Baret, F., Xingfa, G., Qingxi, T., Lanfen, Z., and Bing, Z., 2002. Relating soil surface moisture to reflectance. Remote Sensing of Environment 81: 238–246.

Weidong, L., Baret, F., Xingfa, G., Bing, Z., Qingxi, T., and Lanfen, Z., 2003. Evaluation of models for surface soil moisture estimation from reflectance data. International Journal of Remote Sensing 10(10): 2069-2083.

Whiting, M.L., Li, L., and Ustin, S.L., 2004. Predicting water content using Gaussian model on soil spectra. Remote Sensing of Environment 89: 535-552.

Yitagesu, F.A., Van der Meer, F.D., Van der Werff, H., 2009. Quantifying engineering parameters of expansive soils from their reflectance spectra. Engineering Geology 105: 151–160.

Yitagesu, F.A., Van der Meer, F.D., Van der Werff, H., and Hecker, C., 2011. Spectral characteristics of clay minerals in the 2.5–14 μm wavelength region. Applied Clay Science 53: 581–591.

Yitagesu, F.A., Van der Werff, H., Van der Meer, F.D., and Hecker, C., 2012. On the relationship between plasticity and spectral characteristics of swelling soils: The 3–5 μm wavelength region. Applied Clay Science 69: 67–78.

Yong R.N., and Sethi, A.J., 1978. Mineral particle interaction control of tar sand sludge stability. The Journal of Canadian Petroleum Technology 77(4): 76-83.

Chapter 2 Prediction of Water Content and Normalized Evaporation from Oil Sands Soft Tailings Surface Using Hyperspectral Observations

2.1 Introduction

The oil sands of northern Alberta comprise the third largest proven reserves of petroleum in the world (Alberta Energy 2014). Oil sands are a natural unconsolidated mixture of sand, clays and other minerals, water, and bitumen, a viscous petroleum high in residuals and asphaltenes. Bitumen must be separated from the solids and water so that it can subsequently be upgraded and refined into petroleum products, primarily transportation fuels. Depending on the depth of the oil sand deposits, bitumen extraction is done either by in-situ or surface mining methods. Bitumen does not flow naturally through a deposit, due to its high viscosity at ambient temperatures. In-situ production entails extracting bitumen from underground deposits by injecting steam and solvents to reduce viscosity and allow flow within an artificially created reservoir. Surface mining is done for deposits with overburden of less than approximately 75 meters (National Energy Board 2004). In surface mining, the ore is conditioned with reagents in warm water and agitated to separate bitumen from the oil sand matrix and to aerate bitumen droplets. Aerated bitumen then floats to the top of a separation vessel. The bitumen-rich froth is then diluted with a solvent and put through additional separation steps to reduce the amount of water and fine solids in the bitumen. Non-aqueous bitumen extraction processes are in development; but they have not been commercially implemented. The water-based separation process requires about two barrels of water for each barrel of bitumen produced, resulting in large volumes of tailings, comprising mostly water with sand, silt, clay, and residual bitumen. When the tailings are discharged into the

tailings pond, the coarse sand particles settle to the bottom quickly, forming a beach and trapping some fine solids in interstices. The remaining fine solids settle slowly. This mixture naturally densifies to about 30 wt% fines/fines-plus-water within a few years in a settling basin, forming Mature Fine Tailings (MFT) (MacKinnon 1989). Released water clarifies fairly quickly and is recycled in the extraction process. The MFT remains saturated for decades because of its very slow natural consolidation rate (Kasperski 1992, MacKinnon 1989), and so it has essentially no bearing strength (FTFC 1995).

One of the long-term goals in tailings management is to remove the water from solids so that a trafficable load-bearing surface can be produced (with an undrained shear strength significantly greater than 10 kPa) for terrestrial reclamation (BGC Engineering Inc. 2010). Water removal from saturated tailings is the process of densifying and consolidating tailings. The separation of water from MFT is thus an operational and environmental challenge of tailings management.

In the past few decades, several engineering techniques have been proposed and tested to accelerate water removal and increase the performance of the consolidation process of MFT. The composite tailings or consolidated tailings (CT) process combines gypsum as a coagulant with MFT mixed with tailings sand, which acts as a charge to accelerate densification (FTFC 1995, Boratynec 1998). Thickened tailings processes (TT) use flocculants to form agglomerates in MFT that will settle more quickly and in appropriate conditions to form dense (dewatered) deposits that develop sufficient shear strength to be covered with reclamation material (Scott et al. 2008). New processes use beaching of flocculated tailings in thin lifts to promote faster desiccation, or the process employs centrifugation of flocculated tailings to produce a dense paste deposit with sufficient bearing strength to support a load (Mikula et al. 2009).

Flocculating and drying of MFT has been tested by several oil sands operating companies (COSIA/OSTC 2012). The method typically employs the deposition of layers of in-line flocculated MFT into drying cells where the lifts are allowed to de-water to a solids content with negative pore pressure that - under the right conditions - yields a consolidated soil that meets the specified shear strength requirements. The duration of the drying time required depends on: i) the rate of evaporation associated with the climatic conditions for each day throughout the spring, summer and fall seasons, ii) precipitation, iii) the degree of drying and associated values of total suction at the surface of the MFT for each lift, iv) the thickness of the lift, and v) the soil property functions of the MFT (i.e. Soil-water characteristic curve and hydraulic conductivity functions). Optimization of the drying operation with respect to the key cycling parameters of lift thickness and drying time requires real-time quantification of the actual rate of evaporation at the surface of the tailings, which in turn depends on atmospheric forcing conditions as well as the water content and associated total suction at the surface of the MFT as the material progresses through each evaporation cycle.

The present work investigates the potential of using remote sensing methods to develop techniques for the estimation of water content and evaporative fluxes from the optically sensed portion of the tailings surface (<a few 100μm). Hyperspectral time-series laboratory observations are collected from MFT samples that are allowed to evaporate from an initial state of water saturation to an air-dried state. From these data several spectral features are evaluated to predict water content and normalized evaporation rate. The ability to quickly measure the water content and evaporation flux of tailings surfaces from a standoff distance could allow for estimation of drying progress of treated tailings without physical sampling campaigns (which are laborious and expensive) (Lipsett et al. 2014). Simple surveying of the surface of a treated area may provide

insights into the effectiveness of tailings processes that allow decisions on scheduling the deposition of new lifts, and when placement of reclamation material can be done.

2.2 Background

Potential evaporation (PE) can be defined as the maximum rate of evaporation from a pure water surface under a given climatic condition. The term was first introduced by Thornthwaite (1948) who developed a method to calculate PE based on mean monthly temperature. The rate of evaporation from a water surface can be simply computed using the well-known Dalton's equation (Gray 1970):

(1) $$E = f(u)(e_s - e_a)$$

where E is the rate of evaporation (mm/day), $f(u)$ is the transmission function which depends on the mixing characteristics of the air above the evaporating surface, e_s is the saturation vapour pressure of water at the surface temperature (kPa), and e_a is the air vapour pressure in the atmosphere above the water surface (kPa). According to Dalton's equation, evaporation can be described by Fick's Law as a function of the difference between the vapour pressure of the evaporating surface and that of the air above it. The application of Dalton's equation to calculate the evaporation in field settings can be challenging mainly because of difficulties in: i) determining the temperature of the evaporating surface and thus the saturation vapour pressure (Gray 1970), and ii) evaluating the transmission function, which needs to be established empirically (Gray 1970) or on the basis of rigorous aerodynamic profiles and eddy diffusion similarity theory (Wilson et al. 1997). Although Dalton's equation often remains indeterminate, it

is the basis of the widely used Penman method (Penman 1948) in which the energy balance and the net radiation available to the evaporating water surface are used to resolve the difficulty associated in determining the surface temperature. Penman also presented a method based on measurement of the mean wind speed to determine the transmission function. The Penman method, however, assumes that water is always freely available to the surface and thus is applicable for the estimation of evaporation from a saturated soil surface. Accordingly, the actual evaporation (AE) from a soil surface is approximately equal to the potential evaporation from a free water surface as long as the soil is fully saturated (Penman 1948). However, as the surface begins to dry and becomes unsaturated, the Penman model becomes inaccurate in the estimation of actual evaporation due to soil suction forces.

Traditional models developed for the calculation of potential evaporation provide an overestimation of evaporation when applied to unsaturated soil surfaces, because the basic assumption in these models is that water is freely available to the surface (Morton 1985; Granger 1989a). Numerous efforts have been implemented to evaluate the actual evaporation (AE) from unsaturated soil surfaces. It has been shown that AE begins to decrease when the availability of water becomes limited and the soil is no longer saturated (Gray 1970; Morton 1975; Brutsaert 1982). Figure 2.1a shows the typical relationship between normalized evaporation (AE/PE) defined as the ratio of actual evaporation to the potential evaporation and water availability for sand and clay soil surfaces, after Holmes (1961) and Gray (1970). AE/PE equals unity for both sand and clay soils when the soil surface is saturated or the water content is high. The normalized evaporation starts to decline when water availability decreases. The behaviour of curves in Figure 2.1a is not constant for different soils; and it depends on the water availability, soil texture, and drying rate (Wilson et al. 1997). Empirical models have been developed to estimate

the evaporation from unsaturated soil surfaces (Hillel 1980; Yanful et al. 1993), because of the difficulty in determining the soil characteristics that control the evaporation from unsaturated soils.

Efforts have also been made to develop models on the basis of the soil variables that control evaporation from unsaturated soil surfaces (Barton 1979; Hammel et al. 1981; Granger 1989b; Wilson et al. 1994). Wilson et al. (1997) found that the decline in actual evaporation from unsaturated soil surfaces happens when the total suction exceeds the value of approximately 3000 kPa. As the total suction increases the evaporation decreases to reach zero. The relationship between total suction and AE/PE was found to be consistent for all the soil types and independent of water content, texture, and mineralogy, as illustrated in Figure 2.1b. According to Wilson et al. (1997), if the soil, water, and air temperature are approximately the same, then AE/PE can be computed as:

$$\frac{AE}{PE} = \left[\frac{exp\left[\frac{\psi g W_v}{RT}\right] - h_a}{1 - h_a}\right] \tag{2}$$

where ψ is total suction expressed as equivalent matric suction (head) and has a negative value (m), g is acceleration due to gravity (m/s^2), W_v is the molecular weight of water (0.018 kg/mol), R is the universal gas constant (8.314 J/(mol.K)), T is the soil temperature (K), and h_a is the relative humidity of the air. Although Eq. (2) provides a good mean to estimate AE/PE, measuring total suction and temperature of the soil surface is still required.

In general, to provide good estimates of evaporative fluxes, both climatic parameters and soil properties must be measured, which is a difficult task in field applications. Therefore, the

objective of this paper is to evaluate the potentials of remote hyperspectral technology in estimation of normalized evaporation and moisture content in which there is no need to measure soil and climatic properties. The spectral models are developed by performing evaporation tests and collecting spectral time series in the laboratory. A range of tailings samples are examined to assess the robustness of spectral estimators against the tailings composition.

2.3 Materials and Methods

2.3.1 Sample suite

A suite of 4 MFT samples was provided by a major oil sands operator in northern Alberta. The samples were characterized for Methylene Blue Index (MBI), bitumen content, solid content, and particle size distribution (PSD) (Table 2.1). MBI is an indicator of the swelling potential of the tailings and depends on the type and relative abundance of clay minerals and their total content in the sample. According to Da Silva et al. (2014), a typical MFT is predominantly comprised of approximately 40 wt% quartz, 30 wt% kaolinite, 10 wt% illite and contains traces of siderite, albite, microcline, greigite, pyrite, dolomite, calcite, tenorite, halite, rutile, and anatase. In addition, pore water of MFT contains nearly 12 (mg/L) Ca^{2+} and has a pH of approximately 8, both of which play a significant role in the dispersion and flocculation of MFT (Da Silva et al. 2014). The samples were exposed to the evaporation tests to assess the sensitivity of the spectral measurements to the sample composition. Each sample was stirred to create a homogenous mixture before conducting the experiments in April 2014, as the samples had segregated after long-term storage in their polyethylene storage containers. Air-dried condition of the samples examined is shown in Figure 2.2a.

2.3.2 Experimental approach

The experimental approach was selected to derive a prediction of MFT moisture content and AE/PE from the optically sensed portion of the tailings surface (<a few 100μm) using hyperspectral observations. The evaporation tests were conducted using the experimental setup developed by Wilson et al. (1997). Spectral time-series data were collected for MFT samples at variable moisture conditions to determine the spectral metrics of greatest sensitivity and to derive predictive models. Each evaporation test was performed using two identical circular evaporation pans (polystyrene petri dish), with 150 mm diameter, to measure AE and PE concurrently. One pan contained a thin layer of MFT to measure the actual evaporation rate (AE) and the second contained water to measure the potential evaporation rate (PE). Each container was put on a scale to continually monitor the mass change of the MFT sample and water, to determine the moisture content and actual and potential rates of evaporation.

Two identical 50 W quartz halogen lamps were used to illuminate each of the containers and thus to create an identical heat source over each container. Two thermocouples were embedded in the perimeter of each petri dish to monitor the temperature of tailings and water. Air temperature and relative humidity were also measured using a digital relative humidity and temperature sensor.

The evaporation experiments were started when tailing samples were initially saturated and continued until the samples were completely air dried. The mass and temperature of MFT and water, the temperature and relative humidity of air, and the spectra of MFT were simultaneously measured every 4 minutes, as drying took place. Each experimental trial took 2-2.5 hours. Figure 2.2b shows the experimental setup used to conduct the evaporation tests.

The MFT samples were made as thin as possible due to two reasons: 1) to minimize the effect of water content below the evaporating surface as the total suction at the soil surface controls the evaporation characteristics of AE/PE, and 2) to minimize decoupling between spectral measurements and tailings bulk properties, as the reflectance is a surface phenomenon collected from a few hundred microns in depth. Extensive effort was exerted to create a thin layer of tailings with a uniform thickness. Approximately 20 g of tailings was poured onto the petri dish and then a plastic spoon was used to gently spread the materials over the entire pan and create a thin sample of uniform thickness. Thickness uniformity was assessed qualitatively by visual inspection. The tailings were not viscous and some spreading occurred naturally.

Tailings samples with known varying degree of swelling potential (determined with MBI) and residual bitumen were tested to assess the robustness of spectral estimators against the tailings composition. Spectral features, such as reflectance and absorption depth, were derived from the collected spectral time series. Linear regression analysis was used to link the spectral features to the moisture content and the normalized evaporation. Coefficients of determination (R^2) were calculated to assess the accuracy of the spectral models. A summary of the evaporation tests is provided in Table 2.2.

2.3.3 Collection of optical measurements

Reflectance spectra of MFT surfaces were obtained using an ASD Fieldspec 3 Max spectrometer with a spectral range of 350-2500 nm, and a nominal spectral resolution of 1 nm. In this paper, however, focus was on the Short Wave Infra-Red (SWIR) region that extends from 1000 to 2500 nm.

Illumination of the sample was provided by a 50W lamp positioned at an incidence angle of approximately 20^{o}. The radiance spectrum from the sample was collected with the ASD pointing at a normal viewing angle to the sample surface and sensing a sample footprint almost equal to the petri dish diameter (150 mm). A spectrum was acquired at each time interval of 4 minutes and was the result of averaging 25 measurements, a process that took less than 3 seconds. To obtain a reflectance spectrum, the sample radiance spectrum was normalized to that of a standard white reference panel measured at the beginning of the experiment. Example reflectance spectra of the wet and dry MFT1 sample are shown in Figure 2.2c.

2.3.4 Spectral metrics evaluated

The reflectance spectra collected from the tailings samples during evaporation are affected by variations of the samples water content over time. Using the time series data (AE/PE, moisture content and reflectance spectra) different spectral metrics were compared in terms of their ability to estimate the water content and normalized evaporation of MFTs. The spectral features examined comprised reflectance values, absorption depths, and the normalized soil moisture index (NSMI) (Haubrock et al. 2008). To determine appropriate wavelengths at which to examine reflectance, a correlation analysis was performed between the reflectance at all SWIR bands and water content and normalized evaporation, taking all the samples into account. The depth of absorption features attributable to water and centered at 1450 and 1925 nm was evaluated as a potential spectral metric for moisture content and evaporation estimation. For this purpose, the depth of the absorption band at 1450 nm and at 1925 nm were calculated using the continuum removed spectra between 1375 nm and 1550 nm and 1850 and 2150 nm. Lastly this study examined the normalized soil moisture index (NSMI) suggested by Haubrock et al. (2008).

NSMI is calculated as the normalized difference of the reflectance at 1800 and 2119 nm wavelengths. This index has proven to be a good water content estimator for a range of natural soils.

2.3.5 Calculation of moisture content and AE/PE

The gravimetric water content (GWC) at each time step of the experiments was calculated by measuring the weight of the sample and comparing it to the weight of the dried solids obtained at the end of the test.

(3) $$GWC = \frac{W_{sample} - W_{solids}}{W_{sample}} . 100$$

where Wsample and Wsolids are the weight of the sample (water plus solids) and weight of dried solids, respectively. The normalized evaporation, AE/PE, was calculated using the changes in mass of the tailings and water measured at each time interval.

2.4 Results

2.4.1 Behaviour of water content and AE/PE over time

Figures 2.3a and 2.3b show the moisture content and AE/PE with respect to time for all samples tested in this study. The offset between the behaviour of MFT1 and other samples is due to the lower initial water content of this sample.

The behaviour of curves shown in Figure 2.3b is similar to those shown in Figure 2.1a given by Holmes (1961), except that AE/PE has been plotted as a function of time rather than

water availability. According to Holmes (1961), when the soil is saturated or the water content is high, the AE is equal to PE and thus the normalized evaporation (i.e. AE/PE) equals unity for the clay and sand soils. For the samples tested in this study, however, the normalized evaporation is greater or less than unity as seen in Figure 2.3b. This deviation from unity is mainly attributed to decoupling between the water and soil temperature as the aerodynamic condition above the water and tailings containers was the same during each experiments. Knowing the temperature of the tailing and water, the potential evaporation can be corrected and thus the normalized evaporation. The potential evaporation is adjusted using the tailings temperature (i.e. the potential rate of evaporation is calculated at the tailings temperature using the Dalton's equation). Nevertheless, due to the bias existing between the actual tailings temperature and its temperature measured by the thermocouples, it was not possible to correct the normalized evaporation using the tailings temperature. This temperature discrepancy is due to embedding the thermocouple in the perimeter of the tailings container so that it is not seen by the spectrometer sensor. The tailings temperature measured with the thermocouple is thus not fully representative of the average temperature of the entire sample. Therefore, to correct the normalized evaporation for each curve, the average of the AE/PE was calculated before the AE/PE starts to decline from its constant behaviour and all the data values were divided by this average value. Figure 2.3c shows the corrected normalized evaporation versus time. AE/PE is approximately unity for all the samples at the start of the evaporation tests. These corrected normalized evaporation values were then used for further analysis.

2.4.2 Relationship between AE/PE and water content

The AE/PE versus gravimetric water content is shown in Figure 2.3d. All the curves show a similar behaviour and one comparable to that shown in Figure 2.1a by Holmes (1961). When the water content is high, all the samples continue to evaporate at a near potential rate and then start to decline as the availability of water is decreased. The normalized evaporation reaches zero when each sample becomes air dried. For all samples examined in this study, the normalized evaporation declines at a water content of approximately 30 wt%. This drop in evaporation at a water content of 30 wt% is in close agreement with the results obtained by Wilson et al. (1997) for Regina Clay samples. The slight variation in behaviour between the samples is attributed to the variations in the composition and thickness of the samples, as well as relative humidity of the air at the time of each experiment.

2.4.3 Relationship between spectral features and water content

2.4.3.1 Reflectance

The correlation coefficient between water content and reflectance for each SWIR wavelength is shown in Figure 2.4a. In general, reflectance in the SWIR has a high negative correlation with water content. The highest correlation was observed at 1985 nm. Plots of water content versus reflectance at 1985 nm for all the samples are shown in Figure 2.4b. The behavior of the 1985 nm reflectance above approximately 30 wt% water content is significantly affected by specular reflection where water is present within the field of view. Below 30 wt% moisture content, the data define two groups formed by MFT samples 1 & 3 and samples 2 & 4. The separation between these groups appears to be mainly due to non-uniform drying patterns rather than the composition of the samples. The effects of specular reflection and non-uniform drying

patterns on the reflectance spectra are expanded upon in the Discussion section. Although MFT samples 1 & 3 show almost the same behaviour below 30 wt%, MFT3 shows a lower reflectance than MFT1 below 10 wt% water content because of its higher bitumen concentration. It can be concluded that when the sample is wet (nominally above 10 wt% moisture content), the impact of bitumen on the reflectance is insignificant; but it lowers the reflectance when the sample surface dries (below ~10 wt% water content). Also, it is observed that below approximately 5 wt% moisture content, the behavior of the reflectance at 1985 nm is nonlinear. This reflects the progressive loss of sensitivity of the spectral measurement to the dehydration process when the surface is dry. Deeper parts of the sample likely then loose moisture due to the progressive development of fractures. If one were to use the reflectance at 1985 nm for imagery acquired outdoors (e.g. tailings illuminated by sunlight), the presence of water vapor in the intervening atmosphere would severely impact the quality of the spectral measurements. Consequently, the reflectance at 2205 nm was also examined (Figure 2.4c) as it is minimally impacted by atmospheric effects. As can be seen in Figure 2.4c, the behaviour of graphs is similar to the 1985 nm reflectance except for having a smaller range of variation (0.1 to 0.3 compared to 0.05 to 0.33 in case of 1985 nm reflectance). Because the variation of both the 1985 nm and 2205 nm reflectance above 30 wt% water content is affected by specular reflection from the water surface, the potential of these spectral features was evaluated only below 30 wt%. To account for the nonlinear behavior of the reflectance at 1985 nm and 2205 nm below 5 wt% moisture content, second-order polynomials were employed to fit the data. R^2 values of 0.95 and 0.94 were achieved for reflectance at 1985 nm and 2205 nm, respectively. Although both these features are of value for the estimation of water content in the laboratory, only the reflectance of 2205 nm is of value for outdoor scenarios due to its robustness against atmospheric conditions.

2.4.3.2 Absorption depth

Figures 2.4d and 2.4e show the changes in absorption depths at 1450 nm and 1925 nm with respect to water content for each sample, respectively. Both of these features appear to be sensitive to the changes in water content for the entire moisture regime, with a slight decline in sensitivity of 1450 nm depth below 8 wt% moisture content. The absorption depth at 1925 nm, however, shows a higher range of variation than the 1450 nm band depth. The range of variation for the 1925 nm depth is roughly from 0 to 0.7 compared to 0 to 0.35 in case of 1450 nm depth. Similar to reflectance at 1985 nm, samples form two populations in 1925 nm absorption depth attributed to the non-uniform dehydration. The 1450 nm absorption depth, on the other hand, seems to be more robust against the pattern of dehydration (Figure 2.4d). In general, both features are insensitive to the tailings composition including bitumen. R^2 values of 0.96 and 0.95 were obtained by fitting a second-order polynomial considering the entire set of data points for 1450 nm and 1925 nm absorption features, respectively. Such a polynomial accounts for the changes in the data patterns as the sample goes from encompassing standing water to losing standing water at a moisture content of approximately 40 wt%. This pattern is observed for the band depth at 1450 nm, 1925 nm and the NSMI results of the next section.

Although there is a strong correlation between the absorption bands at 1450 nm and 1925 nm and water content, both spectral regions would be of diminished value for the analysis of imagery acquired outdoors due to the strong absorption of sunlight by water vapor in the intervening atmosphere.

2.4.3.3 NSMI

The relationship between NSMI and water content for each tailings sample is shown in Figure 2.4f. The data shown in this figure suggest that NSMI shows a good level of robustness against tailings composition. Furthermore, it is sensitive to the variation in water content for the entire moisture regime. R^2 of 0.97 was achieved by fitting a second-order polynomial to the data. This high R^2 value and the fact that this index is not affected by the atmosphere make NSMI an appropriate water content estimator in field condition.

2.4.4 Relationship between spectral features and AE/PE

Since for all the tailings samples examined, the AE/PE was approximately unity above 30 wt% water content, the relationship between spectral features and AE/PE was evaluated below this moisture level.

2.4.4.1 Reflectance

A correlation analysis was performed between AE/PE and the reflectance at SWIR wavelengths, as shown in Figure 2.5a. Although reflectance in the SWIR generally has a high correlation with AE/PE, the highest correlation value was observed at 1920 nm. Since 1920 nm is located at the centre of the water absorption band, reflectance at 2205 nm was also examined. Figures 2.5b and 2.5c show plots of AE/PE versus reflectance at 1920 nm and 2205 nm for all the samples, respectively. Both features show a similar pattern with respect to AE/PE; the reflectance increases with decreasing evaporation. The reflectance at 2205 nm, however, shows a less range of variation than the 1920 nm. The range of variation for the 2205 nm reflectance is roughly from 0.15 to 0.29 compared to 0.1 to 0.32 in case of 1920 nm. Both features show a

good level of robustness against the tailings composition. However, it seems that reflectance at 2205 nm is more affected by bitumen concentration. The sample MFT3 shows generally a lower reflectance at 2205 nm than the other samples, but this behaviour is not evident in the 1920 nm diagram until the evaporation regime of less than 0.1. The behaviour can be explained by the presence of more bitumen in sample MFT3. Since both the 1920 nm and 2205 nm reflectance values showed a nonlinear trend with respect to the AE/PE, second-order polynomials were employed for model development. This nonlinear behaviour (also observed in sections below) is presumably associated with the nonlinear relationship between AE/PE and total suction (Figure 2.1b). R^2 of 0.97 and 0.95 were obtained for the reflectance at 1920 nm and 2205 nm, respectively. R^2 values of greater than 0.9 indicate that reflectance can be considered to be capable of measuring normalized evaporation from oil sands tailings. Atmospheric effect is, however, an obstacle for the use of 1920 nm reflectance under the field conditions.

2.4.4.2 Absorption depth

The changes in band depths at 1450 nm and 1925 nm with changes in AE/PE are shown in Figures 2.5d and 2.5e, respectively. In both cases, the depth decreases with decreasing evaporation. For the absorption depth at 1450 nm, the sensitivity of the feature is lost below an AE/PE value of 0.4, a behavior that is not observed for the absorption depth at 1925 nm. As can be seen in Figures 2.5d and 2.5e, these absorption depths are not sensitive to the composition of tailings. Moreover, the absorption depths appear not to be affected by bitumen concentration as the sample with more bitumen content (MFT3) does not show a distinct behaviour. Second-order polynomials were used to model the variations of evaporation with variation of absorption depths at 1450 nm and 1925 nm. R^2 values of 0.94 and 0.96 were calculated for the 1450 nm and 1925

nm absorption depths, respectively. Although these spectral features are successful in prediction of evaporation from the tailings surface under the laboratory conditions, they are not applicable on the spectral data collected in the field due to the effect of the atmosphere on these absorption bands.

2.4.4.3 NSMI

The values of NSMI were calculated and plotted for all the samples examined. Figure 2.5f shows the relationship between the NSMI and normalized evaporation. Between AE/PE evaporation rates of 0.2 to 0.8, this index seems to be insensitive to the tailings composition. However, above 0.8 and below 0.2 evaporation rate, the index starts to show some variations. In particular, when the rate of evaporation is very low (below 0.1), NSMI appears to be sensitive to the samples composition including the bitumen concentration. An R^2 value of 0.95 was achieved by fitting a second-order polynomial to the data. As the NSMI is not affected by the atmospheric conditions, it can be a good estimator of normalized evaporation (AE/PE) when using the field data.

2.5 Discussion

2.5.1 Field applications

The predictive models developed in this study are intended to apply to hyperspectral data acquired in field settings by imaging the MFT tailings and sensing the top few hundred microns of the surface. Thus, the spectral sensing is able to estimate moisture content and AE/PE from the very top surface of the tailings. This is valuable information for tailings management and could help to assess when the deposit has stopped drying at the surface as part of a decision

process to determine when the next lift should be deposited. In addition, the moisture content and normalized evaporation at the surface can contribute to the estimation of the water profile under the surface using empirical models, a topic of future research.

2.5.2 Estimation of total suction at the tailings surface

The results of this study demonstrate the capability of remote hyperspectral technology for the estimation of normalized evaporation. Since there exists a relationship between the normalized evaporation and the total suction (i.e. matric suction plus osmotic suction) as described by Wilson et al (1997) that is independent of water content and soil composition, one can estimate the total suction for the top few hundreds of microns of the surface by measuring the normalized evaporation from hyperspectral observations. According to Eq. (2), to measure the total suction, it is required to measure the normalized evaporation, the surface temperature of the soil, and the relative humidity of the air. The normalized evaporation can be estimated using the hyperspectral data as presented in this study. Long Wave Infra-Red (LWIR) hyperspectral data, on the other hand, can be used to estimate the surface temperature of the soil in field applications. Therefore, by employing the SWIR and LWIR hyperspectral technology, measuring the total suction of the surface in field applications is feasible.

2.5.3 Effect of specular reflection

The behaviour of the 1985 nm and 2205 nm reflectance with varying water content in the high moisture regime (approximately above 20 wt% moisture content) appeared to be counterintuitive. As can be seen in Figures 2.4b and 2.4c the initial decrease in water content results in an increase in reflectance as expected. But a peak in reflectance is then observed

nominally around 40 wt% moisture content where reflectance is higher than expected (a hump in the curves). The expected pattern in reflectance resumes at lower moisture content (e.g. 20-30 wt%). Our investigations revealed that this unexpected behaviour is attributable to the contribution of specular (e.g. mirror like) reflections from the water surface in domains of the sample undergoing the onset surface exposure from the water film. It is an ephemeral phenomenon that disappears as the sample dries. This phenomenon was documented using a series of photos (Figure 2.6) taken at a normal view to the MFT sample (the same position as the sensor) during a dehydration experiment. As can be seen in these photos, the sample surface is initially covered by a continuous water film that progressively thins. The photo at 50.4 wt% water content displays the first evidence of specular reflection (areas with very high reflection) in the left part of the sample. The presence of these reflections are attributed to the formation of surface microtopography as drying occurs that provided localized mirror like bright returns. Their extent increases in subsequent photos for lower moisture content but they clearly have begun to wane for the photo at 39.1 wt% moisture content as standing water has largely disappeared. This phenomenon is the cause for the observed increase in the reflectance at 1985 nm and 2205 nm, as the water content decreases to approximately 20-30 wt% moisture regime.

2.5.4 Effect of non-uniform drying pattern

It was observed during the experiments that non-uniform drying pattern of the samples introduces variability in spectral measurements. The non-uniform drying pattern on the sample surface is mainly attributed to non-uniform sample thickness and illumination. Although the footprint of the spectrometer was adjusted to cover the whole sample area, it was observed that the central part in the field of view contributes more to the final spectra collected than the edge.

As a result, for instance, a sample at certain moisture content with wet central part shows a lower reflectance and deeper water absorption band than a sample at the same moisture content with dry central part. Figure 2.7 shows all the samples examined in the evaporation tests at 20 wt% moisture content. The central part of MFT samples 2 & 4 is wetter than the central part of MFT samples 1 & 3, resulting in a lower reflectance and deeper water absorption depth at 20 wt% moisture content. This explains the offset between the behaviour of the MFT samples 1 & 3 and MFT samples 2 & 4 in Figure 2.4.

2.5.5 Stability assessment of the spectrometer

A test performed in the laboratory to assess the stability of the ASD instrument showed that by warming up the instrument for about 2 hours, the instrument would be stable enough and there is therefore no need to measure the white panel frequently during the experiment. Thus, normalization of each measurement to that of a standard white reference panel for calculation of reflectance was only conducted at the beginning of each experiment. It should be noted that measuring the white panel during the experiment could introduce errors in measuring the actual evaporation rate as the tailing container needed to be replaced by the panel in order to measure the white reference panel spectrum. This disturbance could cause fluctuations in the rate of evaporation.

2.6 Conclusions

This paper investigated the use of SWIR hyperspectral remote sensing data for estimating the moisture content and normalized evaporation of oil sands soft tailings surfaces. Measurements of the moisture content and the exchange of water between the soil surface and

the atmosphere are of importance for many geotechnical problems. In the case of tailings management, the remote estimation of moisture content and evaporation helps to assess the drying process, to determine when the deposit has stopped drying and to decide when the next lift should be deposited.

All SWIR spectral features examined were of value for the estimation of water content and normalized evaporation of the MFTs. For the estimation of moisture content, the best result was achieved using the NSMI index ($R^2 = 0.97$). The reflectance at 1920 nm was found to be the best spectral estimator of normalized evaporation ($R^2 = 0.97$) with the NSMI index also being of value ($R^2 = 0.95$). However, NSMI appears to be sensitive to the sample composition including the bitumen concentration when the evaporation rate is very low. In both instances the NSMI index may be of value for estimations in the field while the reflectance at 1920nm may not due to its sensitivity to atmospheric conditions.

The samples examined in this study were obtained from a single mine and were processed using the same tailings operation technology. Future work could incorporate samples from different mines and tailings process to assess the robustness of our findings to tailings composition. The long term goal is to develop a new tool to monitor moisture content and evaporation over a wide range of tailings and generate real-time maps of tailings properties. In future efforts, the models obtained from this laboratory investigation will be assessed for their applicability in field settings and validated using concurrent sampling. Developing such a remote mapping capability offers a key enabling technology to assess key characteristics of tailing deposits as a supplement to standard geotechnical testing and sampling campaigns.

Acknowledgments

The authors would like to acknowledge the Institute for Oil Sands Innovation (IOSI) at the University of Alberta, the Canada's Oil Sands Innovation Alliance (COSIA), and Shell Canada for their support of this research.

Table 2.1 Characteristics of MFT samples examined.

Sample No.	Solids (wt%)	Bitumen (wt%)	MBI (meq/100g)	PSD (wt%)		
				< 2 µm	< 44 µm	< 74 µm
MFT1	52.16	3.5	2.3	8.90	70.83	83.23
MFT2	46.55	4.0	2.3	9.97	71.65	83.53
MFT3	44.66	4.3	3.5	10.71	82.78	91.53
MFT4	47.96	3.3	3.4	8.39	72.09	83.59

Table 2.2 Summary of key evaporation test parameters.

Sample No.	Initial water content (wt%)	Test duration (min)	Mean room air temperature (^{o}C)	Mean relative humidity of air (%)
MFT1	47.84	108	23.25	22.5
MFT2	53.45	136	24.10	21.4
MFT3	55.34	120	24.30	21.9
MFT4	52.04	140	23.20	35.3

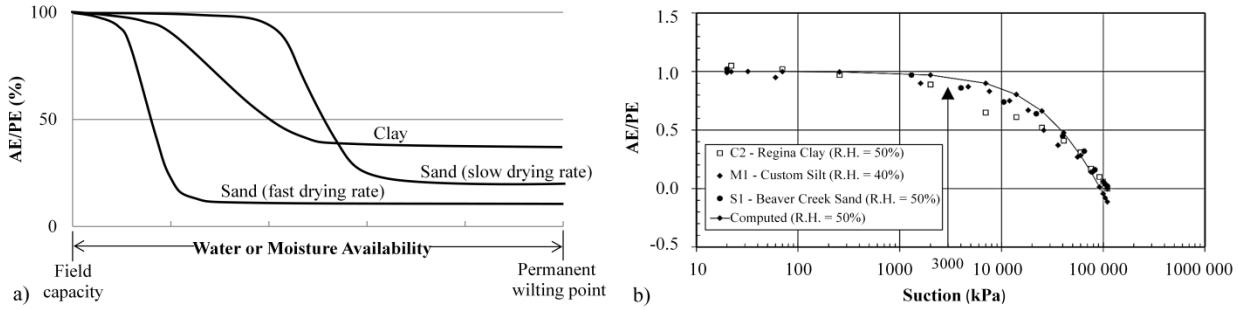

Figure 2.1 (a) Relationship between normalized evaporation (AE/PE) and water availability (after Holmes 1961). (b) Relationship between normalized evaporation (AE/PE) and suction (Wilson et al. 1997).

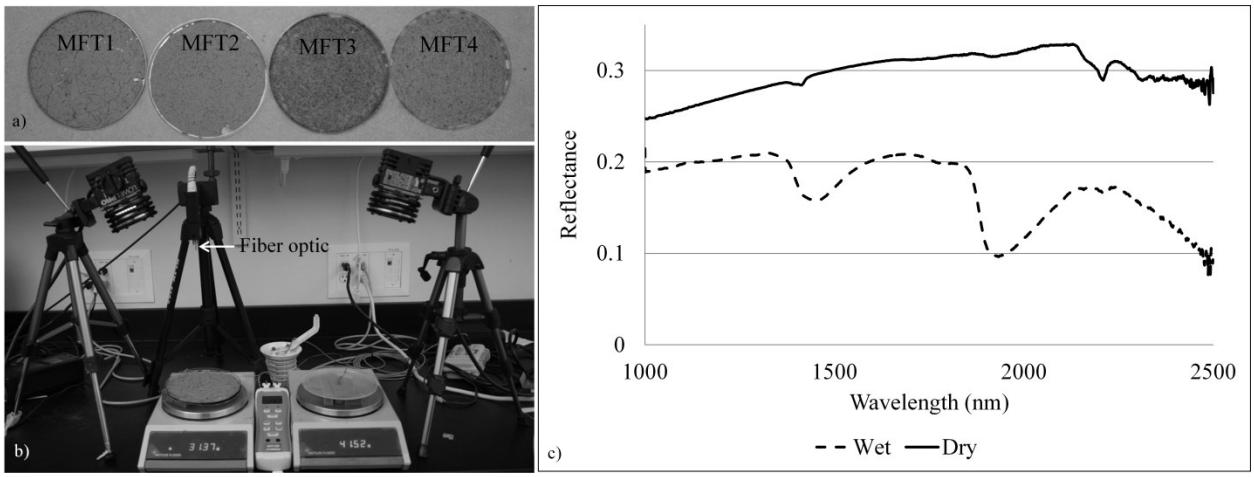

Figure 2.2 (a) Photographs of air-dried samples (b) Experimental setup. Left petri dish contains MFT and right one contains water. (c) Reflectance spectra of dry and wet MFT1.

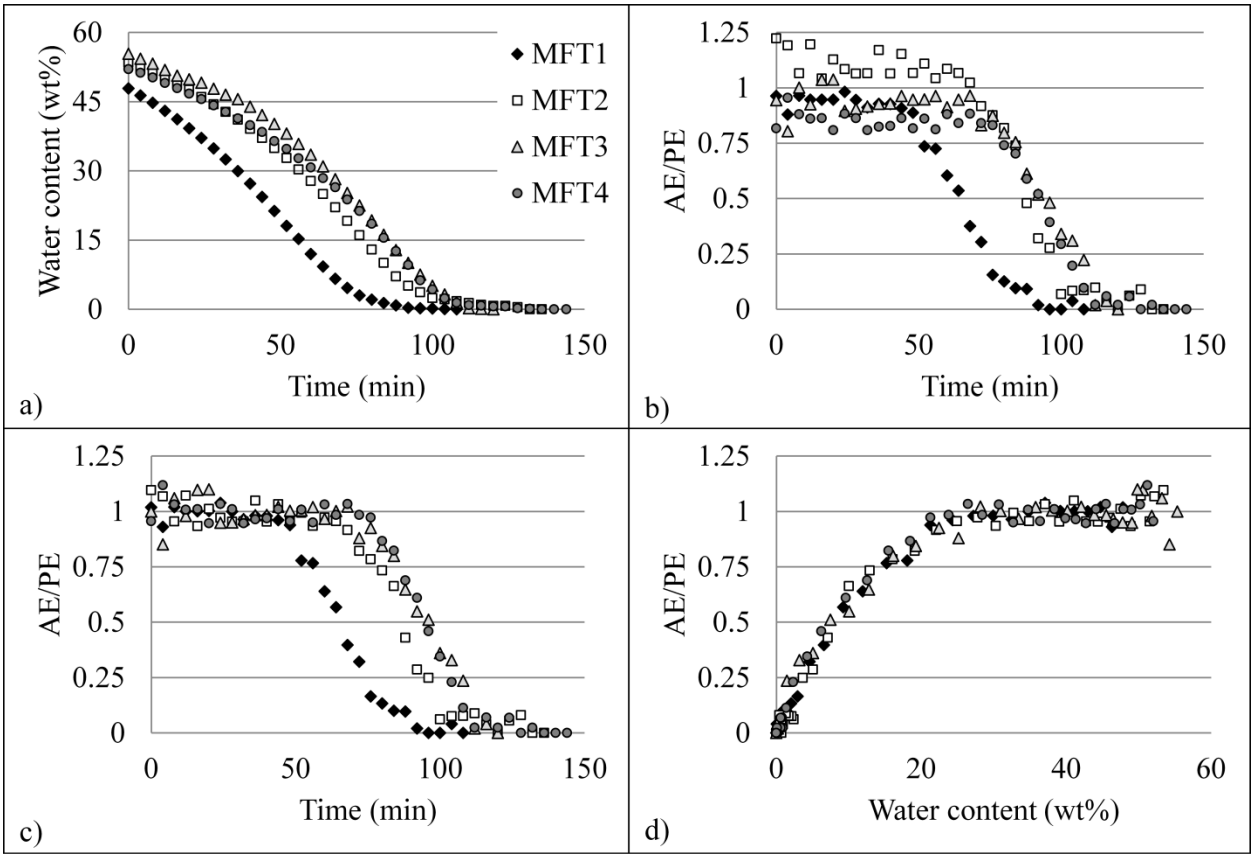

Figure 2.3 Water content and evaporation results: (a) Water content versus time. (b) Normalized evaporation (AE/PE) versus time. (c) Corrected normalized evaporation (AE/PE) versus time. (d) Normalized evaporation (AE/PE) versus water content.

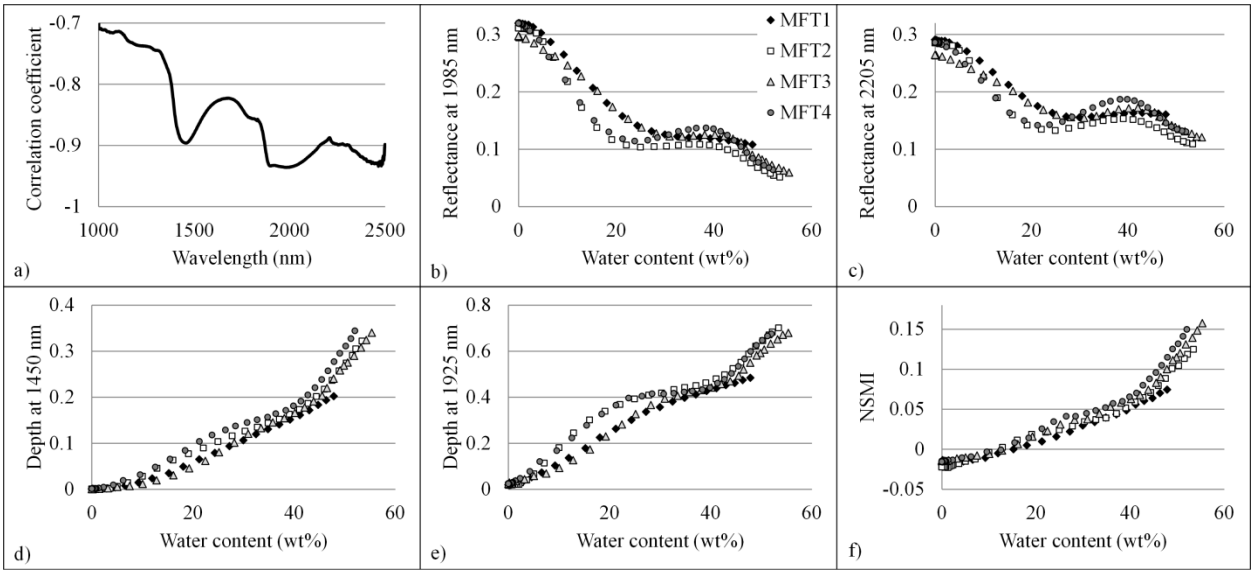

Figure 2.4 Reflectance spectroscopy results: (a) Correlation coefficient between reflectance and water content as a function of wavelength. (b) Reflectance at 1985 nm versus water content. (c) Reflectance at 2205 nm versus water content. (d) Absorption depth at 1450 nm versus water content. (e) Absorption depth at 1925 nm versus water content. (f) NSMI versus water content.

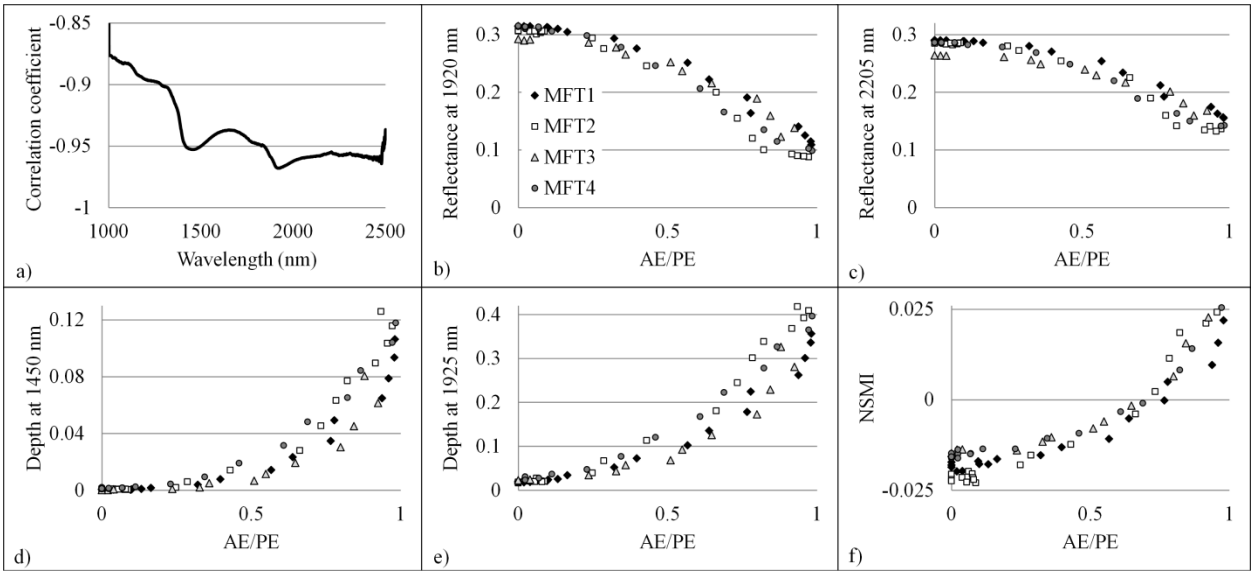

Figure 2.5 Relationship of spectral metrics to AE/PE: (a) for correlation coefficient of reflectance as a function of wavelength. (b) for reflectance at 1920 nm. (c) for reflectance at 2205 nm. (d) for absorption depth at 1450 nm. (e) for absorption depth at 1450 nm. (f) for NSMI.

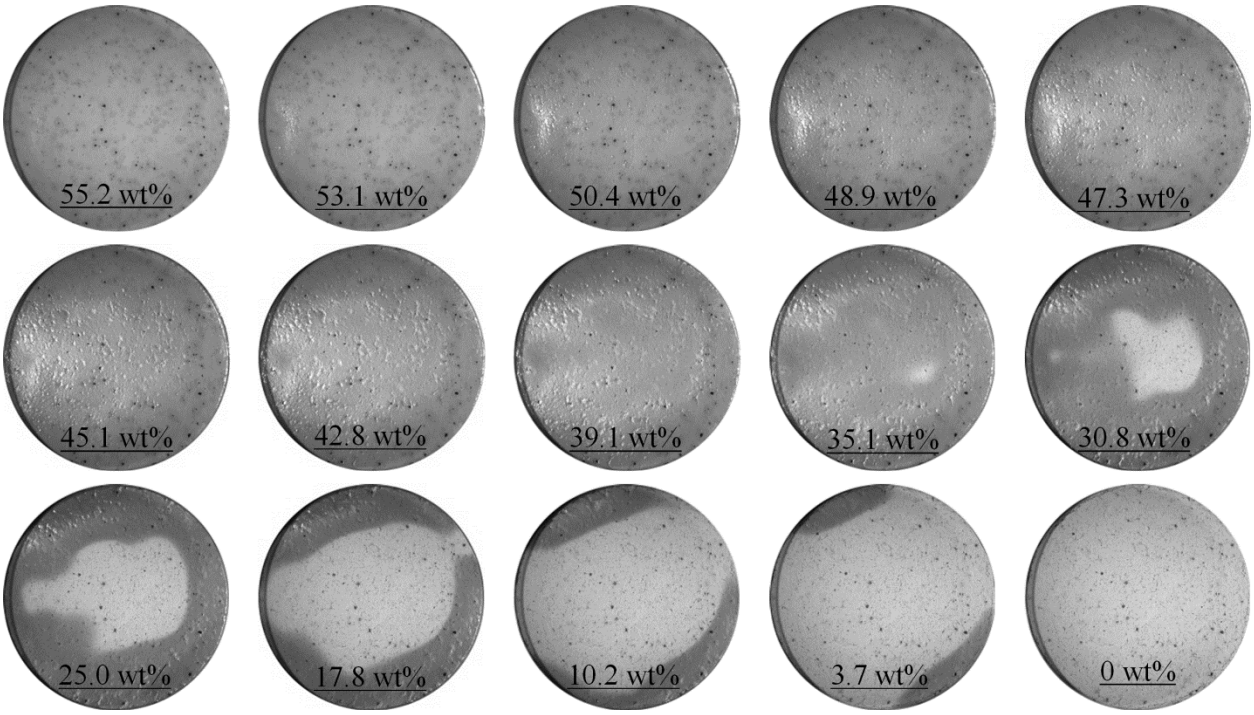

Figure 2.6 Photographs of the MFT sample during a dehydration experiment showing formation and disappearance of the specular reflection.

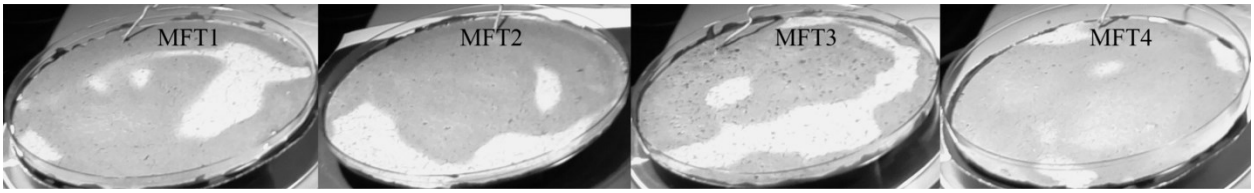

Figure 2.7 Photographs of samples at 20 wt% moisture content.

References

Alberta Energy, 2014. Alberta's oil sands: the facts. Government of Alberta, Edmonton, Alberta, Canada.

Barton, I.J., 1979. A parameterization of the evaporation from non-saturated surfaces. Journal of Applied Meteorology 18: 43–47.

BGC Engineering Inc., 2010. Oil sands tailings technology review. Oil Sands Research and Information Network, University of Alberta, School of Energy and the Environment, Edmonton, Alberta. OSRIN Report No. TR-1. 136 pp.

Boratynec, D.J., Chalaturnyk, R.J. and Scott, J.D., 1998. Experimental and fundamental factors affecting the water release rates of CT. *In* Proceedings of the 51st Canadian Geotechnical Conference, Edmonton, Alberta, Canada, 4-7 October 1998, pp. 607-614.

Brutsaert, W.H., 1982. Evaporation into the atmosphere: theory, history and applications. P. Reidel Publishing Company, Dordrecht, The Netherlands.

COSIA/OSTC, 2012. Technical guide for fluid fine tailings management.

Da Silva, F., Graham, M., Scott, J.D., and Wilson, G.W., 2014. Evaluation of a new treatment technology for improving oil sands tailings management. *In* Proceedings of GeoRegina 2014, Regina, Saskatchewan, Canada, September 28 - October 1, 2014.

FTFC (Fine Tailings Fundamentals Consortium), 1995. Advances in oil sands tailings research. Alberta Department of Energy, Oil Sands and Research Division, Edmonton, Canada.

Granger, R.J. 1989a. An examination of the concept of potential evaporation. Journal of Hydrology 111: 9–19.

Granger, R.J. 1989b. Evaporation from natural non-saturated surfaces. Journal of Hydrology 111: 21–29.

Gray, D.M., 1970. Handbook on the principals of hydrology. Canadian National Committee for the International Hydrological Decade, National Research Council of Canada, Ottawa, Canada.

Hammel, J.E., Papendick, R.I., and Campbell, G.S., 1981. Fallow tillage effects on evaporation and seedzone water content in a dry summer climate. Soil Science Society of America Journal 45: 1016–1022.

Haubrock, S.N., Chabrillat, S., Lemmintz, C., and Kaufmann, H., 2008. Surface soil moisture quantification models from reflectance data under field condition. International Journal of Remote Sensing 29(1): 3-39.

Hillel, D., 1980. Applications of soil physics. Academic Press, New York.

Holmes, R.M. 1961. Estimation of soil moisture content using evaporation data. *In* Proceedings of Hydrology Symposium, No. 2 Evaporation. Queen's Printer, Ottawa, pp. 184–196.

Kasperski, K.L., 1992. A review of properties and treatment of oil sands tailings. AOSTRA Journal of Research 8: 11-15.

Lipsett, M.G., Olmedo, N., Rivard, B., and Wilson, W., 2014. Robotic systems for measuring properties of tailings deposits and collecting samples. Proceedings of Fourth International Oil Sands Tailings Conference (IOSTC 2014), Lake Louise, AB, Canada, 7-10 December 2014, pp. 483-491.

MacKinnon, M.D., 1989. Development of the tailings pond at Syncrude's oil sands plant: 1978–1987. AOSTRA Journal of Research 5: 109–33.

Mikula, R.J., Munoz, V.A., and Omotoso, O., 2009. Centrifugation options for production of dry stackable tailings in surface mined oil sands tailings management. Journal of Canadian Petroleum Technology 48(9): 19-23.

Morton, F.I., 1975. Estimating evaporation and transpiration from climatological observations. Journal of Applied Meteorology 14(4): 488-497.

Morton, F.I., 1985. The complementary relationship areal evapotranspiration model: How it works. Proceedings of the National Conference on Advances in Evapotranspiration, American Society of Agricultural Engineers, Chicago, Illinois, pp. 377–384.

National Energy Board, 2004. Canada's Oil Sands: opportunities and challenges to 2015 [Pamphlet], Calgary, AB.

Penman, H.L., 1948. Natural evapotranspiration from open water, bare soil and grass. Proceedings of the Royal Society of London, Series A, 193: 120-145.

Scott, J.D., Jeeravipoolvarn, S., Donahue, R. and Ozum, B., 2008. Characterization of oil sands thickened tailings. *In* Proceedings of First International Oil Sands Tailings Conference, Edmonton, Alberta, Canada, 7-10 December 2008, pp. 132-142.

Thornthwaite, C.W., 1948. An approach toward a rational classification of climate. Geographical Review 38: 55-94.

Wilson, G.W., Fredlund, D.G., and Barbour, S.L., 1994. Coupled soil–atmosphere modeling for soil evaporation. Canadian Geotechnical Journal 31: 151–161.

Wilson, G.W., Fredlund, D.G., and Barbour, S.L., 1997. The effect of soil suction on evaporative fluxes from soil surface. Canadian Geotechnical Journal 34: 145-155.

Yanful, E.K., Bell, A.V., and Woyshner, M.R., 1993. Design of a composite soil cover for an experimental waste rock pile near Newcastle, New Brunswick, Canada. Canadian Geotechnical Journal 30: 578–587.

Chapter 3 Estimation of Methylene Blue Index in Oil Sands Tailings Using Hyperspectral Data

3.1 Introduction

Canada's oil sands deposits in northern Alberta represent the third largest proven reserves of oil in the world, with established reserves estimated at 28.3 billion cubic meters (National Energy Board 2004). Oil sands are natural mixtures of inorganic materials (primarily quartz sands and clays), bitumen, and water (Kasperski 2001). The bitumen is extracted either through open-pit mining methods or in-situ production techniques. Open-pit mining is applicable for the deposits at a depth of less than approximately 75 meters (National Energy Board 2004), while in-situ methods are used to extract bitumen from deeper deposits. In surface mining, the bitumen is recovered through the general method developed by Karl Clark (Clark and Pasternack 1932), in which the oil sands ore is mixed with hot water and sodium hydroxide, which generates surfactants that promote aeration of the bitumen, after which the resulting slurry is sent to a separation plant for bitumen flotation and treatment to remove water and fine solids from the froth. Ultimately, large volumes of oil sands tailings are produced during open-pit mining. Tailings comprise water with quartz sand, silt, clay, and residual bitumen. There may also be some solvent from the froth treatment process. The tailings are discharged to settling basins, where the coarse sand particles quickly settle to the bottom; but the fine particles (mainly clays) settle slowly and form a saturated mixure of approximately 30 wt% percent solids, which is referred to as fluid fine tailings (FFT). Such FFT cannot be reclaimed and revegetated due to its poor water release and consolidation rate. The separation of water from FFT is thus an operational and environmental challenge of tailings management.

The surface properties of the tailings minerals control the water holding capacity and thus the rate of consolidation of the tailings (Kotlyar et al. 1992). Among the minerals present, clay minerals, which could be inert (e.g. illite, kaolinite, and chlorite) or active (e.g. smectite and vermiculite), constitute a significant fraction of the tailings fine solids. Many studies have shown that kaolinite and illite are dominant clays in the Athabasca oil sands ores and tailings (Kessick 1979; Kotlyar et al. 1995; Mercier et al. 2008). However, other clays including smectite, chlorite, vermiculite and mixed-layer clays such as kaolinite-smectite and illite-smectite have also been observed (Yong and Sethi 1978; Scott et al. 1985; Omotoso and Mikula 2004; Omotoso et al. 2006, Kaminsky 2008). Heavy minerals such as rutile are present in small quantities. Oil sands ore is heterogeneous, and so there is variability in the relative abundance of different clays and their particle size distributions. Estimation of the activity or swelling potential of clays is of great importance for the management of tailings. Swelling potential generally refers to the ability of clays to undergo a large change in volume in the presence of water. The activity of clays significantly affects the settling and consolidation of FFT (Omotoso and Mikula 2004) and the geotechnical stability of a final tailings deposit for reclamation purposes. In addition, the effectiveness of many polymer-based technologies, developed to reduce FFT inventories, depends on the type and abundance of clay minerals (Omotoso and Mikula 2004; Omotoso et al. 2006; Kaminsky et al. 2009; Kaminsky 2014).

A number of swelling potential indices have been introduced to estimate the activity of soils, including Atterberg limits, coefficient of linear extensibility (COLE), cation exchange capacity (CEC), and methylene blue index (MBI). MBI is the most commonly used index to indicate the activity of clays in the ore, froth, and tailings of oil sands. MBI quantifies the CEC of a sample by measuring the amount of methylene blue cations required to cover the total

available surface of the anionic clay particles present in the sample of ore that has had the bitumen and connate water removed so that only solid material remains.

Several studies have examined the effectiveness of reflectance spectroscopy for the detection of swelling clays and for the determination of engineering parameters of expansive soils (Van der Meer 1999; Goetz et al. 2001; Chabrillat et al. 2002; Kariuki et al. 2003, 2004; Shouxun and Jin 2004; Yitagesu et al. 2009, 2012). Depending on the instrument used, spectral measurements collect radiation in the visible, short-wave infrared (SWIR) and long-wave infrared (LWIR) portions of the electromagnetic spectrum, in which unique features about the measured object are revealed. The spectral response from each material is wavelength dependent and is largely controlled by the chemical composition and crystal structure of the minerals and other materials. Van der Meer (1999) reported that soil mineralogy can be identified using remote sensing methods and potentially used to map swelling soils. Goetz et al. (2001) developed techniques to identify clay-rich soils using field spectrometers. In this case SWIR reflectance spectra of soils were used to distinguish smectite, which swells, from illite and kaolinite. Chabrillat et al. (2002) studied the feasibility of mapping expansive soils using airborne imaging spectrometers and showed that remote sensing technology can be of practical help in the detection and mapping of swelling clays. Kariuki et al. (2003) explored the estimation of cation exchange capacity based on parameters of spectral absorption feature (position, depth, width, and asymmetry of absorption band). Shouxun and Jin (2004) analyzed the correlation between such parameters and the smectite, colloid, and clay contents of swelling soils. Also, Yitagesu et al. (2009, 2012) investigated the relationship between reflectance spectra of swelling soils in the 0.35-2.5 μm and 3-5 μm spectral regions and their engineering expansive parameters.

This study explores the applicability of remote sensing techniques for the estimation of MBI of oil sands soft tailings. We use reflectance spectra collected in the laboratory from tailings samples with known MBI and explore spectral metrics, including features attributed to clay and quartz minerals, to develop predictive models for the estimation of MBI. The sensitivity of the models to variation of moisture content in the tailings is examined to evaluate the effectiveness of the models under different moisture regimes. We also examine the applicability of models when measurements are collected in the presence of a significant atmospheric column (e.g. tens of meters) as is the case for outdoor spectral imaging of tailings ponds. As an illustration of this potential monitoring capability, we apply the MBI models developed in laboratory investigations to hyperspectral imagery acquired in the field and discuss the derived MBI map.

3.2 Materials, Measurements, and Methods

3.2.1 Sample suite, Dean-Stark and methylene blue analysis

Thirteen tailings samples were provided by an oil sands operating company. Six samples were flocculated FFT samples collected from tailings treatment cells. The remaining seven FFT samples were collected from different depths of a settling basin. All tailings samples contained residual bitumen, which was removed from the solids at a commercial laboratory using Dean-Stark soxhlet extraction to evaporate the water and oil from the solids. The Dean-Stark analysis method also provides an estimate of the total bitumen content, reported as a bulk mass fraction.

Methylene blue analysis was then conducted on each sample using the procedure described in ASTM C 870-81 (ASTM, 1992) with some modifications. In this test, the cations along the external and internal structure of the clay mineral are replaced by methylene blue cations. It is therefore a method for estimating the cation exchange capacity and surface area of

the clay minerals present in a solid mixture such as a soil. MBI results are impacted by the type and relative abundance of clay minerals and their total content in the sample. Samples with identical total clay content can display different MBI values because of variation in their clay types.

Table 3.1 lists the MBI of each FFT sample. The flocculated FFT samples showed a small range of MBI values from 2.3 to 3.5 (meq/100g solids). The non-flocculated FFT samples, on the other hand, showed a wider range of MBI values from 0.7 to 10.5 (meq/100g solids). The sample with a MBI of 10.5 was collected from the top of the settling basin and thus is enriched in fine clays. The sample with a MBI of 0.7 is a sample from deep in the settling basin. The sample contains coarse sand particles along with silt and clay, with 82% of the sample volume being of particle size greater than 45 μm.

3.2.2 Collection of spectral measurements

3.2.2.1 Sample preparation

Prior to the acquisition of spectral measurements, each sample was stirred to create a homogenous mixture and remove any effects of segregation after long-term storage. This preparatory stirring ensured that the samples were comparable to the stirred aliquots used for MBI and Dean-Stark analysis. Each sample was poured into a polystyrene petri dish with a diameter of 15 cm to a thickness of approximately 5 mm. The sample was then allowed to air-dry to remove the effect of water from the spectrum - as water significantly darkens the spectrum by occluding the surface of particles and generally reducing reflectance.

3.2.2.2 SWIR imaging

Short-wave infrared spectral imagery of the samples in the petri dishes was collected with a Specim SisuROCK imaging system. The unit contains a SWIR spectral line camera, a stage for moving the specimen past the line camera, and a set of quartz halogen lamps that illuminate the sample. The output data consist of reflectance measured from 1 to 2.5 μm at a spectral resolution of approximately 6 nm (256 spectral bands) for every 1mm pixel of the scene. From these data an average spectrum was calculated for each sample, which typically encompassed more than 60000 spectra.

3.2.2.3 LWIR point spectra

Long-wave infrared reflectance spectra were collected using a Bomem MB102 Fourier transform InfraRed (FTIR) spectrometer equipped with a Mercury/Cadmium/Telluride (MCT) detector and a globar thermal light source to illuminate the sample. As the instrument field of view on the samples in the petri dishes was approximately 1 cm in diameter, five spots were measured on each sample and the resulting spectra were averaged to produce a spectrum per sample. Each of the five measurements per sample consisted of 16 co-adds averaged to improve the signal-to-noise ratio. The data presented in this study were acquired at a spectral resolution of 4 cm^{-1} and span the 8-12 μm wavelength region (217 bands), where the Restrahlen bands (reflectance peaks) due to fundamental molecular vibrations of silicate minerals occur. Reflectance spectra were obtained by normalizing each sample measurement to that of a diffuse gold panel collected prior to each sample measurement.

3.2.2.4 Collection of spectral imagery outdoors

In order to investigate the feasibility of generating MBI maps for tailings ponds using the spectral models developed in this research, hyperspectral images were collected at a tailings structure of a mine at an oil sands operating company in northern Alberta. Flocculated tailings had been poured in the pond prior to imaging and allowed to partially dry. The imagery was collected using the SisuRock SWIR camera described above, but with natural illumination. A 99% Spectralon^{TM} white reference panel was located in the scene to enable normalization of the image measurements to reflectance.

3.2.3 Development of spectral predictive models

Several spectral features were extracted from both the SWIR and LWIR spectra of the tailings sample. Linear regression analysis was used to develop spectral models for the estimation of MBI. In the SWIR, attention was given to ratio of the reflectance at two spectral bands (that is, two different wavelengths) as a measure of the slope of the spectrum, which is affected by the mineral makeup of the sample. Ratios can enhance subtle differences amongst a suite of spectra that otherwise appear similar. We explored all band ratios from the available band set and selected the ratio yielding the highest linear correlation with MBI for the sample suite. In the LWIR, the strength of the reflectance peaks at 9.67 and 11 μm, attributed to clay minerals, were used for model development. Statistical parameters were calculated to assess the statistical significance of each model, including the coefficient of determination (R^2), the root mean square error (RMSE), and the p-value.

3.3 Results

3.3.1 SWIR spectral characteristics and ensuing predictive models

3.3.1.1 Spectral characteristics of the samples

As seen in Figure 3.1, the samples display similar reflectance spectra in the SWIR. All spectra show the overtone and combination absorption bands attributed to the hydroxyl (OH) molecule bound to octahedral cations and water bound to interlayer regions or adsorbed on clay mineral surfaces (Bishop et al. 2008). The absorption feature near 1.4 μm is attributed to water or OH overtones, while the 1.9 μm feature is a water combination band (Kruse and Hauff 1991; Bishop et al. 2008). The strong doublet feature at 2.162 μm and 2.205 μm is the characteristic Al-OH absorption band of kaolinite, which is the dominant clay fraction of oil sands tailings (Bayliss and Levinson 1976; Kasperski 1992). Additional weak absorption bands are observed from 2.3-2.5 μm and are attributed to cation-OH stretching and bending combinations; and these bands may be associated with octahedral layer cations in clay minerals (Kruse and Hauff 1991, Bishop et al. 2008).The presence of residual bitumen causes absorption features near 1.7 μm and 2.3 μm and may affect the clay absorption bands as well.

There are notable variations observed on Figure 3.1. Changes in the slope of the spectra are observed in the 1.4-2.1 μm wavelength region. In this region, the sample with lowest MBI displays the spectrum with largest slope while the lowest slope is observed for the spectrum of the sample with highest MBI. In addition, the sample with the highest MBI displays the spectrum with the deepest absorption depths at 1.414, 1.905, and 2.205 μm.

3.3.1.2 Predictive models for the estimation of MBI

From the samples examined, two spectral ratios have been identified that can be used as predictive models of MBI for oil sands tailings.

Reflectance ratio of 2.111 to 1.992 μm: The ratio with the highest correlation to MBI involved bands at 2.111 and 1.992 μm (R^2 = 0.96, Figure 3.2a). Since there was lack of samples with MBI values between 5.9-10.5 (meq/100g), a linear regression was also performed without the sample with the highest MBI value to assess the robustness of the fitted line. By excluding this sample, the R^2 value decreased to 0.89; but the equation of the regression line remained consistent. The 2.111 to 1.992 μm reflectance ratio appears to be a successful estimator of MBI for air-dried tailings samples over a relatively wide range of MBI values. If all samples are included in the regression, the RMSE is 0.47 meq/100g. The small p-value of 5.6E-09 shows the statistical significance of the results.

Variations in this reflectance ratio are likely attributed to changes in the total clay content or relative abundance of clay to quartz minerals amongst the samples. This variability is examined in more detail in the Discussion section. The reflectance ratio of 2.111 to 1.992 μm does however present limitations for its potential use in the estimation of MBI when spectral observations are collected outdoors, because the 1.9 μm water band incorporated in the ratio is affected by water vapor in the intervening atmosphere.

Reflectance ratio of 1.773 to 1.307 μm: When spectral regions impacted by atmospheric absorption bands (1.34-1.47 μm and 1.79-1.98 μm) are removed, the reflectance ratio of 1.773 to 1.307 μm was found to have the highest correlation with MBI values (Linear regression, R^2 = 0.88, Figure 3.2b). The R^2 value decreases slightly (0.87) when the sample with the highest MBI value is excluded from the regression analysis; and the slope of the fitted line changes (Figure

3.2b). The behaviour of these data is linear and the RMSE is 0.50 (meq/100g) (p-value = 9.1E-06). When the sample with highest MBI is included, the data distribution is distinctly non-linear. A second-order polynomial fitted to these data led to a significant R^2 of 0.93 and RMSE of 0.56 meq/100g, with a p-value of 4.4E-08, as shown in Figure 3.2c.

The relationship between both reflectance ratios is shown in Figure 3.2d. The high correlation observed between these two spectral metrics (R^2 = 0.91) suggests that they both capture the same sample mineralogical characteristics, likely the total clay content or relative abundance of clay to quartz in the tailings samples.

3.3.1.3 Sensitivity analysis of the models to tailings water content

The predictive models described above were developed using air-dried MFT samples. The presence of water in tailings impacts the shape and thus the slope of the resulting reflectance spectra. Here we assess the sensitivity of the linear model (excluding the sample with highest MBI) and polynomial model, developed with the reflectance ratio of 1.773 to 1.307 µm, to variations in tailings water content. For this purpose, the MBI models were applied to spectra collected during drying experiments for a subset of the tailings sample population. Samples with MBI values of 2.3, 3.5, 5.2, and 10.5 were examined. Figures 3.3a and 3.3b show the estimated MBI for these samples as a function of the water content of the samples. For moisture contents below approximately 20 wt%, results in Table 3.2 show that the variation in the MBI values estimated is less than the RMSE value of the model. The largest standard deviation of the MBI values estimated was 0.44 meq/100g for the linear model and 0.53 meq/100g for the polynomial model. These values are comparable to the RMSE of 0.5 and 0.56 meq/100g for these models. The SWIR models based on the 1.773 to 1.307 µm reflectance ratio are therefore considered to

be robust against the variation in the tailings moisture content below 20 wt%, for the samples tested. Above 20 wt% moisture regime, on the other hand, the MBI value is overestimated. Consequently, in case of field imagery, the areas on tailings ponds with less than 20 wt% moisture regimes can be detected by applying spectral models for moisture content estimation (reported elsewhere), after which the MBI models can be applied on such areas.

3.3.2 LWIR spectral characteristics and ensuing predictive models

Long-wave spectral features can also be used for MBI estimation.

3.3.2.1 Spectral characteristics of the samples

Several key Restrahlen features are observed as reflectance peaks in the long-wave spectra of oil sands tailings, shown in Figure 3.4. Quartz typically shows a strong doublet of peaks near 8.2 μm and 8.9 μm, attributed to Si-O vibrations. The reflectance peak near 8.2 μm can be attributed to quartz and the 8.9 μm peak to both quartz and clay minerals, particularly kaolinite (Schuttlefield et al. 2007). The highest MBI sample (highest overall reflectance) is the only sample to display little or no reflectance peak at 8.2 μm. The peak observed near 9.6 μm is a characteristic feature of clay minerals attributed to the stretching vibration of Si-O (Schuttlefield et al. 2007; Bishop et al. 2008). The sample with highest MBI exhibits the highest reflectance and displays a peak shifted towards shorter wavelengths compared to the other samples. A reflectance peak is also seen at 9.9 μm, which is attributable to the presence of kaolinite (Vaughan et al. 2005; Schuttlefield et al. 2007). The two reflectance peaks observed from 10.7-11 μm are attributed to Al_2OH vibrations (Bishop et al. 2008; Schuttlefield et al. 2007). Of these, the most subtle feature is reported to be near 10.7 μm. This feature is only observed in the

spectrum of kaolinite while the peak at 11 μm is seen in illite, montmorillonite, and kaolinite (although it is more pronounced for kaolinite).

3.3.2.2 Predictive models for the estimation of MBI

Two reflectance peaks were found to be useful for MBI estimation:

Reflectance peak at 9.67 μm: The reflectance peak at 9.67 μm, attributed to clay minerals, was correlated with the MBI values of the tailings samples, as shown in Figure 3.5a. Since all clay minerals exhibit this reflectance peak, the strength of this peak can be representative of the total clay content in the tailings samples. Other factors being equal, an increase in total clay content increases MBI response. As seen in Figure 3.5a with black diamond symbols, a positive linear relationship is observed between these two variables, excluding the sample with highest MBI. Inclusion of this sample requires a non-linear fit to the data. Thus two spectral models were developed using this reflectance peak. First a linear fit was applied to the data after excluding the sample with highest MBI value and a R^2 of 0.93, RMSE of 0.37 meq/100g, and p-value of 4.7E-07 were obtained. A logarithmic transformation was then applied on all reflectance values to improve the linearity of the transformed data for the linear regression analysis. As seen in Figure 3.5a with white diamond symbols, a significant R^2 value of 0.96 was achieved by linear regression analysis, with RMSE of 0.45 meq/100g, and p-value of 4E-09).

Reflectance peak 11 μm: The reflectance peak at 11 μm showed a linear relationship with MBI, as shown in Figure 3.5b. A significant R^2 value of 0.96 was found applying a linear analysis on the entire sample suite, with RMSE of 0.47 meq/100g, and p-value of 6.6E-09. The exclusion of the sample with highest MBI led to a slight decrease in the R^2 value to 0.93 and a change in the slope of the fitted line, with RMSE of 0.35 meq/100g, and p-value of 3E-07. As the

11 μm reflectance peak is mainly attributed to kaolinite content, it can be concluded that, for the sample suite tested in this study, kaolinite content increases as MBI increases. For the samples tested, there is a mostly constant 11 to 9.67 μm reflectance ratio for most of the samples, implying a constant relative abundance of kaolinite to total clay content. This would explain why capturing the variation in kaolinite through the 11 μm reflectance peak relates well to modeling of variation in MBI.

3.4 Discussion

Several points are worth noting about how mineralogy affects the slope of the SWIR spectra, and how the predictive models developed in the laboratory can be used to estimate MBI at the surface of a tailings structure.

3.4.1 Impact of mineralogy on SWIR slope of spectra

In the SWIR, the 2.111 to 1.992 μm reflectance ratio was found to have the strongest correlation with MBI. This section examines the relationship of this ratio to several spectral features attributed to quartz and clay minerals, and thus the impact of changes in mineralogy on this reflectance ratio. Figure 3.6 shows the relationships between the 2.111 to 1.992 μm reflectance ratio, reflectance peaks at 9.67 and 11 μm, reflectance ratios of 9.67 to 8.20 μm and reflectance ratios of 11 to 9.67 μm. As can be seen in Figures 3.6a and 3.6b, a negative correlation exists between the 2.111 to 1.992 μm reflectance ratio and the reflectance peaks at 9.67 μm and 11 μm, which are attributed to total clays and kaolinite, respectively. Similarly, a negative correlation is observed between this ratio and the ratio of 9.67 to 8.20 μm, which is representative of the relative abundance of total clay to quartz, as is also seen in Figure 3.6c.

These patterns imply that, as the clay content in the samples increases, the 2.111 to 1.992 μm reflectance ratio decreases. Figure 3.6d shows the relationship between this ratio and the ratio of 11 to 9.67 μm, which is representative of the relative abundance of kaolinite to total clays. There is no apparent correlation between these two spectral metrics as most of the samples show a nearly constant relative abundance of kaolinite to total clays, which is fairly representative of oil sands clay ratios in general. Thus the 2.111 to 1.992 μm reflectance ratio is most likely indicative of the total clay content or relative abundance of clay to quartz mineral; and the ratio is not controlled by the relative abundance of different clay minerals.

3.4.2 Generating MBI map using hyperspectral imagery acquired in the field

The potential monitoring capability of tailings surface characteristics was evaluated using hyperspectral imagery acquired in the field using the same SWIR camera as was used in the laboratory study, with a portable traversing mechanism on a tripod. By applying an MBI model developed using the laboratory relationships, an MBI map is generated for the observed surface of the tailings structure. Figure 3.7 shows the reflectance image at 2.205 μm and the corresponding photo for a portion of the tailings structure imaged. Also shown are type spectra extracted from the hyperspectral image in Figure 3.8, which reveal the impact of atmospheric effects around 1.4 μm and 1.9 μm. This effect of atmospheric absorption demonstrates the need for a predictive model of MBI that does not rely on these spectral regions. Figure 3.9a shows an MBI map of the tailings surface produced using the linear model based on the 1.773 to 1.307 μm reflectance ratio. As expected, this map is rather uniform in terms of its MBI; but a narrow domain of higher MBI is predicted in the center and right portion of the map. The uniformity was expected due to the fairly homogenous nature of the tailings discharged to a treatment cell,

because of the multiple mixing steps during ore blending, separation, initial deposition, and then dredging for treatment. For safety reasons, it was not possible at this stage of the study to collect samples from this tailings structure to attempt to evaluate the accuracy of the predicted MBI values. Validation of the performance of the predictive model in field settings is thus part of the scope of the future work. When the MBI map is compared to a moisture content map generated following the work of Entezari et al. (2014), one observes that the moisture map does not highlight the region of elevated MBI (Figure 3.9). One can infer that the moisture regime is below 20 wt% and reveals an MBI pattern which otherwise would be masked by variability in surface moisture as indicated in the water sensitivity analysis.

3.5 Conclusions

The methylene blue analysis technique is a standard analytical test that quantifies the surface activity of solids and thus the clay swelling potential of a sample. In this study, the relationship between MBI values of a set of oil sands tailings samples and their SWIR and LWIR spectral characteristics were studied to develop spectral models to estimate MBI. In the SWIR, the ratio of reflectance at 2.111 and 1.992 μm and the ratio of 1.773 and 1.307 μm resulted in a high correlation with MBI. The predictive model derived from the latter ratio does not include spectral regions impacted by atmospheric absorption bands (1.34-1.47 μm and 1.79-1.98 μm) and is thus better suited for analysis of spectra acquired outdoors with a standoff distance. It was also observed that the sensitivity of the 1.773 to 1.307 μm reflectance ratio to the moisture content of tailings was minimal at moisture contents below 20 wt%. A prototype test of monitoring capability of tailings surface characteristics was conducted using hyperspectral imagery acquired in the field, from which a map of predicted MBI was generated. The

preliminary results are promising, but remain to be validated, a primary challenge being the collection of samples from soft tailings. Significant results were achieved in the LWIR using the reflectance peaks at 9.67 μm and 11 μm, attributed to total clays and kaolinite, respectively. A mostly constant relative abundance of kaolinite to total clays for the sample suite examined explains why both of these clay features were successful for estimation of MBI. This research contribution has established the foundation for developing quick predictions of MBI on drying tailings based on hyperspectral observations. Such tools may contribute to monitoring of tailings surfaces based on imagery collected outdoors and to the development of more effective measures for tailings management.

Acknowledgements

The authors would like to acknowledge the Institute for Oil Sands Innovation (IOSI) at the University of Alberta and Canada's Oil Sands Innovation Alliance (COSIA) to support this research. Shell Canada Energy is also acknowledged for providing the tailings samples.

Table 3.1 MBI values measured for the tailings samples. Samples 1-6 are flocculated tailings.

Sample	1	2	3	4	5	6	7	8	9	10	11	12	13
MBI (meq/100g)	2.3	2.3	3.1	3.4	3.5	3.4	0.7	2.7	3.4	5.2	5.2	5.9	10.5

Table 3.2 Standard deviation of the MBI values estimated below 20 wt% moisture content.

	Standard Deviation	
Sample MBI	Linear model	Polynomial model
2.3	0.19	0.17
3.5	0.44	0.52
5.2	0.30	0.53
10.5	0.20	0.48

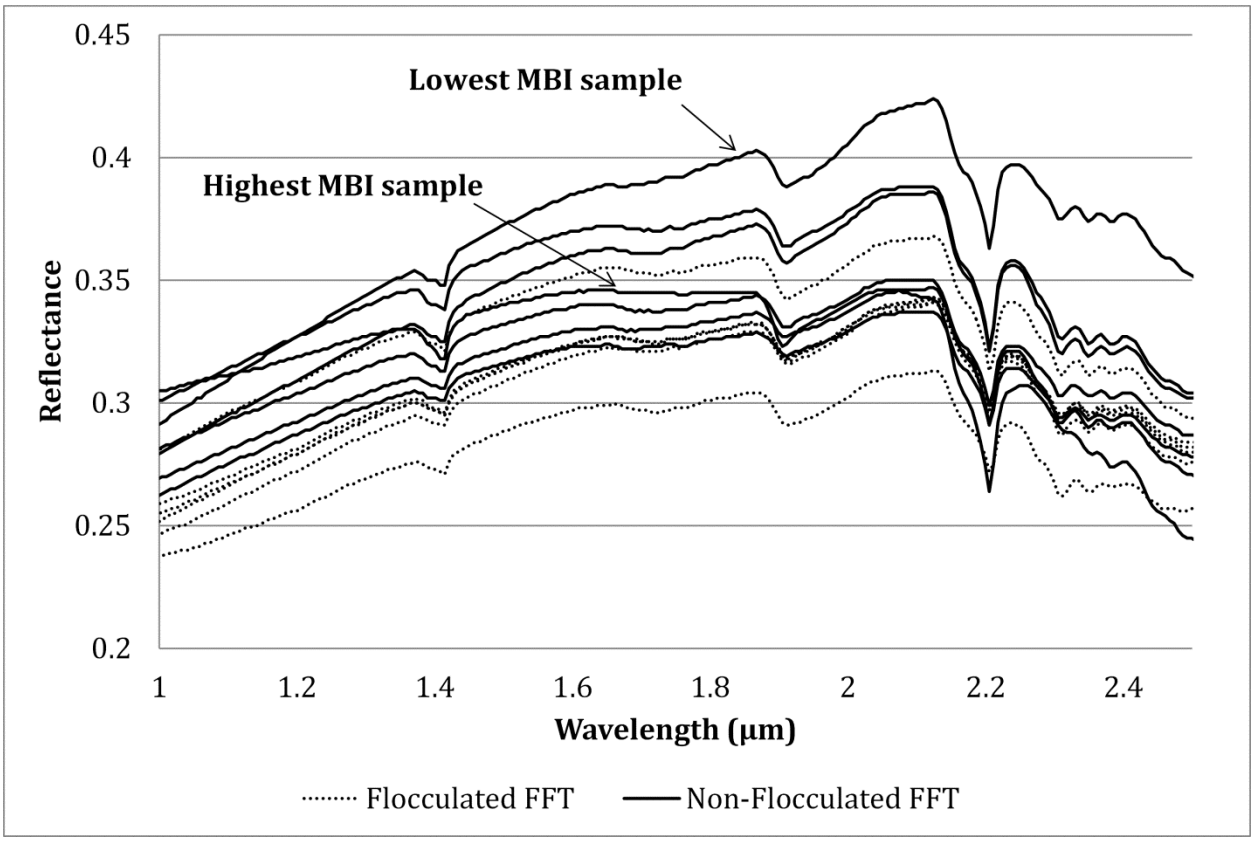

Figure 3.1 Average reflectance spectrum for each tailings samples in the SWIR.

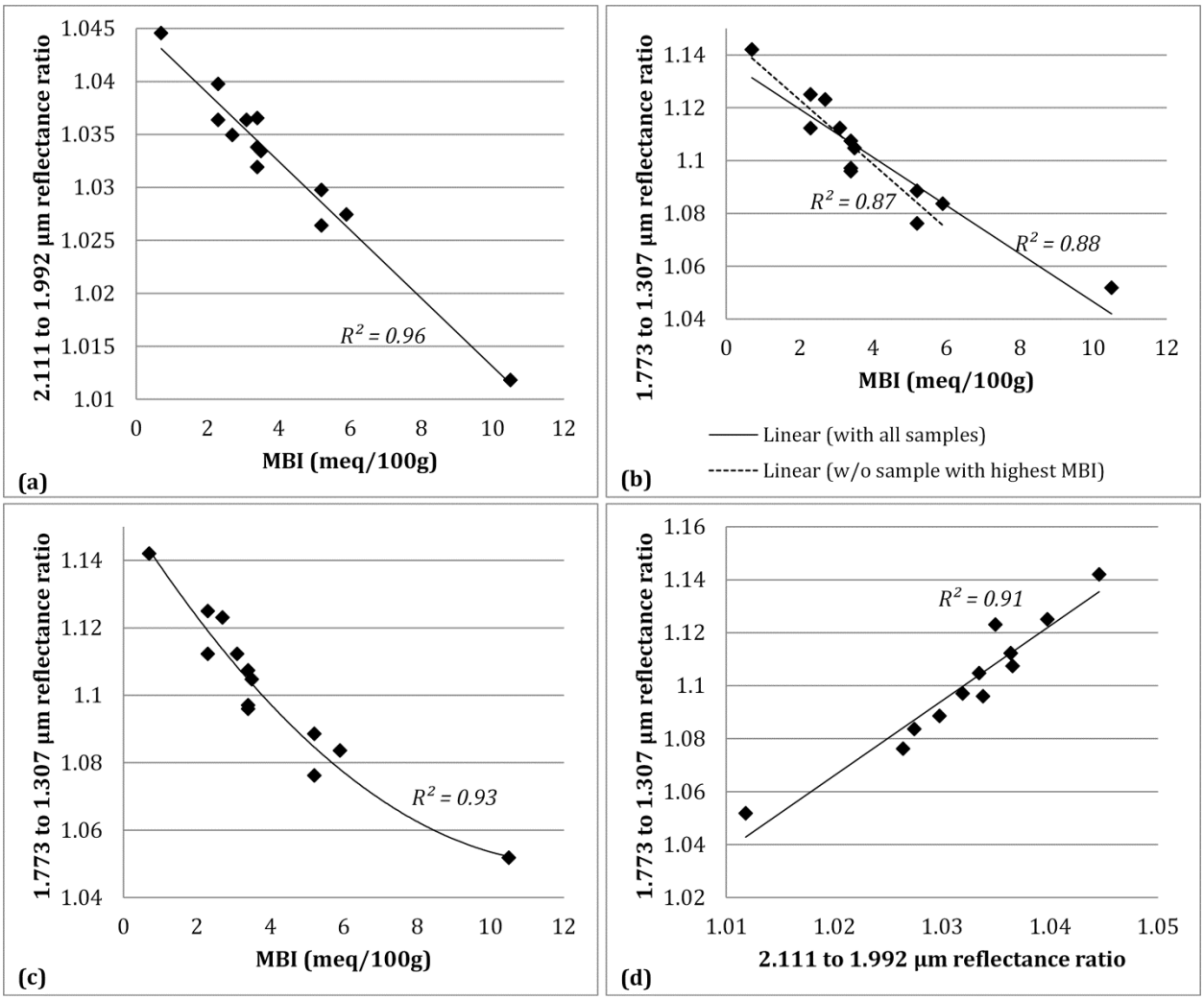

Figure 3.2 Relationship between: (a) MBI and the 2.111 to 1.992 µm reflectance ratio, (b) MBI and the 1.773 to 1.307 µm reflectance ratio, (c) MBI and the 1.773 to 1.307 µm reflectance ratio (nonlinear) and (d) the 2.111 to 1.992 µm reflectance ratio and the 1.773 to 1.307 µm reflectance ratio.

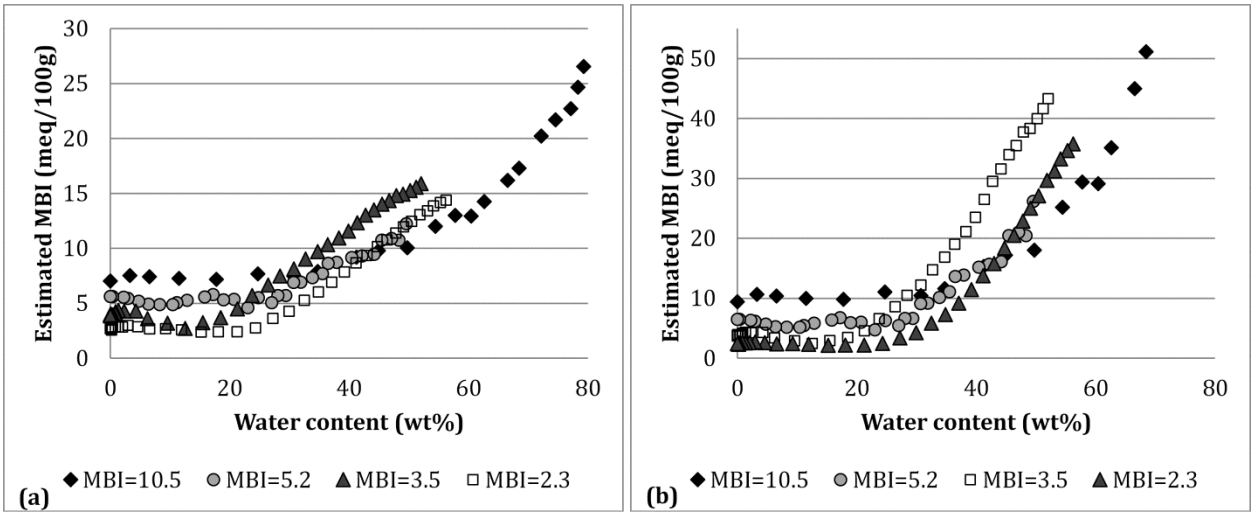

Figure 3.3 Sensitivity of the estimated MBI to water content: (a) linear and (b) polynomial models based on 1.773 to 1.307 μm reflectance ratio.

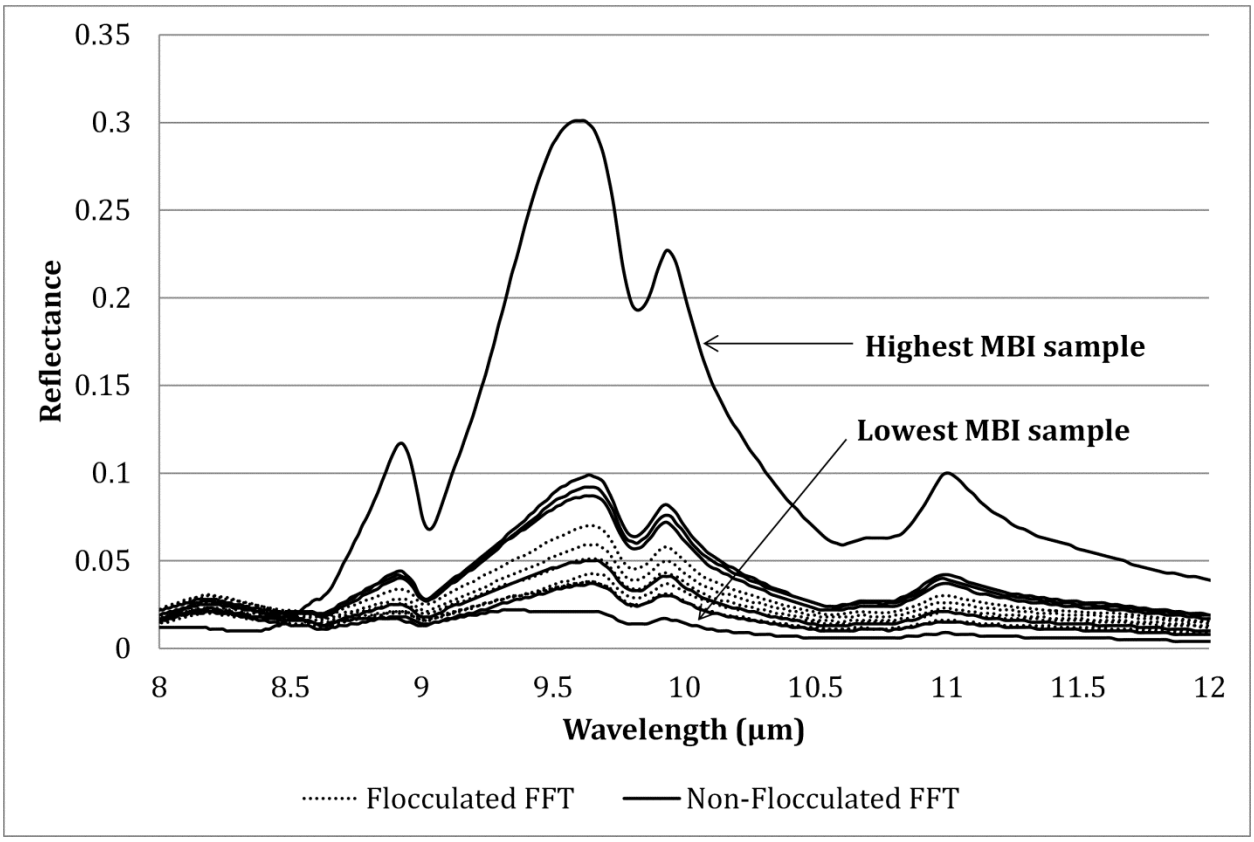

Figure 3.4 Average LWIR reflectance spectrum for each tailing sample.

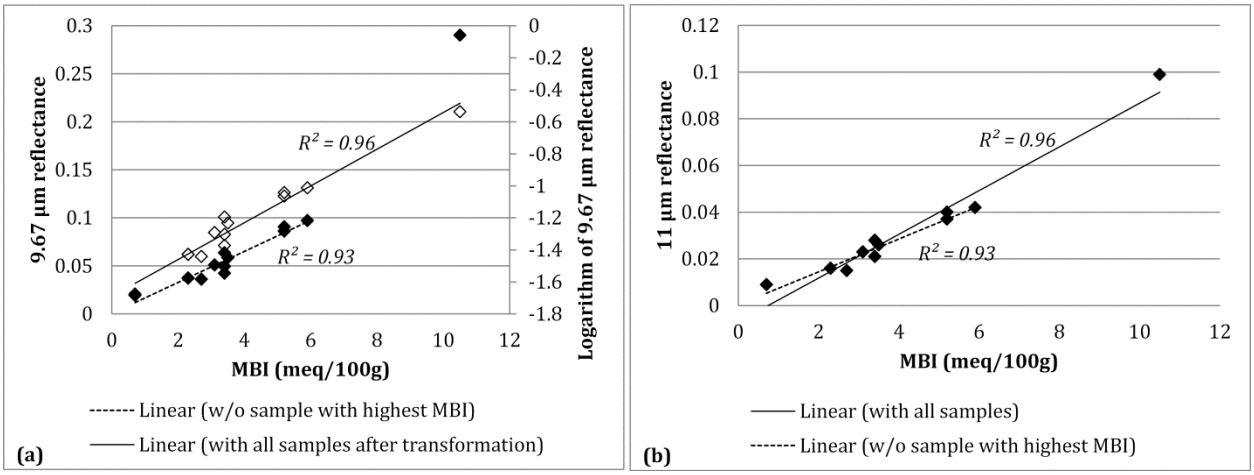

Figure 3.5 Relationship between MBI and: (a) the 9.67 µm reflectance and the logarithm of the 9.67 µm reflectance. White diamonds shows samples after logarithmic transformation (on secondary axis) and (b) the 11 µm reflectance.

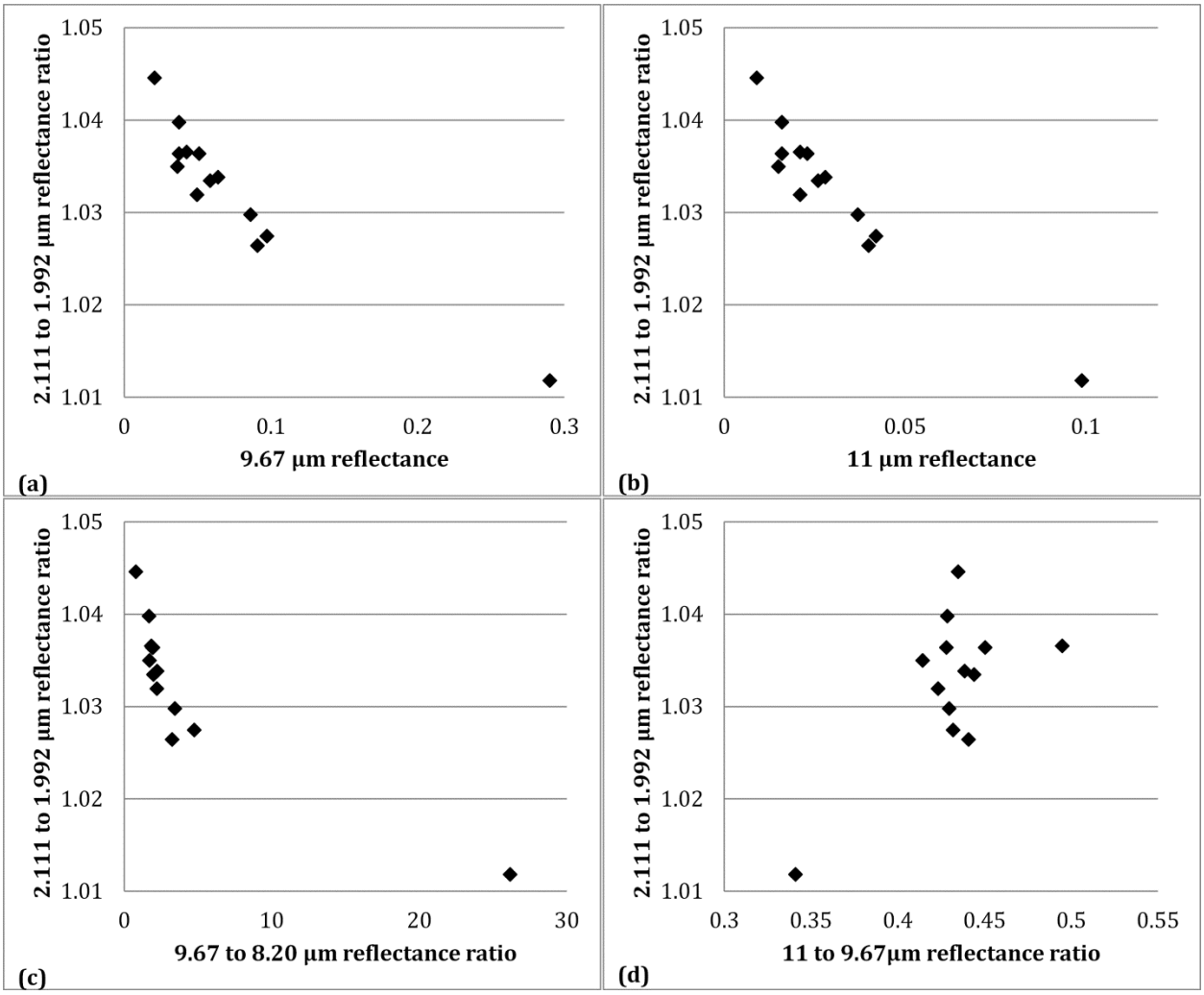

Figure 3.6 Relationship between the 2.111 to 1.992 µm reflectance ratio and: (a) 9.67 µm reflectance, (b) 11 µm reflectance, (c) 9.67 to 8.20 µm reflectance ratio, and (d) 11 to 9.67 µm reflectance ratio.

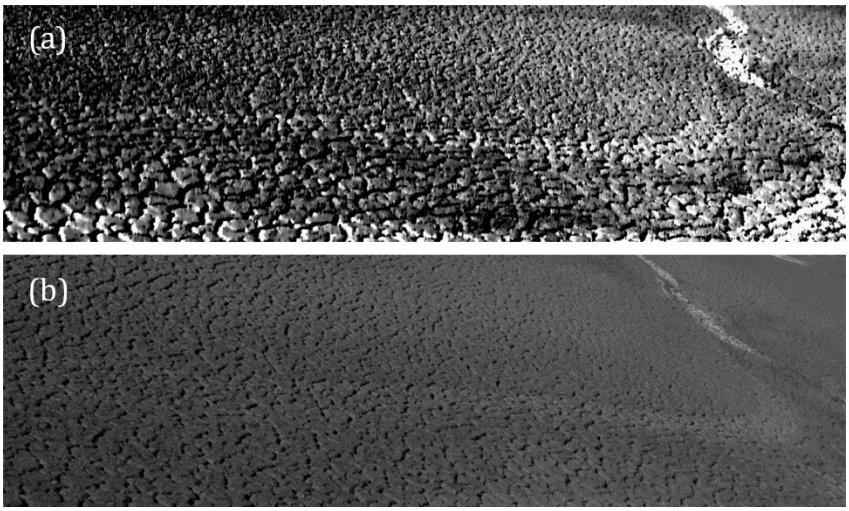

Figure 3.7 Images of the tailings structure analyzed: (a) Reflectance image at 2.205 μm and (b) corresponding photo (from a slightly different position).

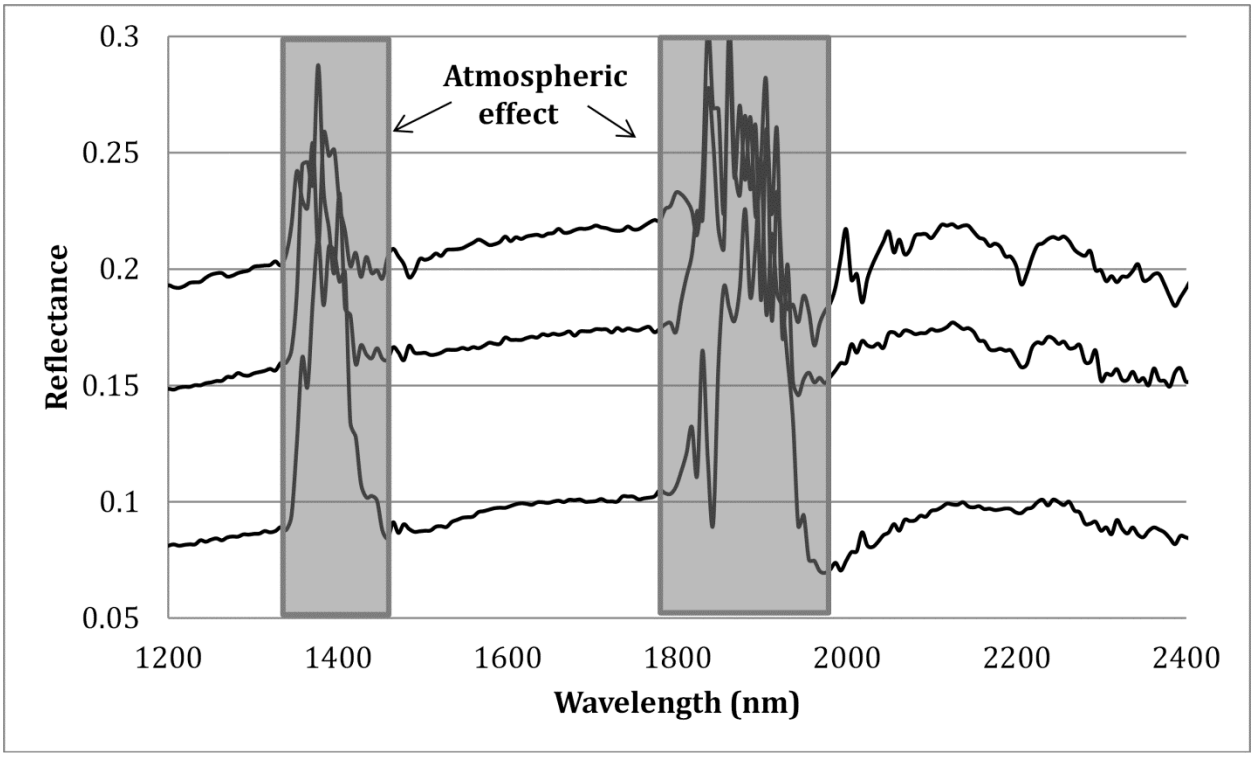

Figure 3.8 Type spectra extracted from the hyperspectral image of the tailings.

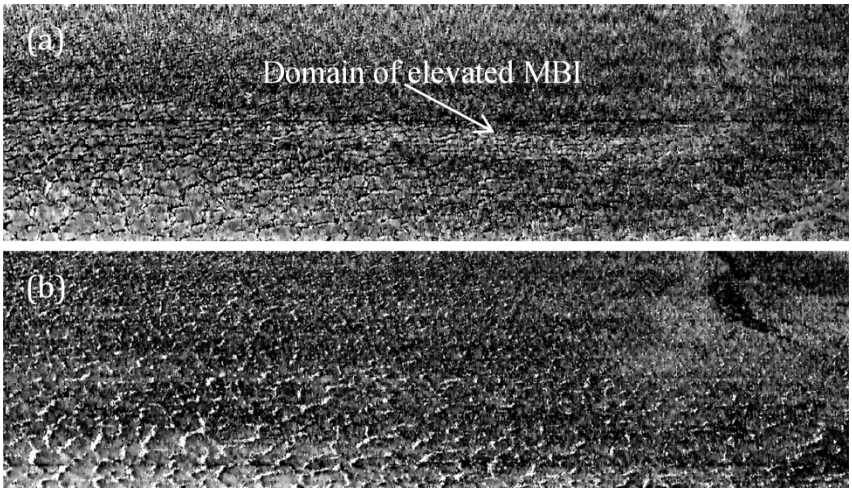

Figure 3.9 Maps of tailings characteristics predicted from the hyperspectral imagery: (a) MBI, generated using the linear SWIR model based on the 1.773 to 1.307 µm reflectance ratio (dark to bright pixels correspond to low to high MBI values) and, (b) moisture content (dark to bright pixels correspond to dry to wet tailings).

References

ASTM, 1992. Standard test method for Methylene Blue Index of clay designation C 837–81, reapproved 1992.

Bayliss, P., and Levinson, A.A., 1976. Mineralogical review of the Alberta oil sand deposits (Lower Cretaceous, Mannville Group). Bulletin of Canadian Petroleum Geology 24(2): 211–224.

Bishop, J.L., Lane, M.D., Dyar, M.D., and Brown, A.J., 2008. Reflectance and emission spectroscopy study of four groups of phyllosilicates: Smectites, kaolinite-serpentines, chlorites and micas. Clay Minerals 43: 35-54.

Chabrillat, S., Goetz, A.F.H., Krosley, L., and Olson, H.W., 2002. Use of hyperspectral images in the identification and mapping of expansive clay soils and the role of spatial resolution. Remote Sensing of Environment 82: 431–445.

Clark, K.A., and Pasternack, D.S., 1932. Hot water seperation of bitumen from Alberta bituminous sand. Industrial and Engineering Chemistry 24(12): 1410-1416.

Entezari, I., Rivard, B., Lipsett, M.G., Feng, J., and Wilson, G.W., 2014. Deployment of hyperspectral imaging instruments for remote monitoring of soft tailings water content. Fourth International Oil Sands Tailings Conference (IOSTC 2014), 7-10 December 2014, Lake Louise, AB, Canada, 493-497.

Goetz, A.F.H., Chabrillat, S., and Lu, Z., 2001. Field reflectance spectrometry for detection of swelling clays at construction sites. Field Analytical Chemistry and Technology 5 (3): 143–155.

Kaminsky, H.A.W., Etsell, T.H., Ivey, D.G., and Omotoso, O., 2009. Distribution of clay minerals in the process streams produced by the extraction of bitumen from Athabasca oil sands. Canadian Journal of Chemical Engineering 87(1): 85-93.

Kaminsky, H., 2014. Demystifying the Methylene Blue Index. Proc. Fourth International Oil Sands Tailings Conference, 7-10 December 2014, Lake Louise, AB, Canada, 221-229.

Kariuki, P.C., Van der Meer, F., and Verhoef, P.N.W., 2003. Cation Exchange Capacity (CEC) determination from spectroscopy. International Journal of Remote Sensing 24(1): 161-167.

Kariuki, P.C., Woldai, T., Van der Meer, F.D., 2004. Effectiveness of spectroscopy in identification of swelling indicator clay minerals. International Journal of Remote Sensing 25(2): 455–469.

Kasperski, K.L., 1992. A review of properties and treatment of oil sands tailings. AOSTRA Journal of Research 8: 11-15.

Kasperski, K. L., 2001. Review of research on aqueous extraction of bitumen from mined oil sands. [Division No. CWRC 01-17 (CF)]. Natural Resources Canada, CANMET-WRC.

Kessick, M., 1979. Structure and properties of oil sands and clay tailings: Journal of Canadian Petroleum Technology 18(1): 49–52.

Kotlyar, L.S., Sparks, B.D., Capes, C.E., and Schutte, R., 1992. Gel-forming attributes of colloidal solids from fine tails formed during extraction of bitumen from Athabasca oil sands by the hot water process. AOSTRA Journal of Research 8: 55-61.

Kotlyar, L.S., Sparks, B.D., Woods, J., Capes, C.E., and Schutte, R., 1995. Biwetted ultrafine solids and structure formation in oil sands fine tailings, Fuel 74: 1146–1149.

Kruse, F.A. and Hauff, P.L., 1991. Identification of illite polytype zoning in disseminated gold deposits using reflectance spectroscopy and X-ray diffraction-Potential for mapping with imaging spectrometers. IEEE Transactions on Geoscience and Remote Sensing 29: 101-104.

Mercier, P.H.J., Le page, Y., Tu, Y., and Kotlyar, L.S., 2008. Powder X-ray diffraction determination of phyllosilicate mass and area versus particle thickness distributions for clays from the Athabasca oil sands. Petroleum Science and Technology 26(3): 307–321.

National Energy Board, 2004. Canada's Oil Sands: opportunities and challenges to 2015 [Pamphlet], Calgary, AB.

Omotoso, O., and Mikula, R., 2004. High surface areas caused by smectitic interstratification of kaolinite and illite in Athabasca oil sands. Applied Clay Science 25: 37-47.

Omotoso, O., Mikula, R., Urquhart, S., Sulimma, H., Stephens, P., 2006. Characterization of clays from poorly processing oil sands using synchrotron techniques. Clay Science 12(2): 88–93.

Scott, J.D., Dusseault, M.B., and Carrier III, W.D., 1985. Behaviour of the clay/bitumen/water sludge system from oil sands extraction plants. Applied Clay Science 1: 207–218.

Schuttlefield, J.D., Cox, D., and Grassian, V.H., 2007. An investigation of water uptake on clays minerals using ATR-FTIR spectroscopy coupled with quartz crystal microbalance measurements. Journal of Geophysical Research 112: D21303.

Shouxun, Y., and Jin, P., 2004. A study on the correlation relationships between smectite contents and spectral absorption indices of swelling soils. Proc. International Geoscience and Remote Sensing Symposium (IGARSS '04), 20-24 Sept. 2004, Anchorage, AK, USA.

Van der Meer, F.D., 1999. Can we map swelling clay with remote sensing? International Journal of Applied Earth Observation & Geoinformation (JAG) 1: 27–35.

Vaughan, R.G., Hook, S.J., Calvin, W.M., and Taranik, J.V., 2005. Surface mineral mapping at Steamboat Springs, Nevada, USA, with multi-wavelength thermal infrared images. Remote Sensing of Environment 99: 140–158.

Yitagesu, F.A., Van der Meer, F.D., Van der Werff, H., 2009. Quantifying engineering parameters of expansive soils from their reflectance spectra. Engineering Geology 105: 151–160.

Yitagesu, F.A., Van der Werff, H., Van der Meer, F.D., and Hecker, C., 2012. On the relationship between plasticity and spectral characteristics of swelling soils: The 3–5 μm wavelength region. Applied Clay Science 69: 67–78.

Yong R.N., and Sethi, A.J., 1978. Mineral particle interaction control of tar sand sludge stability. The Journal of Canadian Petroleum Technology 77(4): 76-83.

Chapter 4 Hyperspectral Characterization of Alberta's Oil Sands

4.1 Introduction

Oil sands located in northern Alberta, Canada, contains a vast reserve of heavy oil. Alberta oil sands are natural mixtures comprised of 55-80 wt% minerals (primarily quartz and clays), 2-15 wt% water, and 4-18 wt% bitumen a highly thick and viscous oil (Kasperski 2001). Currently, two methods are employed to extract bitumen from oil sands deposits, open-pit mining and in-situ production. Bitumen production through open-pit mining uses a water based process that results in production of large volumes of tailings; mixture of solids, water, and residual bitumen. Among the factors affecting the bitumen recovery efficiency, ore mineralogy plays a critical role. Silicates and phyllosilicates, sulfides and sulphates, oxides and hydroxides, phosphates, and carbonates, are the mineral classes found in Alberta's oil sands (Bichard 1987; Hepler and His 1989). Clay minerals are particularly important, as a relationship exists between increased clay content in oil sands ore and decreased bitumen recovery (Liu et al. 2004). Kaolinite and illite have been observed to comprise a major fraction of clays in oil sands (Kessick 1979; Kotlyar et al. 1995; Mercier et al. 2008). However, evidence of the presence of minor amounts of chlorite, vermiculite, smectite, and mixed layer clays including illite-smectite and kaolinite-smectite has been reported in several studies (Yong and Sethi 1978; Scott et al. 1985; Omotoso and Mikula 2004; Omotoso et al. 2006, Kaminsky 2008). It has been reported that active clays (mainly interstratified and ultra-fine illite and kaolinite) are responsible for poor bitumen recovery and slow settling of tailings (Kasongo et al. 2000, Wallace et al. 2004, Omotoso and Mikula, 2004). Consequently, characterization of the abundance and type of clay

minerals is of importance to the oil sands industry due to their influence on ore processability and tailings operations.

Several techniques are employed for the characterization of minerals in oil sands. As summarized by Kaminsky (2008), energy-dispersive x-ray spectroscopy (EDX) analysis and x-ray fluorescence spectroscopy (XRF) are used to investigate elemental composition, electron diffraction (ED) and x-ray diffraction (XRD) are employed to determine the mineralogy, quantitative XRD (QXRD) methods are used to determine the quantitative content of minerals in the samples, and transmission and scanning optical and electron microscopy (TEM and SEM) techniques are used to study the morphology and interactions between minerals. These methods are time-consuming, expensive, and require extensive sample preparation prior to data collection and analysis.

Reflectance spectroscopy is a quick and reliable method widely used for mineral detection and quantification. Hyperspectral sensors measure the natural radiation reflected or emitted from the materials surface in narrow (typically < 10 nm) and contiguous spectral intervals across a wide portion of the electromagnetic spectrum (e.g. 400-2500 nm). The spectral response from each material is controlled by the chemical composition and crystal structure of the minerals and materials within, and is wavelength dependent. The spectroscopy of clay minerals has been investigated in several studies (e.g. Farmer and Russell 1964; Oinuma and Hayashi 1965; Clark et al. 1990; Salisbury et al. 1991; Gates 2005; Bishop et al. 2008, 2011; Yitagesu et al. 2011). In general, clay minerals can be identified using characteristic absorption features caused by vibrations of the hydroxyl (OH) group and structural water molecules as well as vibrations involving silicon, oxygen, and octahedral, tetrahedral, and interlayer cations.

In this study we make use of oil sands samples characterized for their quantitative mineralogy, obtained from QXRD (Osacky et al. 2013a, 2013b), to gain an understanding of changes in the reflectance spectra of oil sands with changes in mineralogy. The sample suite includes bitumen-removed oil sands ore samples (bulk samples; enriched in quartz) and their different fine size fractions (fine fraction samples; enriched in clay species). We then derive spectral metrics applicable to the prediction of quartz and clay contents in oil sands ore and tailings. Focus is given to defining the best spectral metrics correlating with sample content in total 2:1 clays (total of illite and illite-smectite) and kaolinite, as clays impact bitumen extraction and tailings treatment. In doing so, we aim to gain an insight in the ratio of swelling to non-swelling clays in oil sands ore and tailings. The ability to quickly analyze oil sands (ores and tailings) and assess their mineral content characteristics, in particular that of clay minerals, may allow for improved extraction processes and tailings management.

4.2 Materials, Measurements and Methods

4.2.1 Sample description

Three sample suites were used in this study: 1) a suite of Dean-Stark extracted (bitumen-removed) oil sands samples with quantitative mineralogy that was obtained in a prior study, 2) a suite of oil sands ore samples, and 3) a suite of oil sands tailings samples. Each sample suite is described in the section below. The first suite was used to define spectral metrics with the strongest correlation to mineral content (clays and quartz). The other two suites were used for investigating the applicability of the spectral metrics for the mineral characterization of ore and tailings.

4.2.1.1 Dean-Stark extracted oil sands samples with quantitative mineralogy

The quantitative mineralogy of four bitumen-removed oil sand ore samples (bulk samples) and their different size fractions (<2 μm, 0.2-2 μm, and <0.2 μm) was obtained from QXRD analysis (Table 4.1), a portion of these data was reported in Osacky et al. (2013a, 2013b). The ore samples were provided by a major oil sands company and collected from a mine in Alberta. The fine fraction (<0.2 μm) was isolated by techniques that included settling and centrifugation of solids suspended in water. The total 2:1 clays shown in Table 4.1 refer to illite and illite-smectite interstratified clays, as QXRD cannot separately quantify the amount of illite and mixed layer clay minerals (Osacky et al. 2013b). Quartz and clay minerals constitute the major fraction of the samples. However, traces of K-feldspar, carbonates (calcite, dolomite, and siderite), pyrite and TiO_2 minerals are also observed. The total clay content generally increases with decreasing size fraction since clay minerals are typically aggregated in the clay fraction (particle size <2 μm) of a soil or an ore.

The content in total clays and quartz are negatively correlated for all the samples (Figure 4.1), consistent with the known trend for oil sand ore mineralogy. Also, the content in total clays and total 2:1 clays are positively correlated. Interestingly, the data patterns exhibited for the total clays versus kaolinite is more complex. There is a positive correlation observed for the bulk samples, but the fine fractions deviate from this trend and show a nearly negative correlation (Figure 4.1c). Similarly, the content in kaolinite and total 2:1 clays are positively correlated for the bulk samples but negatively correlated for the fine fractions. This sample suite is thus well suited for the spectral investigation of this study because it displays a wide variation in quartz (0-72.1 wt%), total clays (16.6-97.6 wt%), total 2:1 clays (7.5-82.7 wt%), and kaolinite (8.9-38.4 wt%) content. Moreover, there are samples that are enriched in total 2:1 clays and depleted in

kaolinite and vice versa. Thus one can investigate changes in reflectance spectra with varying abundances of these clay minerals.

4.2.1.2 Ore and tailings samples

Seven oil sand ore samples were obtained from various mines in Alberta. The bitumen content and percentage of fines (<44 μm) for each sample were measured at a commercial laboratory. The samples were selected by mine geologists and span a range of grade (6.97-14.15 wt% bitumen) and processability. The fines content for the sample suite ranged from 13.83 wt% to 46.24 wt%. In addition, a suite of seven tailings samples was provided by an oil sands operating company. These tailing samples were collected from different depths of a settling basin. The samples were characterized using the Methylene Blue Index (MBI) and percentage of fines. MBI is an indicator of the swelling potential of the tailings and depends on the type and relative abundance of clay minerals and their total content in the sample. The tailings samples have MBI values ranging from 0.7 to 10.5 meq/100g, fines content from 17.80 to 93.85 wt%, and various amounts of residual bitumen. Table 4.2 lists the ore and tailings samples examined in this study as well as their characteristics.

4.2.2 Measurements of reflectance spectra

Reflectance spectral measurements involved the preparation of samples and the acquisition of shortwave (SWIR, 1-2.5 μm) and longwave (LWIR, 7.5-11.5 μm) infrared spectra from the samples, as follows.

4.2.2.1 Sample preparation

The Dean-Stark extracted oil sands samples (bulk and size fractions) were dry and agglomerated in some parts. Each sample was crushed and mixed using a mortar and pestle to achieve a relatively uniform particle size for spectral measurements. The seven ore samples had been frozen (-5^{o}C) to prevent loss of water. They were crushed and mixed using a rotary breaker to have a homogenous mixture and allowed to thaw and air-dry to remove the impact of water on the spectrum, as water significantly darkens the spectrum by absorbing the light. The ore samples contained bitumen at the time of spectral measurements. The seven tailings samples were initially saturated with water. Each sample was stirred to create a homogenous mixture and remove any effects of segregation after long-term storage. Samples were poured into a petri dish and allowed to air-dry. They were then crushed using a mortar and pestle to minimize the potential impact of segregation on the spectral measurements.

4.2.2.2 SWIR and LWIR spectral acquisition

The shortwave infrared (1.0-2.5 μm) reflectance spectra were collected from the samples using a SisuRock imaging system developed and manufactured by Specim, Finland. SisuRock is a scanner platform equipped with a visible-near infrared (VNIR; 0.4-1 μm) and a short-wave infrared (SWIR; 1-2.5 μm) camera, a set of quartz halogen lamps to illuminate the samples, a translation platform to hold the samples, and a white panel to normalize the radiance spectra acquired to a measure of reflectance. This study made use of the SWIR camera as clays are spectrally active in this wavelength region. The output data consist of reflectance measured from 1 to 2.5 μm at a spectral resolution of approximately 6 nm (256 bands) for every 1mm pixel of

the scene. From the imagery, the average spectrum of each sample was then calculated by averaging the spectrum of the pixels encompassing each sample (~ 1500 pixels).

Additionally long-wave infrared (LWIR; 7.5–11.5 μm) reflectance spectra from the samples were measured relative to a diffuse gold panel (InfragoldTM, 96% reflectance) using a Bomem MB100 fourier transform infrared (FTIR) spectrometer. The spectrometer is equipped with a mercury/cadmium/telluride (MCT) detector and a globar light source. Spectra were collected at a resolution of 4 cm^{-1} (308 bands). As the instrument field of view on the samples was approximately 1 cm in diameter, 2-3 spots were measured on each sample and these spectra were averaged to produce a spectrum for each sample. Each spot measurements consisted of 128 co-adds averaged to improve the signal-to-noise ratio.

4.2.3 Spectral analysis

Reflectance spectra were analyzed with the objective of identifying spectral metrics correlated with the content in clays (total 2:1, kaolinite, and total clays) and quartz obtained from QXRD data. Band ratios (i.e. reflectance ratio) were calculated to capture the variation in overall shape and slope amongst spectra as it relates to sample mineralogy. Ratios of all possible band combinations were calculated for the available SWIR and LWIR bands respectively. Linear regression analysis was then performed between these band ratios and QXRD data to define the band ratios of highest correlation with quartz and clay mineral content. The coefficient of determination (R^2) and root-mean-square error (RMSE) were calculated to evaluate the goodness of fit and accuracy of the regression analysis.

The bulk and fine fraction samples were analyzed together in the regression analysis because they were considered to represent quartz-rich and clay-rich samples, respectively. Using

these samples as a single population expanded the range in clay content, for comparison with that observed for both the oil sands ore and tailings (as quartz-rich and clay-rich materials).

4.3 Results

4.3.1 SWIR spectral properties of samples

The SWIR spectral characteristics of the Dean-Stark extracted bulk and fine fraction samples (Figure 4.2a) show variation in overall spectral shape and absorption features near 1.4, 1.9, and 2.2 μm. The absorption feature near 1.4 μm is attributed to water or OH overtones whereas the 1.9 μm feature is a water combination band (Kruse and Hauff 1991; Bishop et al. 2008). The existence of the 1.9 μm feature relates to the presence of smectitic clays which have water in their interlayer structure. However, adsorbed water on the surface of minerals or impurities in the samples can also produce this absorption feature (Bishop et al. 2008). The sharp absorption feature at 2.2 μm is the OH stretching and bending combination vibration diagnostic of all clay minerals. For most of the samples, this feature is in the form of a doublet feature at 2.162 μm and 2.205 μm, confirming the presence of kaolinite in the samples. The weak absorption bands observed from 2.3-2.5 μm are attributed to OH stretching and bending combinations and may be associated with octahedral layer cations in the clays structure (Kruse and Hauff 1991, Bishop et al 2008). Carbonate minerals also have vibrational absorption features in this wavelength region due to carbonate anions (Hunt and Salisbury 1971; Gaffey 1987), which interferes with the clays absorption bands.

4.3.2 LWIR spectral properties of samples

The spectral characteristics of the Dean-Stark extracted samples in the LWIR are shown in Figure 4.2b. The bulk samples show distinct spectra due to the existence of a strong reflectance peak at ~8.2 μm attributed to quartz and caused by Si-O vibrations (Hunt 1982; Salisbury et al. 1991). The ~8.9 μm reflectance peak is a second quartz feature but can also be attributed to clay minerals as well, particularly kaolinite (Salisbury et al. 1991). The reflectance peak observed at ~9.5 μm is the fundamental characteristic Si-O stretching vibrations feature for clay minerals (Salisbury et al. 1991; Schuttlefield et al. 2007; Bishop et al. 2008). This peak is centred at ~9.24 μm for the bulk samples and between ~9.4 and ~9.6 μm for the fine fraction samples. The reflectance peak at ~9.9 μm is characteristic of kaolinite (Salisbury et al. 1991; Vaughan et al. 2005; Schuttlefield et al. 2007). Kaolinite also has a characteristic reflectance peak near 11 μm but for the samples examined here, this peak is subtle due to the small particle size and volume scattering (Salisbury et al. 1991; Salisbury and Wald 1992).

4.3.3 Correlations between mineralogy and spectral features

This section presents the best spectral metrics correlated with sample content in total 2:1 clays, kaolinite, quartz and total clays. Results are presented for the SWIR and LWIR spectral regions to provide a comparison in the value of these spectral regions for the estimation of quartz and clay minerals in oil sands.

4.3.3.1 Spectral metrics correlated with total 2:1 clays

Spectral analysis in the SWIR showed that the best correlation to total 2:1 clays involved a ratio of bands 1.892 to 1.936 μm (Figure 4.3a). A linear fit to the data produced a R^2 value of

0.79 and a RMSE of 10.68 wt%. These bands are located within the 1.9 μm water absorption band observed in water bearing clays and the ratio captures changes in the shape of this spectral feature with abundance of total 2:1 clays. In the LWIR spectral region, a significant correlation was observed between the total 2:1 clays and ratio of bands 9.428 to 9.276 μm (Figure 4.3b). A linear fit to the data resulted in a R^2 value of 0.89 and a RMSE of 7.69 wt%. This band ratio captures the slope of spectra short of the fundamental clay reflectance peak near 9.5 μm and appears to be more affected by 2:1 clays than other clay types (e.g. kaolinite).

4.3.3.2 Spectral metrics correlated with kaolinite

The ratio of bands 1.879 to 2.080 μm showed the greatest linear correlation with kaolinite content. As shown in Figure 4.4a, a linear fit to the data produced a R^2 value of 0.81 and a RMSE of 4.55 wt%. In the LWIR, a significant correlation was observed between kaolinite content and the ratio of bands 9.858 to 9.783 μm (Figure 4.4b, R^2 = 0.93, RMSE = 2.85 wt%). This reflectance ratio captures the slope of the edge of the 9.9 μm reflectance peak, a feature characteristic of kaolinite. The slope of the edge of this clay feature is apparently more sensitive to the kaolinite content than the amplitude of the peak.

4.3.3.3 Spectral metrics correlated with quartz and total clay

Although quartz is featureless in the SWIR, the band ratio analysis was pursued to investigate the effect of quartz on the overall shape of the spectra. The highest linear correlation with quartz content was observed for the ratio of bands 1.942 to 1.892 μm (Figure 4.5a). However, samples form two separate populations and a regression line does not fit well to the bulk and fine fraction samples when considered separately. More samples are therefore required

to evaluate the success of this spectral feature as a predictor of quartz content. In the LWIR, on the other hand, a significant R^2 of 0.99 with a small RMSE of 3.05 wt% was observed between quartz content and a ratio of bands 8.377 and 9.638 μm, as shown in Figure 4.5b. This is a ratio of quartz to clay features in the LWIR. Although the bulk and fine fraction samples form two separate populations in Figure 4.5b, the regression line appears to fit both populations well and shows a slight deviation from the regression lines fitted to each population. This band ratio thus is of value for the estimation of quartz in samples with a wide range of quartz content.

For each of the two spectral regions, our spectral analysis resulted in the same spectral metrics for the estimation of quartz and total clay content (Figure 4.5c and 4.5d). This relates to the high negative correlation observed between the quartz and total clay content in oil sands samples (see Figure 4.1a). The reflectance ratios of bands 1.942 to 1.892 μm in the SWIR (R^2 = 0.83, RMSE = 11.60 wt%) and bands 8.377 and 9.638 μm (R^2 = 0.95, RMSE = 6.19 wt%) in the LWIR are the best spectral metrics for the estimation of the total clay content. In the LWIR, the data form two populations and the regression line appears to fit the bulk samples better compared to the fine fraction samples (Figure 4.5d). In both the SWIR and LWIR, however, more samples are required to evaluate the potential of these spectral estimators.

4.3.4 Mapping of kaolinite to total 2:1 clays ratio

Figure 4.6 allows an examination of the relative abundance of kaolinite to total 2:1 clays for a suite of samples. Figure 4.6a displays the observed contents for the Dean-Stark extracted samples obtained from QXRD (black and white circles) as well as the estimated values (gray circles) using the LWIR spectral metrics found in this study. The LWIR spectral metrics were employed as they showed a better performance than SWIR ones for the estimation of total 2:1

clays and kaolinite. As seen in this plot, the estimated values follow the observed pattern of kaolinite to total 2:1 clays for both bulk and fine fraction samples, as expected given the models were derived from this sample population. Next, we investigated the applicability of these predictive tools for the characterization of oil sands ore and tailings. Figure 4.6b displays the estimated contents of kaolinite and total 2:1 clays for the ore and tailings samples obtained using the LWIR spectral metrics. Also shown are the estimated values for the bulk and fine fractions shown on figure 4.6a. The data pattern for the ore samples is consistent with that of the bulk samples; kaolinite and total 2:1 clays are positively correlated. The tailings samples are generally aligned with the pattern of the ore samples though they show a higher kaolinite and total 2:1 clay content than the ore samples, owing to their clay-rich nature. Also, some variation in terms of kaolinite to total 2:1 clays ratio is observed for the tailings samples. Five of these samples display a narrow range of kaolinite content, approximately from 26 to 28 wt%, while the total 2:1 clays range from 28 to 52 wt%.

4.3.5 Relationship between total clays and percentage of fines (<44 μm)

The percentage of fines (<44 μm) is a common descriptor of oil sands ore and tailings. It is considered an estimate of total clay content of the samples. To further assess the LWIR spectral metric for the estimation of total clays, we examined the relationship between the total clay content of the ore and tailings samples estimated using the LWIR spectral metric, and the percentage of fines obtained from particle size distribution analysis. A strong positive correlation (R^2 = 0.87) was observed between the estimated total clay content and the observed fines content, as shown Figure 4.7. The LWIR spectral metric thus appears to be of value for the estimation of total clay content.

4.4 Discussion

4.4.1 Reliability of the spectral predictions

From the results it could be argued that the spectral metrics identified for the estimation of total 2:1 clays could potentially be attributed to the effect of total clays given the positive correlation between total 2:1 clay and total clay contents for the samples (Figure 4.1b). However, the SWIR and LWIR spectral metrics yielded a R^2 value of 0.75 and 0.83 with total clay content compared to values of 0.79 and 0.89 for total 2:1 clays, indicating that these metrics are more sensitive to total 2:1 clays. As for predicting kaolinite content, the spectral metrics identified appear to be solely sensitive to kaolinite content given that the content in this mineral was not observed to show a unique correlation with the total clay or total 2:1 clay contents across the sample suite (Figures 4.1c and 4.1d). Moreover, the spectral metric identified in the LWIR for the estimation of kaolinite involved a known kaolinite spectral feature. Quartz and total clays can confidently be quantified using the same LWIR spectral metric involving the ratio of characteristic quartz and clay spectral features. The strong correlation that generally exists between contents in quartz and total clays in oil sands explains why the same spectral metric can be employed for quantification of quartz and total clays. In addition, the strong correlation observed between the estimated total clay content and the observed percentage of fines for ore and tailings samples is another evidence for the reliability of the LWIR spectral metric for the estimation of total clay content.

4.4.2 SWIR versus LWIR results

The spectral metrics derived in the LWIR perform considerably better than those in the SWIR for the estimation of clay and quartz content. The characteristic features of quartz and

clays (in particular the kaolinite feature) in the LWIR explain the better performance of the LWIR spectral metrics. In the SWIR, the spectral band ratios correlated with the contents in total 2:1 clays, kaolinite, and quartz use bands located within or in close proximity of the 1.9 μm water band. This likely reflects the presence of water bearing clays (e.g. smectitic clays) and fluid inclusions in quartz. Adsorbed water, particularly the moisture content in tailings, also affects the results of the SWIR models thus samples must be dry when the SWIR spectral data are collected. In this respect, the SWIR spectral metrics are of lesser value for the analysis of spectra acquired outdoors either for moist targets or simply due to the strong absorption of sunlight by water vapor in the intervening atmosphere near 1.9 μm. Future investigations should explore the sensitivity of the LWIR spectral metrics to sample moisture content.

4.4.3 Application to mapping of kaolinite to total 2:1 clays ratio

The determination of the relative abundance of kaolinite to total 2:1 clays is important for bitumen extraction and tailings management. This relative abundance and the content in total clay play a role in the processability of oil sands ore, and the settling and consolidation behaviour of tailings. The predicted kaolinite to total 2:1 clays ratio for the oil sands ore and tailings samples examined in this study was observed to be nearly constant in general. However, the spectral metrics of this study can potentially be used to detect anomalous samples in terms of their ratio of kaolinite to total 2:1 clays. One might also be able to determine the swelling potential of the tailings through the estimation of kaolinite to total 2:1 clay content, which is an indicator of the ratio of non-swelling to swelling clays. As observed in Figure 4.6b, the variations in kaolinite to total 2:1 clays ratio as well as in the total clay content for the tailings samples may relate to the variation in MBI values.

4.4.4 Effect of tailings compaction on the LWIR spectra

Variations in particle size and degree of compaction impact the overall reflectance (continuum) and the strength of spectral features (Clark and Roush 1984; Salisbury and Wald 1992; Hapke 1993; Cooper and Mustard 1999). In this study, we observed that the LWIR spectra of the tailings samples were notably different when they were measured in a densified state compared to a crushed powder. The lower contrast observed in the crushed powder is likely attributable to an increase in volume scattering (Hapke 1993). As seen in Figure 4.8, both spectra of densified and crushed tailings exhibit the same spectral features, except for the features near 10.7 and 11 μm, attributed to kaolinite. These are distinct in the spectrum of the densified tailings and are not visible in the spectrum of the crushed tailings. However, the strength of the quartz and clay features is remarkably different. The clay features around 8.9, 9.5, and 9.9 μm are stronger in the densified tailings. Also, the ratio of quartz to clay feature (8.377 to 9.638 μm) is considerably lower in the densified tailings. Further analysis revealed that all the LWIR spectral metrics of this study used for the estimation of clay minerals and quartz generally result in higher clay content estimates (total 2:1 clays, kaolinite, and total clays) when they are applied to spectra of densified tailings. The spectral metrics presented perform best for spectra collected from crushed (powder) samples, as they were established using the samples in powder form. It may be possible to recalibrate such results for their application on densified samples.

4.5 Conclusions

This study investigated the application of hyperspectral sensing to Alberta oil sands samples to find spectral metrics correlated with the content of major clay minerals and quartz. Band ratio analysis in both the SWIR and LWIR spectral regions was employed to find the best

spectral metrics correlated with the clays and quartz. In general, the band ratio analysis proved to be an effective spectral analysis method for the estimation of clays and quartz in oil sands. Overall, spectral metrics found in the LWIR resulted in better performance than the ones in the SWIR. The existence of characteristics quartz and clay features in the LWIR explains the better performance of LWIR spectral metrics. The best estimation of total 2:1 clay content was achieved using the 9.428 to 9.276 μm reflectance ratio. The 9.858 to 9.783 μm reflectance ratio resulted in the best efficacy for the estimation of kaolinite. For the estimation of quartz and total clays, the 8.377 to 9.638 μm reflectance ratio was observed to lead to the best results. This study lays the foundation for future work on establishing a quick and reliable in-situ method for determining mineralogy of oil sands ore and tailings based on hyperspectral sensing. In particular, real-time detection and quantification of clay minerals and quartz provides useful insight about bitumen recovery and tailings consolidation and can enhance bitumen production processes and tailings operation.

Table 4.1 Mineral composition (wt%) of the oil sands samples determined by QXRD.

Sample	Size Fraction (μm)	Quartz	K-feldspar	Kaolinite	Total 2:1 clays[2]	Chlorite	Carbonates[3]	TiO_2	Pyrite	Total clay content[4]
MC1[1]	Bulk	72.1	3.9	8.9	7.5	0.2	13.7	0.3	0.1	16.6
	<2	N/A	N/A	N/A	N/A	N/A	N/A	N/A	N/A	N/A
	0.2-2	16.4	1.3	38.4	33.7	1.2	10.0	0.0	0.0	73.3
	<0.2	15.9	3.4	21.5	40.8	1.1	13.7	0.2	0.2	63.4
EC1[1]	Bulk	52.3	2.7	14.4	25.3	1.3	3.3	0.7	0.0	41.0
	<2	4.2	1.0	28.9	58.9	4.6	2.1	0.3	0.0	92.4
	0.2-2	6.9	0.6	37.0	52.6	2.3	0.3	0.3	0.0	91.9
	<0.2	1.2	0.9	21.4	64.8	8.9	2.7	0.3	0.1	95.1
MC2	Bulk	51.7	3.8	11.7	17.8	0.0	14.1	0.2	0.2	29.5
	<2	6.6	0.9	36.7	52.4	0.0	2.9	0.5	0.0	89.1
	0.2-2	N/A	N/A	N/A	N/A	N/A	N/A	N/A	N/A	N/A
	<0.2	0.0	2.4	11.3	82.6	0.0	2.5	0.7	0.0	93.9
EC2	Bulk	62.9	2.0	12.2	20.2	0.0	2.3	0.4	0.0	32.4
	<2	12.4	1.1	28.7	55.9	0.0	0.0	1.2	0.0	84.6
	0.2-2	N/A	N/A	N/A	N/A	N/A	N/A	N/A	N/A	N/A
	<0.2	0.0	1.7	14.9	82.7	0.0	0.0	0.7	0.0	97.6

[1]The mineralogical and chemical composition of the samples MC1 and EC1 have been thoroughly investigated in Osacky et al. (2013a, 2013b).

[2]Total of illite and illite-smectite.

[3]Total of calcite, siderite, and dolomite.

[4]Total of kaolinite, total 2:1 clays, and chlorite.

Table 4.2 Characteristics of the ore and tailings samples examined.

Ore	Fines (wt%)	Bitumen (wt%)	Tailings	Fines (wt%)	MBI (meq/100g)
O1	13.83	14.15	**T1**	93.85	10.5
O2	40.06	7.40	**T2**	76.91	5.9
O3	40.75	9.75	**T3**	81.74	5.2
O4	24.98	7.80	**T4**	75.94	5.2
O5	27.30	12.02	**T5**	70.87	3.4
O6	46.24	6.97	**T6**	54.61	2.7
O7	31.00	8.23	**T7**	17.80	0.7

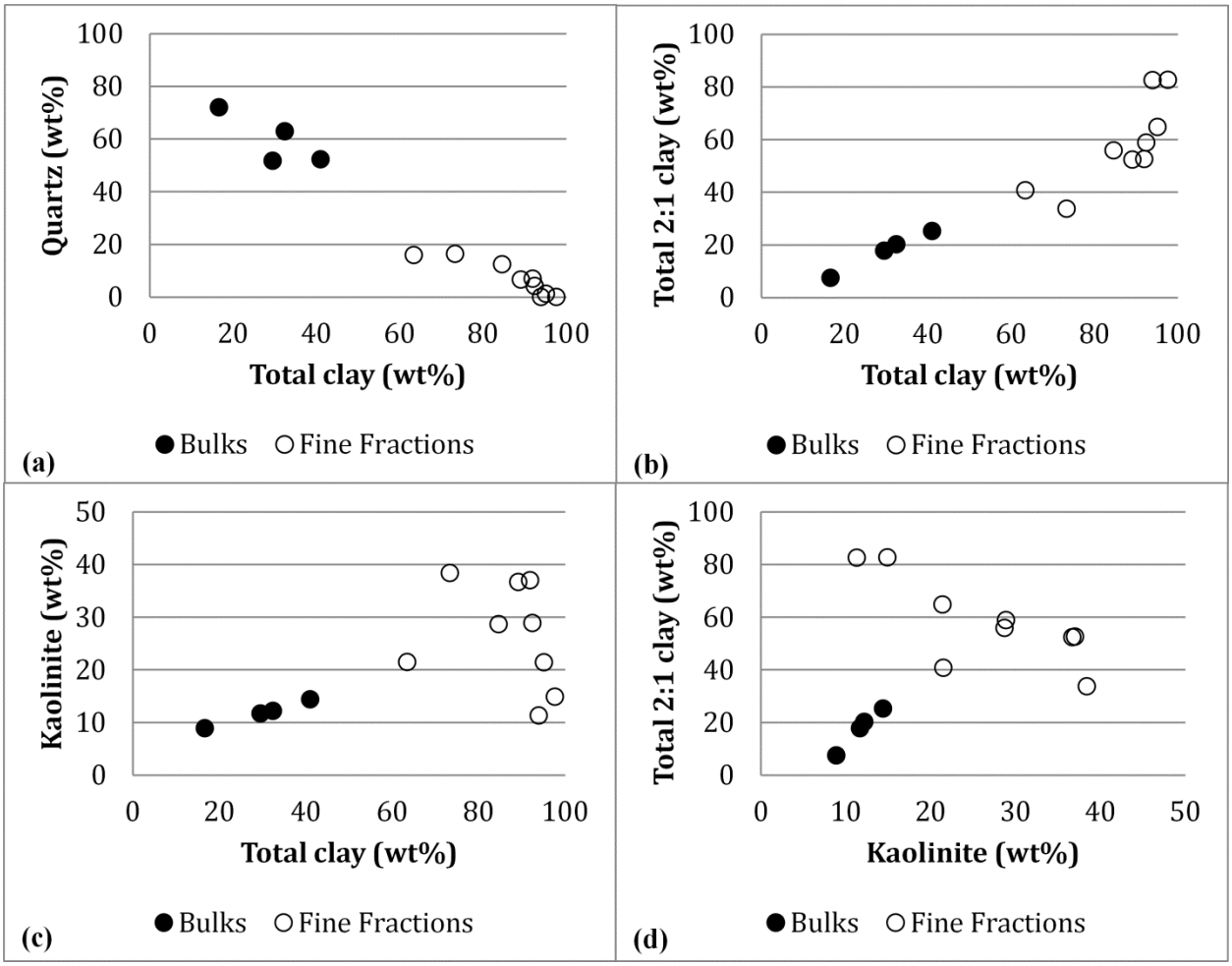

Figure 4.1 Relationships between: (a) total clay and quartz, (b) total clay and total 2:1 clay, (c) total clay and kaolinite, and (d) kaolinite and total 2:1 clay. These relationships were extracted from QXRD data.

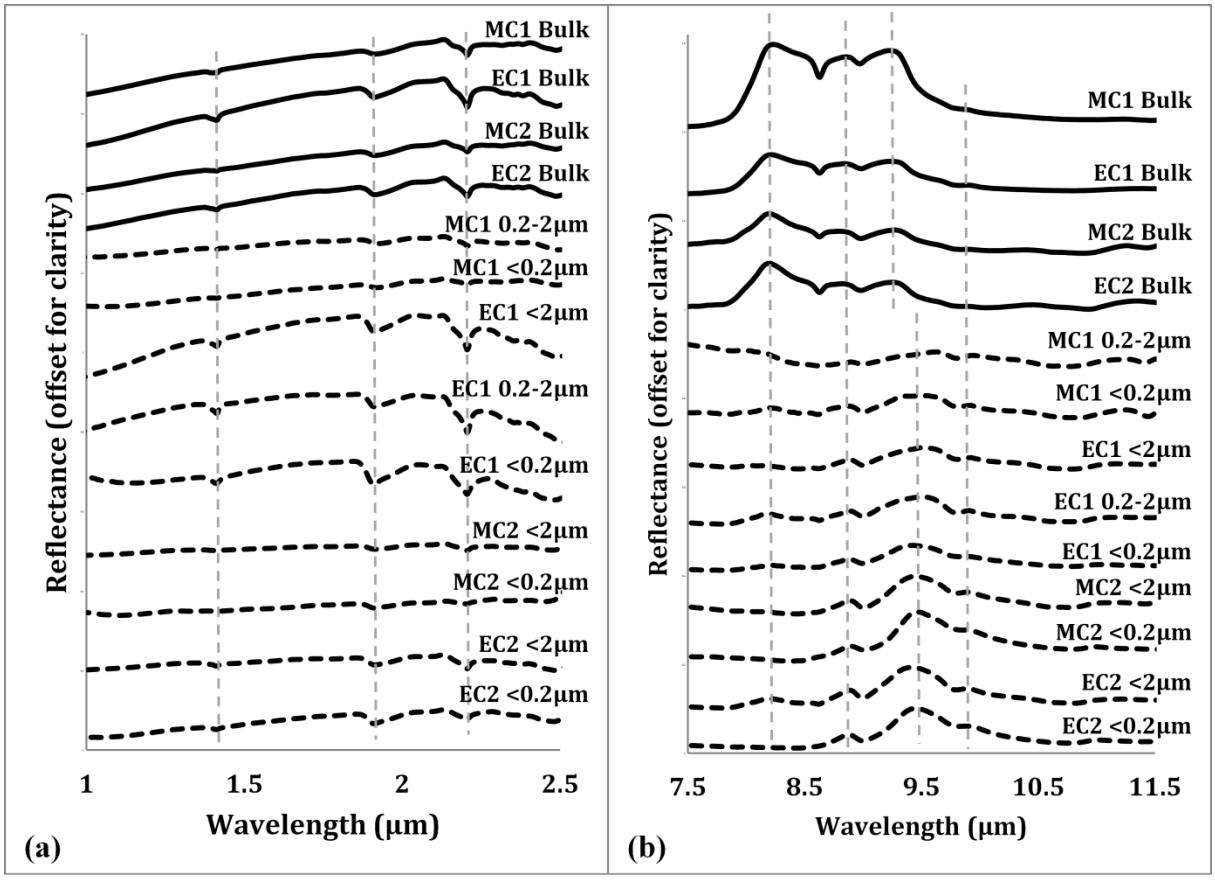

Figure 4.2 Average reflectance spectrum for each sample in the (a) SWIR and (b) LWIR.

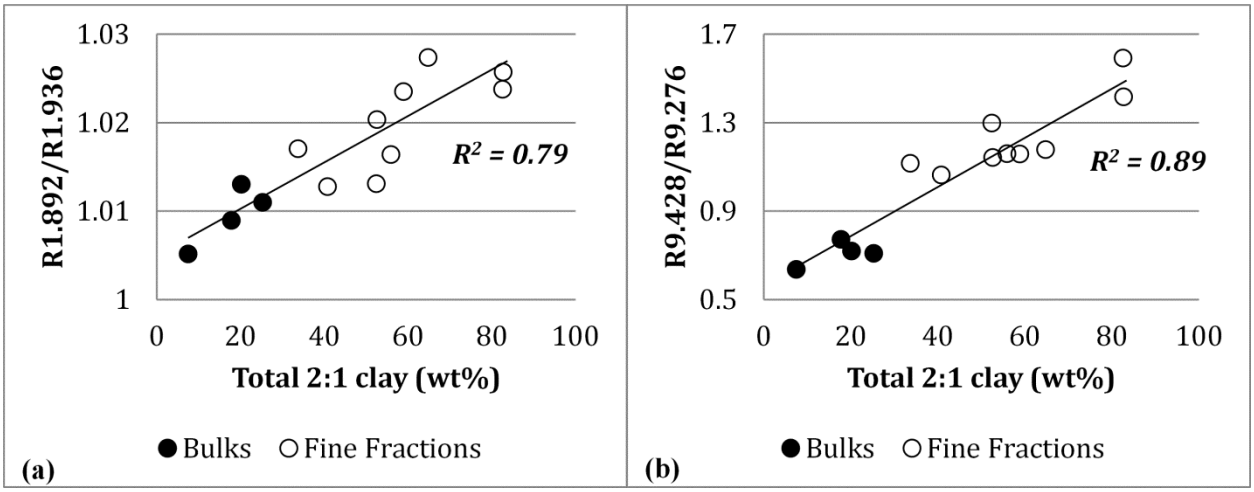

Figure 4.3 Strongest correlations observed between total 2:1 clay content and spectral metrics in the (a) SWIR; the 1.892 to 1.936 µm reflectance ratio and (b) LWIR; the 9.428 to 9.276 µm reflectance ratio.

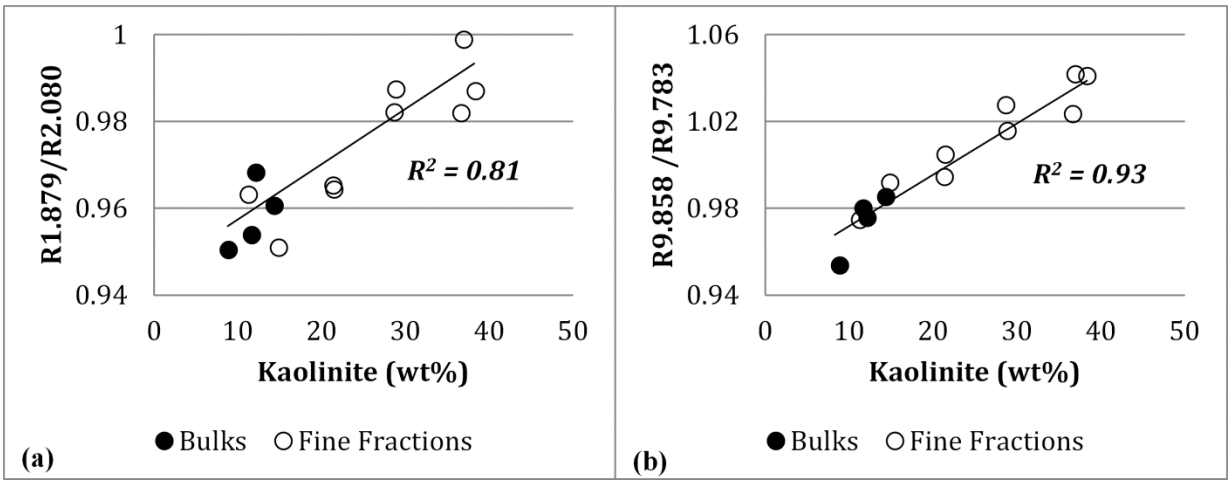

Figure 4.4 Strongest correlations observed between kaolinite content and spectral metrics in the (a) SWIR; the 1.879 to 2.080 µm reflectance ratio and (b) LWIR; the 9.858 to 9.783 µm reflectance ratio.

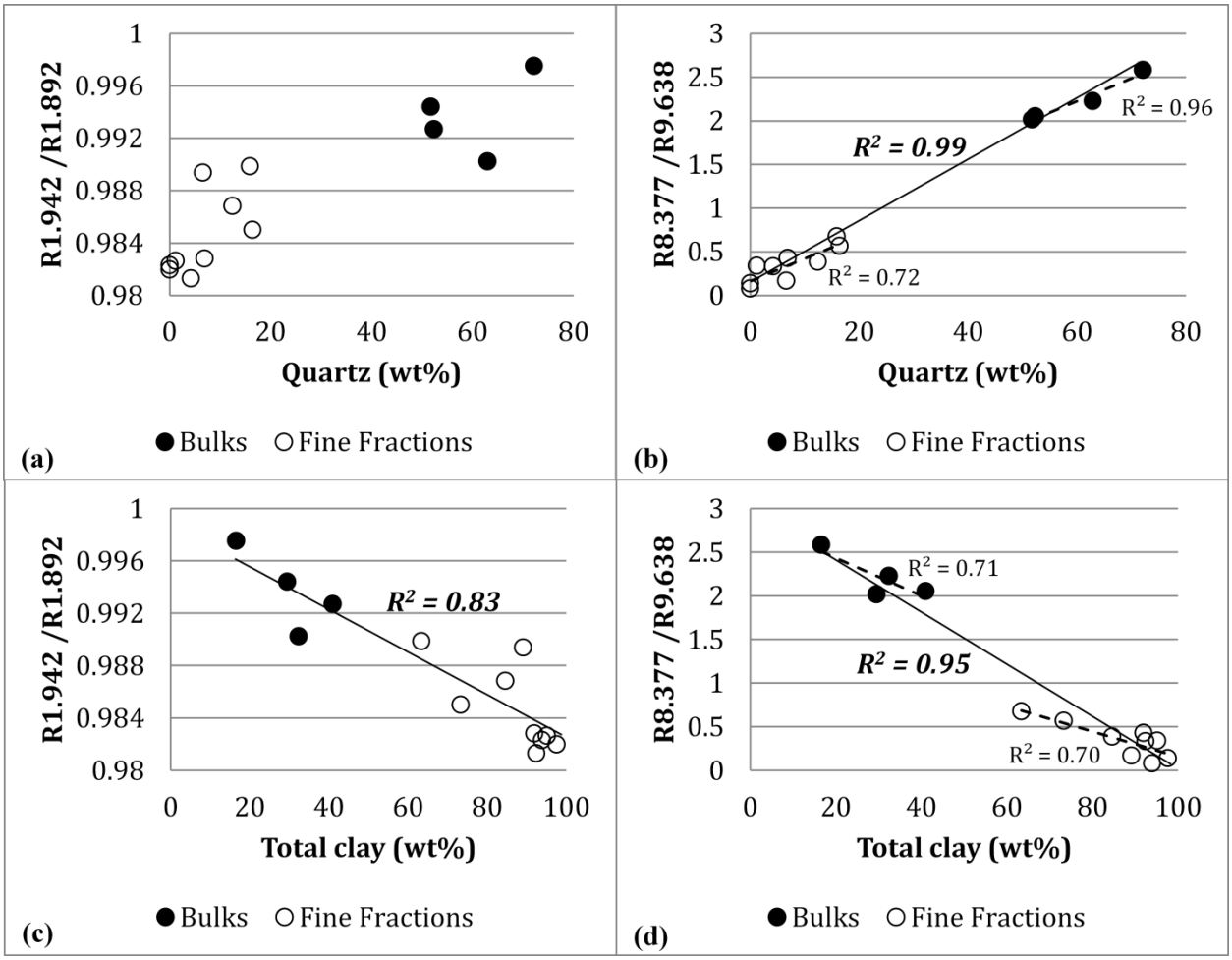

Figure 4.5 Strongest correlations observed for quartz and total clay contents obtained from QXRD, and spectral metrics in the SWIR and LWIR: (a) quartz and the 1.942 to 1.892 µm reflectance ratio in the SWIR, (b) quartz and the 8.377 to 9.638 µm reflectance ratio in the LWIR, (c) total clay and the 1.942 to 1.892 µm reflectance ratio in the SWIR, and (d) total clay and the 8.377 to 9.638 µm reflectance ratio in the LWIR.

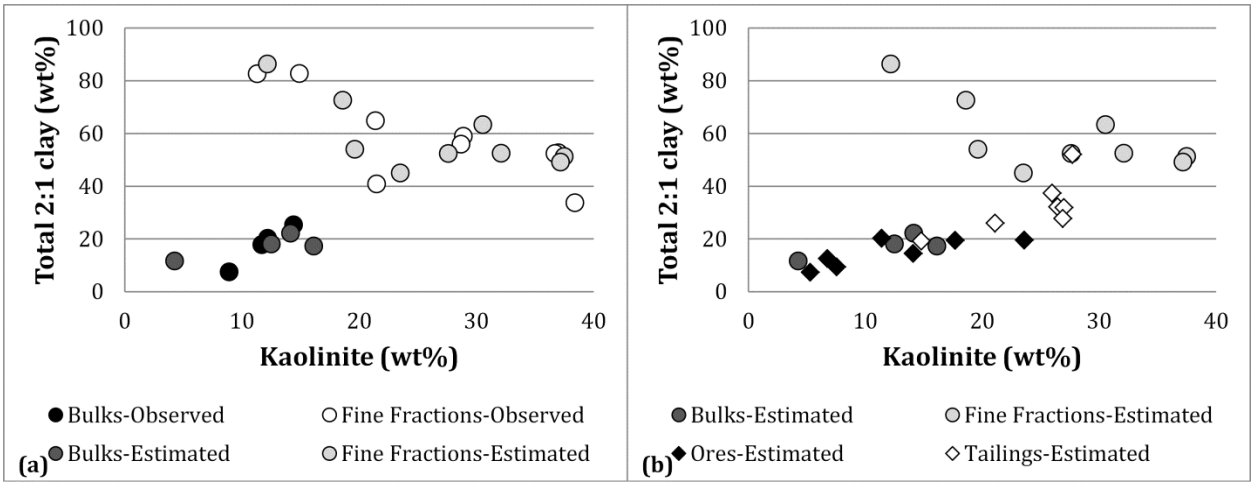

Figure 4.6 Relationship between: (a) kaolinite and total 2:1 clay contents (observed and estimated) and (b) kaolinite and total 2:1 contents estimated from the LWIR models for the ore and tailings samples.

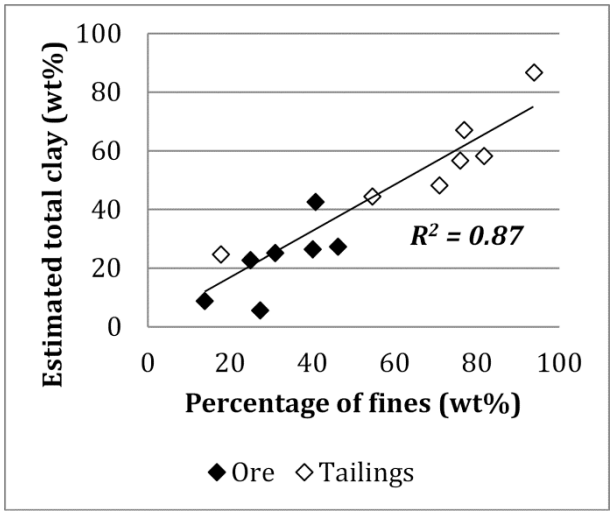

Figure 4.7 Relationship between the observed fines (<44 μm) content and the estimated content in total clay for the ore and tailings samples.

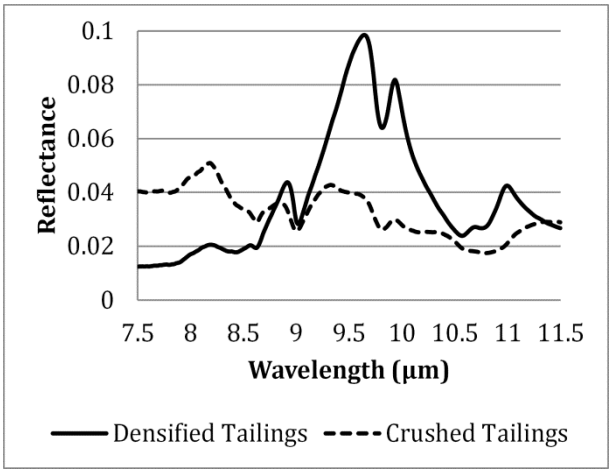

Figure 4.8 LWIR spectra of a tailings sample in densified and crushed states.

References

Bichard, J.A., 1987. Oil sands composition and behaviour research. Edmonton: Alberta Oil Sands Technology and Research Authority.

Bishop, J.L., Lane, M.D., Dyar, M.D., and Brown, A.J., 2008. Reflectance and emission spectroscopy study of four groups of phyllosilicates: Smectites, kaolinite-serpentines, chlorites and micas. Clay Minerals 43: 35-54.

Bishop, J.L., Gates, W.P., Makarewicz, H.D., McKeown, N.K., and Hiroi, T., 2011. Reflectance spectroscopy of beidellites and their importance for Mars. Clays and Clay Minerals 59(4): 378–399.

Clark, R.N., King, T.V.V., Klejwa, M., Swayze, G., and Vergo, N., 1990. High spectral resolution reflectance spectroscopy of minerals. Journal of Geophysical Research 95: 12653-12680.

Clark, R.N. and Roush, T.L., 1984. Reflectance spectroscopy: Quantitative analysis techniques for remote sensing applications. Journal of Geophysical Research 89: 6329−6340.

Cooper, C.D., and Mustard, J.F., 1999. Effects of very fine particle size on reflectance spectra of smectite and palagonitic soil. Icarus 142: 557–570.

Farmer, V.C., Russell, J.D., 1964. The infrared spectra of layer silicates. Spectrochimica Acta 20: 1149–1173.

Gaffey, S.J., 1987. Spectral reflectance of carbonate minerals in the visible and near infrared (0.35–2.55 (Am): Anhydrous minerals. Journal of Geophysical Research 92(B2): 1429–1440.

Gates W.P., 2005. Infrared spectroscopy and the chemistry of dioctahedral smectites. pp. 125-168 in: The Application of Vibrational Spectroscopy to Clay Minerals and Layered Double Hydroxides (J.T. Kloprogge, editors). The Clay Minerals Society, Aurora, Colorado, USA.

Hapke, B., 1993. Theory of Reflectance and Emittance Spectroscopy. Cambridge Univ. Press, Cambridge.

Hepler, L. (ed.) and Hsi, C. (ed.), 1989. AOSTRA technical handbook on oil sands, bitumens and heavy oils. Edmonton: Alberta Oil Sands Technology and Research Authority.

Hunt, G.R., 1982. Spectroscopic properties of rocks and minerals, in Handbook of Physical properties of rocks, Volume I, (R. S. Carmichael, ed.) CRC Press, Boca Raton, 295-385.

Hunt, G.R., Salisbury, J.W., 1971. Visible and near-infrared spectra of minerals and rocks - II: Carbonates. Modern Geology 2: 23-30.

Kaminsky, H., 2008. Characterization of an Athabasca oil sands ore and process streams. PhD Thesis, Department of Chemical and Materials Engineering, University of Alberta.

Kasongo, T., Zhou, Z., Xu, Z., and Masliyah, J., 2000. Effect of clays and calcium ions on bitumen extraction from Athabasca oil sands using flotation. The Canadian Journal of Chemical Engineering 78: 674–680.

Kasperski, K.L., 2001. Review of research on aqueous extraction of bitumen from mined oil sands. [Division No. CWRC 01-17 (CF)]. Natural Resources Canada, CANMET-WRC.

Kessick, M., 1979. Structure and properties of oil sands and clay tailings. Journal of Canadian Petroleum Technology 18(1): 49–52.

Kotlyar, L.S., Sparks, B.D., Woods, J., Capes, C.E., and Schutte, R., 1995. Bitwetted ultrafine solids and structure formation in oil sands fine tailings. Fuel 74: 1146–1149.

Kruse, F.A. and Hauff, P.L., 1991. Identification of illite polytype zoning in disseminated gold deposits using reflectance spectroscopy and X-ray diffraction-Potential for mapping with imaging spectrometers. IEEE Transactions on Geoscience and Remote Sensing 29: 101-104.

Liu, J., Masliyah, J., and Xu, Z., 2004. Role of fine clays in bitumen extraction from oil sands. American Institute of Chemical Engineers Journal 50(8): 1917–1927.

Mercier, P.H.J., Le page, Y., Tu, Y., and Kotlyar, L.S., 2008. Powder X-ray diffraction determination of phyllosilicate mass and area versus particle thickness distributions for clays from the Athabasca oil sands. Petroleum Science and Technology 26(3): 307–321.

Oinuma, K. and Hayashi, H., 1965. Infrared study of mixed-layer clay minerals. American Mineralogist 50: 1213-1227.

Omotoso, O., and Mikula, R., 2004. High surface areas caused by smectitic interstratification of kaolinite and illite in Athabasca oil sands. Applied Clay Science 25: 37-47.

Omotoso, O., Mikula, R., Urquhart, S., Sulimma, H., and Stephens, P., 2006. Characterization of clays from poorly processing oil sands using synchrotron techniques. Clay Science 12(2): 88–93.

Osacky, M., Geramian, M., Dyar, M.D., Sklute, E.C., Valter, M., Ivey, D.G., Liu, Q., Etsell, T.H., 2013a. Characterisation of petrologic end members of oil sands from the Athabasca region, Alberta, Canada. The Canadian Journal of Chemical Engineering 9999: 1–14.

Osacky, M., Geramian, M., Ivey, D.G., Liu, Q., Etsell, T.H., 2013b. Mineralogical and chemical composition of petrologic end members of Alberta oil sands. Fuel 113: 148–157.

Salisbury, J.W., and Wald, A., 1992. The role of volume scattering in reducing spectral contrast in spectra of powdered minerals. Icarus 96: 121–128.

Salisbury J.W., Walter L.S., Vergo N., and D'Aria D.M., 1991. Infrared (2.1-25 mm) Spectra of Minerals. Johns Hopkins University Press, Baltimore, USA.

Schuttlefield, J.D., Cox, D., and Grassian, V.H., 2007. An investigation of water uptake on clays minerals using ATR-FTIR spectroscopy coupled with quartz crystal microbalance measurements. Journal of Geophysical Research, 112: D21303.

Scott, J.D., Dusseault, M.B., and Carrier III, W.D., 1985. Behaviour of the clay/bitumen/water sludge system from oil sands extraction plants. Applied Clay Science 1: 207–218.

Vaughan, R.G., Hook, S.J., Calvin, W.M., and Taranik, J.V., 2005. Surface mineral mapping at Steamboat Springs, Nevada, USA, with multi-wavelength thermal infrared images. Remote Sensing of Environment 99: 140–158

Wallace, D., Tipman, R., Komishke, B., Wallwork, V., and Perkins, E., 2004. Fines/water interactions and consequences of the presence of degraded illite on oil sands extractability. The Canadian Journal of Chemical Engineering 82: 667–677.

Yitagesu, F.A., Van der Meer, F.D., Van der Werff, H., and Hecker, C., 2011. Spectral characteristics of clay minerals in the 2.5–14 μm wavelength region. Applied Clay Science 53: 581–591.

Yong R.N., and Sethi, A.J. 1978. Mineral particle interaction control of tar sand sludge stability. The Journal of Canadian Petroleum Technology 77(4): 76-83.

Chapter 5 Conclusions and Future Work

5.1 Conclusions

The main objective of this thesis was to evaluate the potential of hyperspectral remote sensing for the characterization of oil sands tailings. The focus was to develop spectral models to estimate key and trackable properties of tailings including water content and normalized evaporation, swelling potential and mineral content. Overall, this research contribution has established the foundation for developing quick predictions of some important tailings characteristics based on hyperspectral measurements. Such tools may contribute to monitoring of tailings surfaces based on imagery collected outdoors and to the development of more effective measures for tailings operations and management. The key conclusions of this thesis are summarized below.

5.1.1 Estimation of moisture content and evaporation

The SWIR measurements were of value for the estimation of water content and normalized evaporation of the soft tailings. Reflectance in the SWIR was generally observed to show a high negative correlation with water content and normalized evaporation. The best estimate of moisture content of soft tailings was achieved using the Normalized Soil Moisture Index (NSMI). The reflectance at 1920 nm was found to be the best spectral estimator of normalized evaporation with the NSMI index also being of value. In both instances, the NSMI index shows the most potential for estimations in a field setting, as it is less sensitive to the effects of the intervening atmospheric column between the spectral camera and the target. However, NSMI appears to be sensitive to the sample composition including the bitumen

concentration when the evaporation rate is very low. Measurements of the moisture content and the exchange of water between the soil surface and the atmosphere are of importance for many geotechnical problems. In the case of tailings management, the remote estimation of moisture content and evaporation could help to assess the drying process and to determine when the deposit has stopped drying at the surface, as part of a decision determining when the next lift should be deposited.

5.1.2 Estimation of MBI

Results of laboratory experiments demonstrated that remote sensing methods are generally successful to estimate the swelling potential of oil sands tailings indicated by MBI. In the SWIR, a band ratio of reflectance at 2.111 μm to 1.992 μm was highly correlated with MBI values for air-dried tailings. Towards the estimation of MBI in outdoor settings, where the intervening atmosphere can impact the spectral measurements, a band ratio of reflectance at 1.773 μm to 1.307 μm provided an estimation of MBI of tailings. The water sensitivity analysis showed that the SWIR model based on these bands is robust against variations in the tailings moisture content for values less than 20 wt%. At moisture levels above 20 wt%, the MBI value was overestimated. Of relevance to the estimation of MBI in a field setting, a first step would involve imaging the tailing surfaces to delineate areas with less than 20 wt% moisture using the spectral models of this study for moisture content estimation (as discussed in Chapter 2). In a second step, the MBI predictive models could be then applied to areas with moisture less than 20 wt%. The best MBI predictions were obtained in the LWIR using reflectance peaks at 9.67 μm and 11 μm attributed to total clays and kaolinite, respectively. For the sample suite examined, a mostly constant relative abundance of kaolinite to total clays was observed (using spectral

analysis) which explains why both of these clay features were successful for the estimation of MBI. A first field test to estimate the MBI of soft tailings as they were deposited in a containment cell was conducted using SWIR hyperspectral imagery. A map of predicted MBI was generated and though the preliminary results were promising, they remain to be validated using concurrent sampling.

5.1.3 Prediction of mineral content

In general, the band ratio analysis proved to be an effective spectral analysis method for the estimation of clays and quartz in Dean-Stark extracted oil sand solids. Spectral metrics derived from the LWIR data performed considerably better for the estimation of clay and quartz content. The existence of characteristic quartz and clay features in the LWIR explains the better performance of the LWIR spectral metrics. The best estimation of total 2:1 clay and kaolinite was achieved using a ratio of bands at 9.428 to 9.276 μm and 9.858 to 9.873 μm, respectively. A ratio of reflectance at 8.377 to 9.638 μm was found to be the best spectral estimator of quartz and total clays. These results lay the foundation for future work to establish a quick and reliable in-situ method for determining the mineralogy of oil sands ore and tailings based on hyperspectral sensing. In particular, the real-time detection and quantification of clay minerals and quartz can provide useful insights into bitumen recovery and tailings consolidation and could enhance bitumen production processes and tailings operation.

5.2 Future Work

5.2.1 Validation of results in field settings

The experimental procedures of this study were carried out in the laboratory environment under controlled conditions. In future work, the models obtained from this laboratory investigation should be assessed for their applicability in field settings. The presence of water vapor in the intervening atmosphere can severely impact the quality of the spectral measurements conducted outdoors. In such settings, atmospheric correction of the hyperspectral imagery is necessary as part of pre-processing operations. The imagery can then be analyzed for the estimation of the tailings characteristics including moisture content and normalized evaporation, MBI, and clay content using models developed during this thesis. The estimation results will first require validation through the collection of samples possibly via autonomous means (e.g. robotic sampling) at the time of spectral imaging. As part of this thesis, guidance was provided to the research team of Dr. Lipsett for the development of a robotic tool that can be used to collect adequate samples from areas of tailings ponds where humans cannot collect samples without significant risk (Lipsett et al. 2014).

5.2.2 Estimation of total suction

As discussed in Chapter 2, hyperspectral sensing can be employed to estimate the total suction of tailings surfaces. Future field work should incorporate a SWIR hyperspectral camera to estimate normalized evaporation, a LWIR hyperspectral camera or a forward looking infrared (FLIR) camera to estimate the tailings surface temperature, and sensors to measure the relative humidity of the air. With knowledge of these parameters, one can estimate the total suction (i.e.

matric suction plus osmotic suction) of the tailings surface based on the known relationship between the normalized evaporation and total suction (Wilson et al. 1997).

5.2.3 Expanding the sample suite

The samples examined in Chapters two and three of this study were obtained from a single mine and were processed using the same tailings operation technology. Future work could incorporate samples from different mines and tailings processes to assess the robustness of the findings to tailings composition. The long term goal is to apply the tools of this study to a wide range of tailings and monitor their moisture content, evaporation rate, and MBI and generate real-time maps of these tailings properties. In regards to Chapter four, the samples with quantitative mineralogy were limited to four oil sands ore samples from a single mine. This sample suite should be expanded to include more oil sands ores encompassing a wider range of variation in mineralogy. Ideally one would also perform or access existing QXRD data for some tailings samples to assess the performance of the spectral tools for the estimation of the mineralogy of tailings.

5.2.4 End-of-pipe measurements for improving in-line flocculation

Flocculent treatment for the dewatering of MFTs has been widely implemented by a number of oil sands operating companies (Rao 1980; Scott et al. 2008; COSIA/OSTC 2012). The method typically employs the deposition of layers of in-line flocculated MFT into drying cells where the lifts are allowed to de-water and densify to a solids content that meets a specified shear strength requirement, without additional surcharge material. Initial dewatering performance is affected by the abundance and type of fines present in the MFT being treated.

Tailings treated in a flocculation process are generally discharged from a pipe, either subaerially or subaqueously. As a future research avenue, developing a well-performing hyperspectral technique at the point of discharge (or within pipe) could promptly reveal useful information on the clay species and their abundance in the tailings slurry. End-of-pipe spectral observations could thus be used to assess initial dewatering performance and infer mineral characteristics that can be related to chemical dosage settings to ensure effective flocculation with variable feedstock.

References

COSIA/OSTC, 2012. Technical guide for fluid fine tailings management.

Lipsett, M.G., Olmedo, N., Rivard, B., and Wilson, G.W., 2014. Robotic systems for measuring properties of tailings deposits and collecting samples. Fourth International Oil Sands Tailings Conference (IOSTC 2014), 7-10 December 2014, Lake Louise, AB, Canada: 483-491.

Rao, S.R., 1980. Flocculation and dewatering of Alberta oil sands tailings. International Journal of Mineral Processing 7(3): 245-253.

Scott, J.D., Jeeravipoolvarn, S., Donahue, R. and Ozum, B., 2008. Characterization of oil sands thickened tailings. First International Oil Sands Tailings Conference, 7-10 December 2008, Edmonton, AB, Canada: 132-142.

Wilson, G.W., Fredlund, D.G., and Barbour, S.L., 1997. The effect of soil suction on evaporative fluxes from soil surface. Canadian Geotechnical Journal 34: 145-155.

Literature Cited (Thesis)

Alberta Energy, 2014. Alberta's oil sands: the facts. Government of Alberta, Edmonton, Alberta, Canada.

ASTM, 1992. Standard test method for Methylene Blue Index of clay designation C 837–81, reapproved 1992.

Barnes, E.M., Sudduth, K.A., Hummel, J.W., Lesch, S.M., Corwin, D.L., Yang, C.H., Daughtry, C.S.T., and Bausch, W.C., 2003. Remote- and ground-based sensor techniques to map soil properties. Photogrammetric Engineering and Remote Sensing 69(6): 619–630.

Barton, I.J., 1979. A parameterization of the evaporation from non-saturated surfaces. Journal of Applied Meteorology 18: 43–47.

Bayliss, P., and Levinson, A.A., 1976. Mineralogical review of the Alberta oil sand deposits (Lower Cretaceous, Mannville Group). Bulletin of Canadian Petroleum Geology 24(2): 211–224.

Ben-Dor, E., Chabrillat, S., Dematte, J.A.M, Taylor, G.R., Hill, J., Whiting, M.L., and Sommer, S., 2009. Using imaging spectroscopy to study soil properties. Remote Sensing of Environment 113(1): 38–55.

BGC Engineering Inc., 2010. Oil sands tailings technology review. Oil Sands Research and Information Network, University of Alberta, School of Energy and the Environment, Edmonton, Alberta. OSRIN Report No. TR-1. 136 pp.

Bichard, J.A., 1987. Oil sands composition and behaviour research. Edmonton: Alberta Oil Sands Technology and Research Authority.

Bindlish, R., Jackson, T.J., Wood, E., Gao, H., Starks, P., Bosch, D., and Lakshmi, V., 2003. Soil moisture estimates from TRMM Microwave Imager observations over the southern United States. Remote Sensing of Environment 85(4): 507–515.

Bishop, J.L., Lane, M.D., Dyar, M.D., and Brown, A.J., 2008. Reflectance and emission spectroscopy study of four groups of phyllosilicates: Smectites, kaolinite-serpentines, chlorites and micas. Clay Minerals 43: 35-54.

Bishop, J.L., Gates, W.P., Makarewicz, H.D., McKeown, N.K., and Hiroi, T. 2011. Reflectance spectroscopy of beidellites and their importance for Mars. Clays and Clay Minerals. 59(4): 378–399.

Boratynec, D.J., Chalaturnyk, R.J. and Scott, J.D., 1998. Experimental and fundamental factors affecting the water release rates of CT. *In* Proceedings of the 51st Canadian Geotechnical Conference, Edmonton, Alberta, Canada, 4-7 October 1998, pp. 607-614.

Brutsaert, W.H., 1982. Evaporation into the atmosphere: theory, history and applications. P. Reidel Publishing Company, Dordrecht, The Netherlands.

Chabrillat, S., Goetz, A.F.H., Krosley, L., and Olsen, H.W., 2002. Use of hyperspectral images in the identification and mapping of expansive clay soils and the role of spatial resolution. Remote Sensing of Environment 82: 431-445.

Chalaturnyk, R.J., Scott, J.D, and Ozum, B., 2002. Management of oil sands tailings. Petroleum Science and Technology 20: 1025–1046.

Clark, K.A., and Pasternack, D.S., 1932. Hot water seperation of bitumen from Alberta bituminous sand. Industrial and Engineering Chemistry 24(12): 1410-1416.

Clark, R.N., King, T.V., Klejwa, M., Swayze, G.A., and Vergo, N., 1990. High spectral resolution reflectance spectroscopy of minerals. Journal of Geophysical Research 95(B8): 12653-12680.

Clark, R.N. and Roush, T.L., 1984. Reflectance spectroscopy: Quantitative analysis techniques for remote sensing applications. Journal of Geophysical Research 89: 6329−6340.

Cooper, C., and Mustard, J., 1999. Effects of very fine particle size on reflectance spectra of smectite and palagonitic soil. Icarus 142: 557-570.

COSIA/OSTC, 2012. Technical guide for fluid fine tailings management.

Da Silva, F., Graham, M., Scott, J.D., and Wilson, G.W., 2014. Evaluation of a new treatment technology for improving oil sands tailings management. *In* Proceedings of GeoRegina 2014, Regina, Saskatchewan, Canada, September 28 - October 1, 2014.

Ellis, R.J., and Scott, P.W., 2004. Evaluation of hyperspectral remote sensing as a means of environmental monitoring in the St. Austell China clay (kaolin) region, Cornwall, UK. Remote Sensing of Environment 93: 118-130.

Entezari, I., Rivard, B., Lipsett, M.G., Feng, J., and Wilson, G.W., 2014. Deployment of hyperspectral imaging instruments for remote monitoring of soft tailings water content. Fourth International Oil Sands Tailings Conference (IOSTC 2014), 7-10 December 2014, Lake Louise, AB, Canada, 493-497.

Farmer, V. C., Russell, J.D. 1964. The infrared spectra of layer silicates. Spectrochimica Acta 20: 1149–1173.

FTFC (Fine Tailings Fundamentals Consortium), 1995. Advances in oil sands tailings research. Alberta Department of Energy, Oil Sands and Research Division, Edmonton, Canada.

Gaffey, S.J., 1987. Spectral reflectance of carbonate minerals in the visible and near infrared (0.35–2.55 (Am): Anhydrous minerals. Journal of Geophysical Research 92(B2): 1429–1440.

Gates W.P., 2005. Infrared spectroscopy and the chemistry of dioctahedral smectites. pp. 125-168 in: The Application of Vibrational Spectroscopy to Clay Minerals and Layered Double Hydroxides (J.T. Kloprogge, editors). The Clay Minerals Society, Aurora, Colorado, USA.

Granger, R.J. 1989a. An examination of the concept of potential evaporation. Journal of Hydrology 111: 9–19.

Granger, R.J. 1989b. Evaporation from natural non-saturated surfaces. Journal of Hydrology 111: 21–29.

Gray, D.M., 1970. Handbook on the principals of hydrology. Canadian National Committee for the International Hydrological Decade, National Research Council of Canada, Ottawa, Canada.

Goetz, A.F.H., Chabrillat, S., and Lu, Z., 2001. Field reflectance spectrometry for detection of swelling clays at construction sites. Field Analytical Chemistry and Technology 5(3): 143-155.

Hammel, J.E., Papendick, R.I., and Campbell, G.S., 1981. Fallow tillage effects on evaporation and seedzone water content in a dry summer climate. Soil Science Society of America Journal 45: 1016–1022.

Hapke, B., 1993. Theory of reflectance and emittance spectroscopy. Cambridge Univ. Press, Cambridge.

Haubrock, S.N., Chabrillat, S., Lemmintz, C., and Kaufmann, H., 2008. Surface soil moisture quantification models from reflectance data under field condition. International Journal of Remote Sensing 29(1): 3-39.

Hepler, L. (ed.) and Hsi, C. (ed.), 1989. AOSTRA technical handbook on oil sands, bitumens and heavy oils. Edmonton: Alberta Oil Sands Technology and Research Authority.

Hillel, D., 1980. Applications of soil physics. Academic Press, New York.

Holmes, R.M. 1961. Estimation of soil moisture content using evaporation data. *In* Proceedings of Hydrology Symposium, No. 2 Evaporation. Queen's Printer, Ottawa, pp. 184–196.

Hooshiar Fard, M.A., 2011. Characterization of clay minerals in the Athabasca oil sands in water extraction and nonaqueous solvent extraction processes. Ph.D. Thesis, Department of Chemical and Materials Engineering, University of Alberta, Canada.

Hunt, G.R., 1982. Spectroscopic properties of rocks and minerals, in Handbook of Physical properties of rocks, Volume I, (R. S. Carmichael, ed.) CRC Press, Boca Raton, 295-385.

Hunt, G.R., Salisbury, J.W., 1971. Visible and near-infrared spectra of minerals and rocks - II: Carbonates. Modern Geology 2: 23-30.

Kaminsky, H., 2008. Characterization of an athabasca oil sands ore and process streams. PhD Thesis, Department of Chemical and Materials Engineering, University of Alberta.

Kaminsky, H., 2014. Demystifying the Methylene Blue Index. Proc. Fourth International Oil Sands Tailings Conference, 7-10 December 2014, Lake Louise, AB, Canada, 221-229.

Kaminsky, H.A.W., Etsell, T.H., Ivey, D.G., and Omotoso, O., 2009. Distribution of clay minerals in the process streams produced by the extraction of bitumen from Athabasca oil sands. Canadian Journal of Chemical Engineering 87(1): 85-93.

Kasperski, K.L., 1992. A review of properties and treatment of oil sands tailings. AOSTRA Journal of Research 8(1): 11–53.

Kasperski, K. L., 2001. Review of research on aqueous extraction of bitumen from mined oil sands. [Division No. CWRC 01-17 (CF)]. Natural Resources Canada, CANMET-WRC.

Kariuki, P.C., Van der Meer, F., and Verhoef, P.N.W., 2003. Cation exchange capacity (CEC) determination from spectroscopy. International Journal of Remote Sensing 24(1): 161-167.

Kariuki, P.C., Woldai, T., Van der Meer, F.D., 2004. Effectiveness of spectroscopy in identification of swelling indicator clay minerals. International Journal of Remote Sensing 25(2): 455–469.

Kasongo, T., Zhou, Z., Xu, Z., and Masliyah, J., 2000. Effect of clays and calcium ions on bitumen extraction from Athabasca oil sands using flotation. The Canadian Journal of Chemical Engineering 78: 674–680.

Kessick, M., 1979. Structure and properties of oil sands and clay tailings. Journal of Canadian Petroleum Technology 18(1): 49–52.

Kotlyar, L.S., Capes, C.E., and Sparks, B.D., 1992. Gel-forming attributes of colloidal solids from fine tails formed during extraction of bitumen from Athabasca oil sands by the hot water process. AOSTRA Journal of Research 8: 55-61.

Kotlyar, L.S., Sparks, B.D., Woods, J., Capes, C.E., and Schutte, R., 1995. Bitwetted ultrafine solids and structure formation in oil sands fine tailings. Fuel 74: 1146–1149.

Kruse, F.A. and Hauff, P.L., 1991. Identification of illite polytype zoning in disseminated gold deposits using reflectance spectroscopy and X-ray diffraction-Potential for mapping with imaging spectrometers. IEEE Transactions on Geoscience and Remote Sensing 29: 101-104.

Lipsett, M.G., Olmedo, N., Rivard, B., and Wilson, W., 2014. Robotic systems for measuring properties of tailings deposits and collecting samples. Proceedings of Fourth International Oil Sands Tailings Conference (IOSTC 2014), Lake Louise, AB, Canada, 7-10 December 2014, pp. 483-491.

Liu, J., Masliyah, J., and Xu, Z., 2004. Role of fine clays in bitumen extraction from oil sands. American Institute of Chemical Engineers Journal 50(8): 1917–1927.

MacKinnon, M.D., 1989. Development of the tailings pond at Syncrude's oil sands plant: 1978–1987. AOSTRA Journal of Research 5: 109–33.

Mercier, P.H.J., Le page, Y., Tu, Y., and Kotlyar, L.S., 2008. Powder X-ray diffraction determination of phyllosilicate mass and area versus particle thickness distributions for clays from the Athabasca oil sands. Petroleum Science and Technology 26(3): 307–321.

Mikula, R.J., Munoz, V.A., and Omotoso, O., 2009. Centrifugation options for production of dry stackable tailings in surface mined oil sands tailings management. Journal of Canadian Petroleum Technology 48(9): 19-23.

Morton, F.I., 1975. Estimating evaporation and transpiration from climatological observations. Journal of Applied Meteorology 14(4): 488-497.

Morton, F.I., 1985. The complementary relationship areal evapotranspiration model: How it works. Proceedings of the National Conference on Advances in Evapotranspiration, American Society of Agricultural Engineers, Chicago, Illinois, pp. 377–384.

National Energy Board, 2004. Canada's Oil Sands: opportunities and challenges to 2015 [Pamphlet], Calgary, AB.

Oinuma, K. and Hayashi, H., 1965. Infrared study of mixed-layer clay minerals. American Mineralogist 50: 1213-1227.

Omotoso, O., and Mikula, R., 2004. High surface areas caused by smectitic interstratification of kaolinite and illite in Athabasca oil sands. Applied Clay Science 25: 37-47.

Omotoso, O., Mikula, R., Urquhart, S., Sulimma, H., and Stephens, P., 2006. Characterization of clays from poorly processing oil sands using synchrotron techniques. Clay Science 12(2): 88–93.

Osacky, M., Geramian, M., Dyar, M.D., Sklute, E.C., Valter, M., Ivey, D.G., Liu, Q., Etsell, T.H., 2013a. Characterisation of petrologic end members of oil sands from the Athabasca region, Alberta, Canada. The Canadian Journal of Chemical Engineering 9999: 1–14.

Osacky, M., Geramian, M., Ivey, D.G., Liu, Q., Etsell, T.H., 2013b. Mineralogical and chemical composition of petrologic end members of Alberta oil sands. Fuel 113: 148–157.

Penman, H.L., 1948. Natural evapotranspiration from open water, bare soil and grass. Proceedings of the Royal Society of London, Series A, 193: 120-145.

Rao, S.R., 1980. Flocculation and dewatering of Alberta oil sands tailings. International Journal of Mineral Processing 7(3): 245-253.

Rivard, B., Lyder, D., Feng, J., Gallie, A., Cloutis, E., Dougan, P., Gonzalez, S., Cox, D., and Lipsett, M.G., 2010, Bitumen content estimation of Athabasca oil sand from broad band infrared reflectance spectra. The Canadian Journal of Chemical Engineering 88: 830–838

Salisbury, J. W., and Wald, A., 1992. The role of volume scattering in reducing spectral contrast in spectra of powdered minerals. Icarus 96: 121–128.

Salisbury J.W., Walter L.S., Vergo, N. and D'Aria D.M., 1991. Infrared (2.1-25 mm) spectra of minerals. Johns Hopkins University Press, Baltimore, USA.

Schuttlefield, J.D., Cox, D., and Grassian, V.H., 2007. An investigation of water uptake on clays minerals using ATR-FTIR spectroscopy coupled with quartz crystal microbalance measurements. Journal of Geophysical Research 112: D21303.

Scott, J.D., Dusseault, M.B., and Carrier III, W.D., 1985. Behaviour of the clay/bitumen/water sludge system from oil sands extraction plants. Applied Clay Science 1: 207–218.

Scott, J.D., Jeeravipoolvarn, S., Donahue, R. and Ozum, B., 2008. Characterization of oil sands thickened tailings. First International Oil Sands Tailings Conference, 7-10 December 2008, Edmonton, AB, Canada: 132-142.

Shouxun, Y., and Jin, P., 2004. A study on the correlation relationships between smectite contents and spectral absorption indices of swelling soils. Proc. International Geoscience and Remote Sensing Symposium (IGARSS '04), 20-24 Sept. 2004, Anchorage, AK, USA.

Speta, M., Rivard, B., Feng, J., Lipsett, M., and Gingras, M.K., 2015, Hyperspectral imaging for the determination of bitumen content in Athabasca oil sands core samples: AAPG Bulletin 99(7): 1245–1259.

Thornthwaite, C.W., 1948. An approach toward a rational classification of climate. Geographical Review 38: 55-94.

Van der Meer, F.D., 1999. Can we map swelling clay with remote sensing? International Journal of Applied Earth Observation & Geoinformation (JAG) 1: 27–35.

Vaughan, R.G., Hook, S.J., Calvin, W.M., and Taranik, J.V., 2005. Surface mineral mapping at Steamboat Springs, Nevada, USA, with multi-wavelength thermal infrared images. Remote Sensing of Environment 99: 140–158.

Wallace, D., Tipman, R., Komishke, B., Wallwork, V., and Perkins, E., 2004. Fines/water interactions and consequences of the presence of degraded illite on oil sands extractability. The Canadian Journal of Chemical Engineering 82: 667–677.

Weidong, L., Baret, F., Xingfa, G., Qingxi, T., Lanfen, Z., and Bing, Z., 2002. Relating soil surface moisture to reflectance. Remote Sensing of Environment 81: 238–246.

Weidong, L., Baret, F., Xingfa, G., Bing, Z., Qingxi, T., and Lanfen, Z., 2003. Evaluation of models for surface soil moisture estimation from reflectance data. International Journal of Remote Sensing 10(10): 2069-2083.

Whiting, M.L., Li, L., and Ustin, S.L., 2004. Predicting water content using Gaussian model on soil spectra. Remote Sensing of Environment 89: 535-552.

Wilson, G.W., Fredlund, D.G., and Barbour, S.L., 1994. Coupled soil–atmosphere modeling for soil evaporation. Canadian Geotechnical Journal 31: 151–161.

Wilson, G.W., Fredlund, D.G., and Barbour, S.L., 1997. The effect of soil suction on evaporative fluxes from soil surface. Canadian Geotechnical Journal 34: 145-155.

Yanful, E.K., Bell, A.V., and Woyshner, M.R., 1993. Design of a composite soil cover for an experimental waste rock pile near Newcastle, New Brunswick, Canada. Canadian Geotechnical Journal 30: 578–587.

Yitagesu, F.A., Van der Meer, F.D., Van der Werff, H., 2009. Quantifying engineering parameters of expansive soils from their reflectance spectra. Engineering Geology 105: 151–160.

Yitagesu, F.A., Van der Meer, F.D., Van der Werff, H., and Hecker, C., 2011. Spectral characteristics of clay minerals in the 2.5–14 μm wavelength region. Applied Clay Science 53: 581–591.

Yitagesu, F.A., Van der Werff, H., Van der Meer, F.D., and Hecker, C., 2012. On the relationship between plasticity and spectral characteristics of swelling soils: The 3–5 μm wavelength region. Applied Clay Science 69: 67–78.

Yong R.N., and Sethi, A.J., 1978. Mineral particle interaction control of tar sand sludge stability. The Journal of Canadian Petroleum Technology 77(4): 76-83.